

5-2022

## A Geochemical and Mineralogical Evaluation of the Mona Lisa Turquoise Mine, Polk County, Arkansas

Alexander Arai Goodsumh  
*University of Arkansas, Fayetteville*

Follow this and additional works at: <https://scholarworks.uark.edu/etd>



Part of the [Geochemistry Commons](#), [Geology Commons](#), and the [Mineral Physics Commons](#)

---

### Citation

Goodsumh, A. A. (2022). A Geochemical and Mineralogical Evaluation of the Mona Lisa Turquoise Mine, Polk County, Arkansas. *Graduate Theses and Dissertations* Retrieved from <https://scholarworks.uark.edu/etd/4420>

This Thesis is brought to you for free and open access by ScholarWorks@UARK. It has been accepted for inclusion in Graduate Theses and Dissertations by an authorized administrator of ScholarWorks@UARK. For more information, please contact [scholar@uark.edu](mailto:scholar@uark.edu), [uarepos@uark.edu](mailto:uarepos@uark.edu).

A Geochemical and Mineralogical Evaluation of the Mona Lisa Turquoise Mine,  
Polk County, Arkansas

A thesis submitted in partial fulfillment  
of the requirements for the degree of  
Master of Science in Geology

by

Alexander Arai Goodsuhm  
Baylor University  
Bachelor of Science in Geology, 2020

May 2022  
University of Arkansas

This thesis is approved for recommendation to the Graduate Council.

---

Thomas R. Paradise, Ph.D.  
Thesis Director

---

Adriana Potra, Ph.D.  
Committee Member

---

Gregory Dumond, Ph.D.  
Committee Member

## ABSTRACT

The presence of turquoise in Arkansas has long been disputed by geologists and gem collectors. Despite the prevalence of other phosphate minerals in Arkansas, such as planerite, wavellite, and variscite, the absence of an obvious copper (Cu) source required for turquoise formation was considered too great of an obstacle for turquoise mineralization. In this study, geologic, mineralogical, and geochemical techniques provide overwhelming evidence that the novaculite-hosted Mona Lisa Mine in Arkansas does produce turquoise. X-ray diffraction and Raman spectroscopy have confirmed the structural nature of the material and identified other phosphate minerals, such as crandallite, often found in assemblage with turquoise. Elemental concentrations of Cu up to 5.82 wt.% analyzed on a Thermo Scientific™ iCAP Q ICP-MS clearly show that Cu is a major chemical component. Lead and strontium isotope signatures have been used in studies of the southwestern U.S.A. turquoise to determine the origin of archaeological turquoise. This study applies Lead (Pb) isotope analyses determined on a Nu Plasma multi-collector ICP-MS to constrain the sources of Cu and its potential path prior to mineralization. The determined  $^{208}\text{Pb}/^{204}\text{Pb}$ ,  $^{207}\text{Pb}/^{204}\text{Pb}$ , and  $^{206}\text{Pb}/^{204}\text{Pb}$  ratios indicate that the Pb was derived from the host Arkansas Novaculite. However, the novaculite does not contain enough Cu to be the primary Cu source for turquoise. Therefore, an additional, yet unknown Cu source is required which has negligible lead content. Sr isotope analyses ( $^{87}\text{Sr}/^{86}\text{Sr}$  ratios between 0.71229 and 0.71916) indicate the crustal (basement) source of the material and combined with Pb ratios to provide a unique isotopic signature of Mona Lisa turquoise that can be used as a database for future artifact provenance study. Studying the petrogenesis of Mona Lisa turquoise provided the necessary background for future assessment of potential turquoise sites in the southeastern U.S.A. By combining these analytical techniques with a gemological evaluation, the

current study takes an innovative and inclusive look at each aspect of the Mona Lisa Mine and its potential as a source of gem-quality American turquoise in the future.

*Keywords:* Mona Lisa Mine, turquoise, lead and strontium isotopes, x-ray diffraction, Raman spectroscopy

©2022 by Alexander Arai Goodsum  
All Rights Reserved

## **ACKNOWLEDGEMENTS**

First, I would like to thank Mr. James Zigras and Avant Mining LLC for providing access to the Mona Lisa Mine and access to samples from the site to be used in my research.

Uncovering the history of the mine was possible through accessing Avant's files for preliminary information and viewing the Wigley nugget at the Avant Mining Fisher Mountain location served as motivation to understand this unique locality.

Next, I am grateful to a variety of contributors at the University of Arkansas for their insights and time. Dr. Thomas R. Paradise provided motivation, opportunities, and a fantastic look into the world of minerals and gemstones, while also changing the way I think about graphics and maps. Dr. Adriana Potra spent many hours explaining how lead isotopes are used and provided the lab area and guidance necessary to even begin an isotope project requiring such precision. Dr. Gregory Dumond broke out his incredible 4WD skills on multiple occasions to access the mine site, even before the mine road was graded. Additionally, he provided an extensive background in tectonics and structural geology that proved vastly important to this study. Other contributors include Dr. John R. Samuelsen and Dr. Andrian V. Kuchuk for spending many hours analyzing turquoise samples, Dr. Kenneth S. Befus of Baylor University for allowing access to the Raman microscope in his experimental petrology lab, and Noah Morris for helping me with column chemistry, dilution calculations, and probably cleaning more than his fair share of pipette tips.

Lastly, I am grateful for my family and my girlfriend Morgan for their support and motivation throughout my time in grad school, their interest in my project, and their reminders that life exists outside of school.

# CONTENTS

1. Introduction .....	1
2. Study Site & Geologic Setting .....	4
2.1 Mona Lisa Mine .....	4
2.2 Local Geology .....	8
3. Literature Review .....	22
3.1 Turquoise History & Value .....	22
3.1.1 Global .....	22
3.1.2 North, Central, and South America .....	28
3.2 Turquoise Mineralogy .....	34
3.2.1 Turquoise Group .....	34
3.2.2 Planerite-Turquoise Solid-Solution .....	37
3.2.3 Turquoise-Chalcosiderite Solid-Solution .....	39
3.2.4 Mineralization .....	40
4. Methodology .....	43
4.1 Mapping .....	43
4.1.1 Isohypsometry .....	43
4.1.2 Seam Diagrams .....	43
4.1.3 Structural Orientations .....	44
4.2 Mineralogy .....	45
4.2.1 Physical Properties .....	45
4.2.2 X-Ray Diffraction .....	46
4.2.3 Raman Spectroscopy .....	47

4.3 Geochemistry .....	48
4.3.1 Elemental Concentrations .....	48
4.3.2 Lead and Strontium Isotope Signatures .....	49
5. Results .....	52
5.1 Maps and Stereonets.....	52
5.2 Color and Hardness .....	55
5.3 X-Ray Diffraction Patterns .....	57
5.4 Raman Spectra .....	62
5.5 Elemental Concentrations .....	64
5.6 Sr Isotope Ratios .....	66
5.7 Pb Isotope Ratios .....	68
6. Discussion .....	72
6.1 Local Geology .....	72
6.2 Gemological Value .....	74
6.3 Solid-Solution Relationships .....	79
6.4 Pb & Sr Isotopes .....	80
7. Conclusions & Implications .....	83
7.1 Geologic History .....	83
7.2 Copper Source .....	84
7.3 Further Exploration & Economics .....	84
7.4 Future Directions .....	85
8. References .....	87
9. Appendices .....	93



## LIST OF TABLES

Table 1: CMYK color and hardness values of Mona Lisa samples. ....	56
Table 2: Cu, Fe, Zn, Pb, and Sr concentrations of Mona Lisa samples added to the Mona Lisa concentrations analyzed by Laney (2020). ....	65
Table 3: Cu, Fe, Zn, Pb, and Sr concentrations of Arkansas Novaculite, from Philbrick (2016) and Cains (2019). ....	66
Table 4: $^{87}\text{Sr}/^{86}\text{Sr}$ ratios from select Mona Lisa samples. ....	67
Table 5: $^{208}\text{Pb}/^{204}\text{Pb}$ , $^{207}\text{Pb}/^{204}\text{Pb}$ , and $^{206}\text{Pb}/^{204}\text{Pb}$ isotope ratios of Mona Lisa samples. ....	68

## LIST OF FIGURES

Figure 1: Wigley turquoise nugget, a 245-lb nugget recovered from the Mona Lisa Mine by Jack Wigley in 1982. ....	6
Figure 2: Mena, AR climograph (US Climate Data, 2022). ....	8
Figure 3: Mona Lisa turquoise veins in Arkansas Novaculite gangue. ....	9
Figure 4: Mona Lisa Mine location. ....	11
Figure 5: Extent of the Ouachita Orogeny in the southern United States ....	13
Figure 6: Ouachita structural provinces, from Cervantes and Wiltschko (2010). ....	15
Figure 7: Ouachita wedge model, from Houseknecht and Matthews (1985). ....	17
Figure 8: Seismic reflection interpretations of the Ouachitas, from Lillie et al. (1983). ....	19
Figure 9: Ouachita subsurface integrated gravity model, from Mickus and Keller (1992). ....	20
Figure 10: Chinese turquoise carving, photo courtesy of T. Paradise. ....	25
Figure 11: Turquoise-inlaid Mayan mask, photo courtesy of T. Paradise. ....	30
Figure 12: Map of turquoise sites in the American Southwest and Mexico, from Thibodeau et al (2018). ....	33
Figure 13: Unit cell of turquoise with labeled crystallographic sites (Abdu et al., 2011). ....	36
Figure 14: Variance in the turquoise-planerite solid-solution series based on water content and vacancies (Foord and Taggart, 1998). ....	38
Figure 15: Isohypse map on the Mona Lisa trench, March 2021. ....	53
Figure 16: Seam diagrams of Mona Lisa turquoise, from Avant Mining videos. ....	54
Figure 17: Bedding orientations at/near the Mona Lisa Mine, represented on a contoured stereonet. ....	54
Figure 18: Joint surface orientations at the Mona Lisa Mine on a contoured stereonet. ....	55
Figure 19: Example comparison between Pantone™ CMYK color set and Mona Lisa turquoise. ....	57
Figure 20: 7 Mona Lisa sample x-ray diffraction patterns with matched patterns. ....	58-60

Figure 21: XRD patterns of Mona Lisa matrix material. ....	61
Figure 22: Raman spectrum of sample TQ-A1 compared with turquoise reference. ....	62
Figure 23: Additional mineral phases identified by Raman analysis. ....	63
Figure 24: $^{87}\text{Sr}/^{86}\text{Sr}$ ratios from Mona Lisa samples, compared with novaculite and southwestern turquoise ratios. ....	67
Figure 25: Covariate thorogenic and uranogenic plot of Mona Lisa samples compared with regional strata and ores. ....	69
Figure 26: Thorogenic and uranogenic covariate plots comparing Mona Lisa material with turquoise deposits in the American Southwest. ....	70
Figure 27: Pb isotope composition chart of $^{208}\text{Pb}/^{204}\text{Pb}$ vs $^{207}\text{Pb}/^{204}\text{Pb}$ , contrasting Mona Lisa ratios from southwestern sources. ....	71
Figure 28: Stereonet of averaged conjugate fracture orientations at the Mona Lisa Mine. ....	74
Figure 29: Turquoise seam along the south side of the Mona Lisa Mine. ....	76
Figure 30: Mona Lisa turquoise cabochons. ....	78
Figure 31: Mona Lisa turquoise necklace. ....	79

## Chapter 1: Introduction

Turquoise, the copper aluminum phosphate mineral, has been treasured throughout history for its decorative properties and distinctive color. Typically found in high altitude, arid environments, turquoise forms as a result of the alteration of copper deposits and subsequent mineralization within voids and fractures of pre-existing rock (Lowry and Lowry, 2018). The mineralogy of turquoise is complex -- it exhibits solid-solution relationships with other turquoise-group minerals and features extreme compositional variability within single samples (Foord and Taggart, 1998; Abdu et al., 2011). In the United States, turquoise has long been associated with Native American cultures and trade between indigenous groups (Carpenter, 2020). Recently, however, an Avant Mining LLC-owned trench (the Mona Lisa Mine) has opened for the commercial production of turquoise in western Arkansas, near Mena. The presence of gem-quality turquoise in this location poses significant questions about when, why, and how the conditions allowed for turquoise precipitation. This research, conducted in cooperation with Avant Mining, establishes the first characterization of the Mona Lisa Mine Turquoise, providing insight into the (a) detailed phosphate mineralogy in the open mine trench, (b) lead (Pb) and strontium (Sr) isotopic ratios of Mona Lisa turquoise, (c) implications for turquoise petrogenesis at the mine, and (d) future economic potential of the mine and material.

A wide range of procedures have been employed to gather data for this study. An initial visit to the site yielded several turquoise samples, ranging in quality from gem-quality to chalky and friable material. Ten of these samples, representing the spectrum of collected material, were analyzed by Andrian Kuchuk at the University of Arkansas Nanocenter using x-ray diffraction for mineral identification. For further confirmation, I analyzed the samples at the Baylor University Igneous Petrology Lab using Raman spectroscopy. The combination of Raman and

XRD techniques has provided extensive mineralogical data for the mined turquoise. Pb and Sr isotope data have been collected at the University of Arkansas Radiogenic Isotope Laboratory from the same samples and additional samples of turquoise rough collected in the summer of 2021. Trips to the mine site in 2021 and 2022 resulted in isohypsometric and seam mapping of the trench. The fieldwork also provided the opportunity to measure the orientations of bedding and >200 joints at the Mona Lisa Mine. From these mineralogical data, maps, and comparison with other phosphate mineralization sites, conclusions about the origins of the turquoise have been analyzed, interpreted, and inferred. Finally, Avant Mining LLC records of turquoise prices will be compared with the geologic implications to determine the extent of turquoise mineralization and ensuing economic potential for the company. The results of this study of a new American turquoise source offer key geochemical evidence determining why turquoise mineralized in Arkansas and whether further deposits in the area are to be expected.

The study of the Mona Lisa Mine will have mineralogical, geochemical, and economic impacts. Initially, the site is in a much different climatic and geologic setting than most turquoise deposits. Implications about how turquoise formed here could have wider-reaching impacts on the discovery of future turquoise deposits in Arkansas and abroad. The weathering of phosphates remains poorly understood due to the complex nature of phosphate mineralogy. In this proposed research, precise measurements of Pb and Sr isotopic ratios were used to indicate the primary source of the turquoise's elemental components and how the Arkansas material relates to other U.S. localities. The research will also benefit Avant Mining by better describing and possibly forecasting the value of the mined material. After relative depletion of many famous Southwestern turquoise mines, a substantial amount of turquoise currently being sold in the US is imported, with significant amounts coming from China (Chen et al., 2012). An increase in

domestic turquoise production from a site in Arkansas would decrease the U.S. market's reliance on foreign sources in favor of sustainably mined American turquoise. The scope of this research adds to our understanding of the gemological, geochemical, and mineralogical features of the Mona Lisa Mine, a new, viable source of American turquoise.

## Chapter 2: Study Site & Geologic Setting

### *2.1 Mona Lisa Mine*

Phosphate minerals in Arkansas were first described in 1877 (Chester, 1877) from a variscite locality in Montgomery County. Soon after, Arkansas wavellite was also described (Kunz, 1883). Mining for “phosphate rock” in multiple Arkansas counties commenced in the 20<sup>th</sup> century (Stroud et al., 1969). In the years prior to World War II, the Work Projects Administration (WPA) and other government agencies uncovered other aluminum phosphate localities (including the Mona Lisa site) as they explored the potential for manganese resources in western Arkansas (Barwood and deLinde, 1989). The Mona Lisa Mine site, located on the ridge of Little Porter Mountain, was first opened in 1958 with the purpose of mining phosphate for agricultural fertilizers (Laney, 2020), specifically for use as superphosphate and triple superphosphate (Stroud et al., 1969). Larger scale phosphate mining in other counties (e.g., Searcy, Van Buren, Independence, Pulaski) decreased the demand from the Mona Lisa Mine, leading to the site being closed before 1963 (Stroud et al., 1969). In 1978, the mine reopened as a turquoise mine and was then located on the McBride property (Erickson et al., 1983), and known by some as the McBride Mine.

From 1978-1986, the mine remained at least partially active as a turquoise mine, owned initially by Jack Wigley, a construction contractor from Dallas with an interest in mining (Wigley, 2006). Reports from a Caney Creek Wilderness mineral study (Erickson et al., 1983), estimated the total turquoise production as under 600 pounds. A description of the mining operations from March 1978 is as follows: “...workings consisted of a ridge crest and an adit driven to intersect the turquoise zone about 30 ft lower” (Erickson et al., 1983). This description also identifies the presence of multiple mineralized zones on the McBride property. The evidence

of multiple turquoise sites remains apparent today, with the remnants of a smaller trench visible less than 100 meters to the east of the main trench. During this first period of turquoise production, a 245-lb (after cutting and polishing) nugget of turquoise (Figure 1) was recovered from the mine by Jack Wigley (Avant Mining LLC). Wigley himself described the nugget as being 380 lbs. when it was removed from the mine after a large chunk (~100 lbs.) broke off during extraction (Wigley, 2006). This first-hand observation would put the complete nugget's total weight at close to 500 lbs. The material from the mine in this early period of production was likely marketed and sold as Southwestern turquoise, creating difficulties in evaluating the true amount and value of turquoise from the Mona Lisa (Archuleta and Renfro, 2018). Wigley estimates that between 25000 and 30000 lbs. of material was mined over the course of this period of operation, with significant material lost due to unfamiliarity with stabilization processes (Wigley, 2006). A competitive turquoise market caused operations to close in 1986, with further reports that the trench had been "mined out" (Wigley, 2006). From 1989-1991, the mine was reclaimed (Laney, 2020).





Figure 1: Photograph of the Wigley nugget, a 245-lb nugget discovered by Jack Wigley in 1982 that was presented by Avant Mining at the 2018 Tucson Gem and Mineral Show. (From Archuleta and Renfro, 2018, photographed by Robert Weldon).

In 2017, James Zigras, founder and owner of Avant Mining LLC, purchased the mining claim, leasing the subsurface mineral rights from the Bureau of Land Management (Targeted News Service, 2020). The mine is located on National Forest Service land, in the Ouachita National Forest area. An Avant Mining test trench in early 2018 produced ~1000 lbs. of

turquoise within one week (Archuleta and Renfro, 2018), an amount suitable for further development. The 245-lb nugget was located, purchased, and first displayed by Avant at the 2018 AGTA gem show in Tucson, after being polished by Michael Beck (Copper Canyon Lapidary & Jewelry, Sedona, AZ). After this dramatic re-entrance into the market, the Mona Lisa Mine has been operating sporadically, with minor delays caused by COVID-19, weather, and equipment issues. Mine production has recently begun once more in early 2022.

The Mona Lisa Mine entrance is accessible via Polk County Road 402 (FS Road 176) from Highway 246 between the towns of Vandervoort and Athens. With Avant Mining permission, 4-wheel drive vehicles may access the trench by climbing the mine road. The trench is located at an elevation of ~1420 feet. The Cossatot River (part of the National Wild and Scenic Rivers system) lies less than half a mile northwest of the ridge, and the Caney Creek Wilderness area begins less than a mile to the northeast.

The climate at the Mona Lisa Mine in the Ouachita Mountains of Arkansas contrasts with the arid climates in the turquoise mining districts of the American Southwest. Figure 2 shows a climograph of temperature and precipitation in Mena, Arkansas. The climate is temperate, with the most precipitation falling in the fall and spring seasons. Total precipitation averages at 150 cm per year in the Ouachita Mountains region (National Climatic Data Center, 2009). This is above the national average for rainfall. The annual mean temperature is 16°C, the result of hot summers and milder winters. The plant growth and outcroppings on Ouachita ridges is dependent upon the exposure to sunlight, with some areas densely forested and others sparsely.

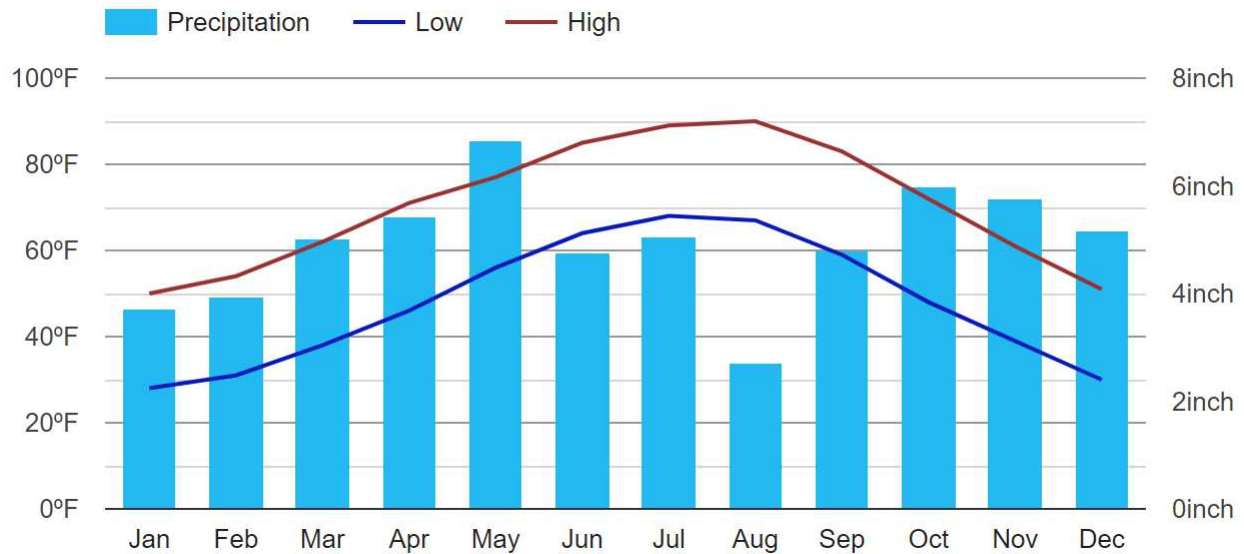


Figure 2: This climograph details average precipitation (in inches) and mean high and low temperatures (in °F) in Mena, AR. Mena is the largest city and county seat for Polk County. (From U.S. Climate Data, 2022).

## ***2.2. Local Geology***

The Mona Lisa Mine is composed of an open trench dug into weathered and fractured Arkansas Novaculite along the ridge of Little Porter Mountain in Polk County, Arkansas. Figure 3 shows turquoise in the host novaculite. The trench is located near the contact and transition between the Missouri Mountain Shale and Arkansas Novaculite, with thin beds of Missouri Mountain Shale are visible just south of the trench and sporadically interbedded in novaculite within the trench. The presence of the older (Silurian) Missouri Mountain Shale along the ridge suggests an overturned anticlinal structure, but the bedding orientations and facing directions are needed to further detail the structural nature of Little Porter Mountain.



Figure 3: Monalisa turquoise in Arkansas Novaculite host rock. (Photo by T. Paradise).

The Arkansas Novaculite formation consists of variably-colored, high-purity cryptocrystalline silica that derives its name (novaculite) from the Latin for “razor” due to the prevalent usage of the material for whetstones (Goldstein, 1959). Novaculite is differentiated from chert by having a generally lighter color, a lack of lamination and chalcedony, and less organic and clastic materials (Goldstein, 1959). However, a firm petrographic distinction has not been established, as both novaculite and chert units in the Ouachita Mountains experience variable metamorphic micro-textures depending on their adjacency to the core of the uplift (Keller et al., 1985). The Arkansas Novaculite is Late Devonian to Early Mississippian in age and often formally divided into upper, middle, and lower members (Goldstein, 1959). The distribution of the Arkansas Novaculite lithology in the county in reference to the study area is illustrated in Figure 4.

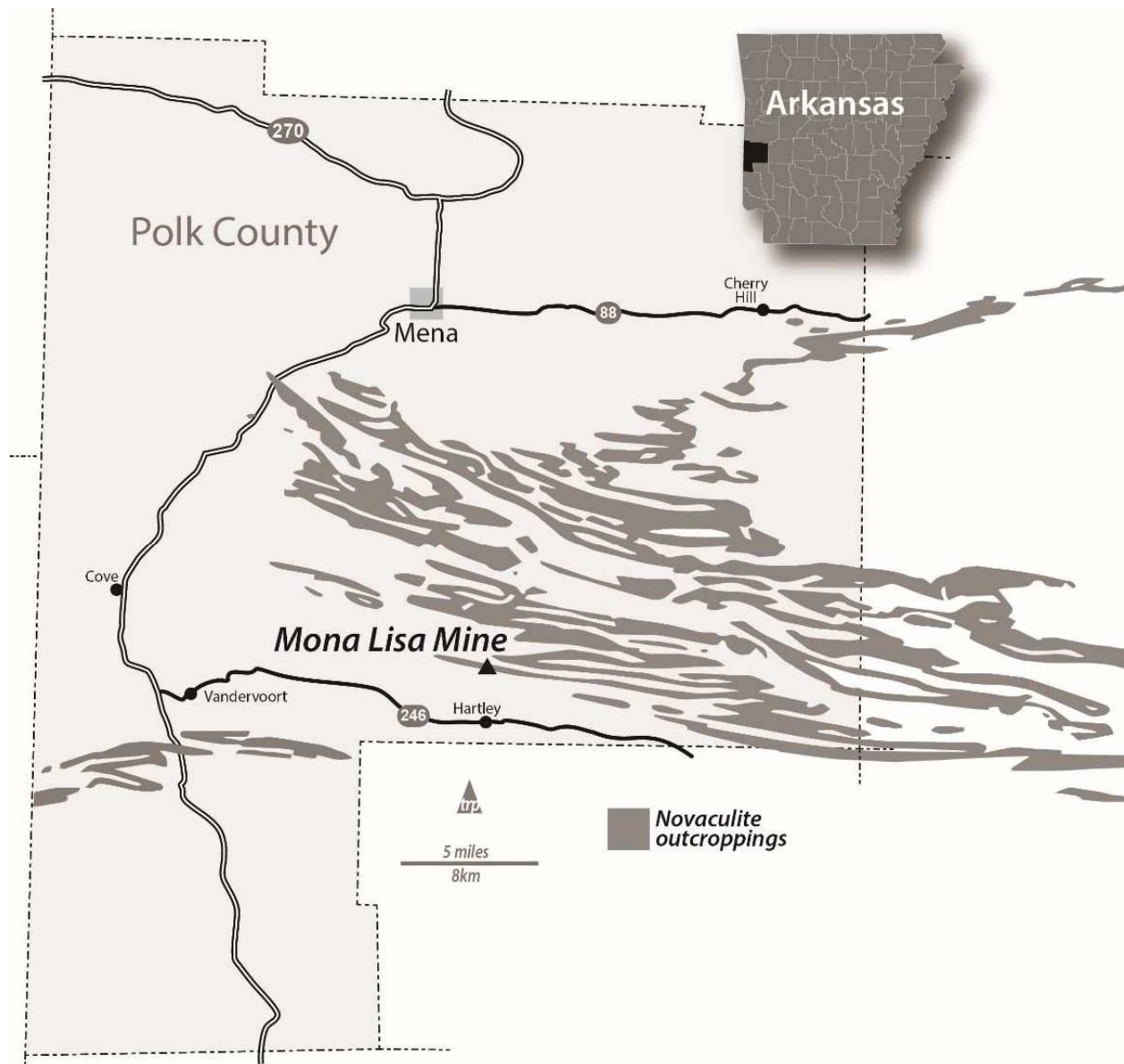


Figure 4: The Mona Lisa Mine location in Polk County, AR. Outcroppings of Arkansas Novaculite included (cartography by T. Paradise).

The deposition of the Arkansas Novaculite remains a complicated topic. The presence of radiolarians, spores, and sponge spicules offer evidence that some of the silica was derived organically; conversely, evidence of these organisms is not present throughout the formation, indicating possible compression (Goldstein, 1959). The idea that organic material from microorganisms could provide sufficient silica for the deposition of the thick novaculite succession is

contested as well. Elemental concentrations of the Arkansas Novaculite show reasonable resemblance to a boninitic magmatic body, caused by the deposition of volcanic ash into the ocean from arcs generated by the collision between the North American craton and the Gondwana landmass (Philbrick, 2016). Arkansas Novaculite represents the final passive margin formation that was deposited prior to the onset of the Ouachita Orogeny (Blythe et al., 1988).

The Ouachita Orogeny is a segment of the southern Laurentia orogenic system, along with the Appalachian Orogeny (Johnson et al., 2019). The Ouachita orogenic belt is >2100 km long, extending from the Appalachians in the northeast to the Coahuila Uplift in Mexico (Richards et al., 2002), but the vast majority of the system is covered by Gulf Coastal Plain sediment (Figure 5). The Ouachita Mountains are the best exposure of the system, trending east to west from central Arkansas to south-eastern Oklahoma (Houseknecht and Matthews, 1985), although the belt is also exposed at the Marathon Thrust Belt Province of West Texas. The position of the orogeny was south of the paleo-equator in the late Paleozoic, accounting for the carbonate deposition along the southern margin of the North American craton (Gutschick and Sandberg, 1981). The stratigraphic setting of the Ouachitas can be divided into pre-orogenic and syn-orogenic successions (Richards et al., 2002).

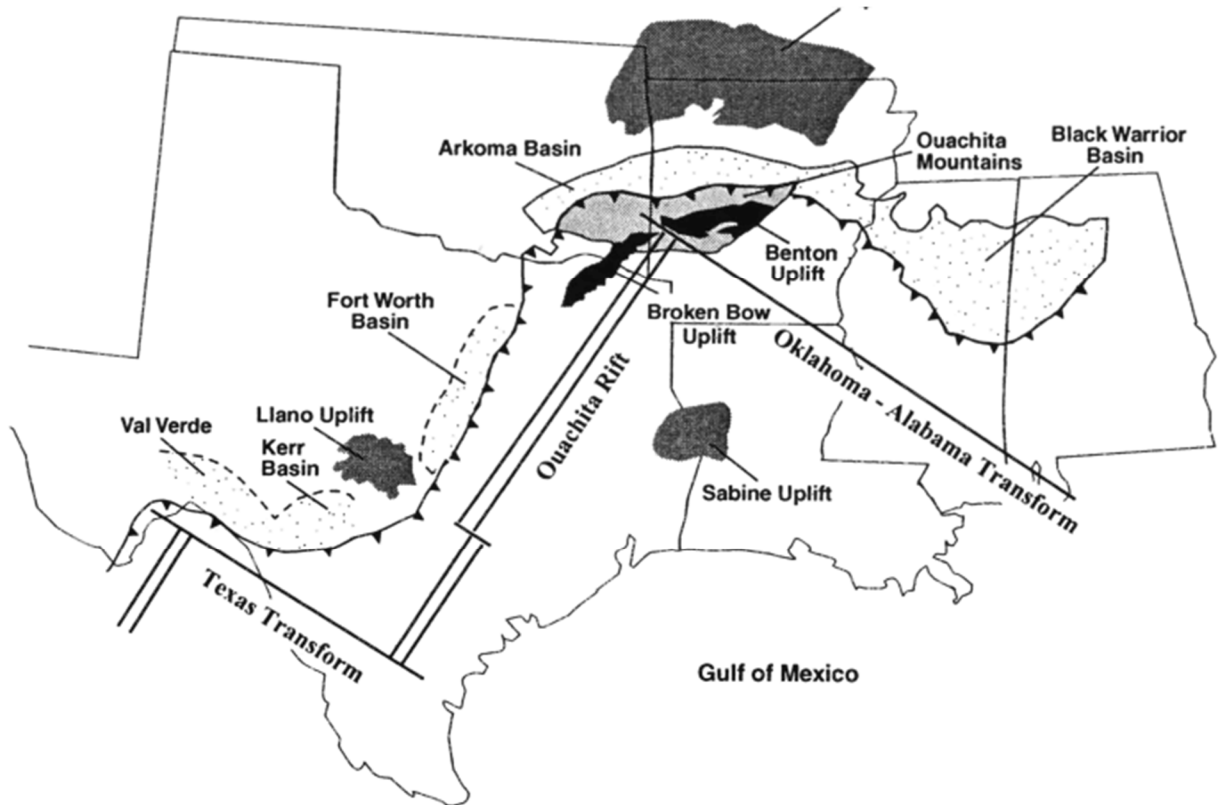


Figure 5: This map shows the extent of the Ouachita Orogeny, although most of orogenic belt is covered by younger sedimentation. (From Harry and Mickus, 1998).

The opening of an ocean basin in the Late Proterozoic and Early Cambrian provided the passive margin setting on the southern edge of the North American craton in which the pre-orogenic strata were deposited (Richards et al., 2002). The general nature of passive margin deposition can be described as Early Ordovician thin shale, sandstone, and micrite layers that grade into siliceous shale, chert, and novaculite in the Devonian and Early Mississippian (Richards et al., 2002). The oldest formation found in the Ouachitas is the Collier Shale, a thin layer composed of black shale, siliceous limestone, and minor black chert (Richards et al., 2002). The Crystal Mountain Sandstone, Mazarn Shale, Blakely Sandstone, Womble Shale, Bigfork Chert, and Polk Creek Shale represent alternating layers of sandstone, shale, limestone, and chert in the late Ordovician Period (Richards et al., 2002). The Silurian formations are the Blaylock



Sandstone and the Missouri Mountain Shale, both characterized by increasingly lighter-colored, more siliceous beds (Richards et al., 2002). The Arkansas Novaculite, with shale, chert, and novaculite beds, was deposited during the Devonian Period and signifies the end of passive margin deposition before the commencement of the orogeny (Blythe et al., 1988).

The onset of the Ouachita Orogeny is defined by the first deposition of Stanley Shale sediment. The Stanley Shale marks the start of a very thick (>13 km) flysch sequence of clastic, deep-water sediments, deposited during the Carboniferous (Blythe et al., 1988). The clastic wedge sequence includes the Stanley Shale, Jackfork Sandstone, and Johns Valley Shale. A >3 km thick formation, the Stanley Shale is composed of sandy and shaly continental detritus. The Jackfork Sandstone represents a turbidite deposit, which is resistant to weathering and thus forms some of the ridges in the Ouachitas. The Johns Valley Shale, made up of light-colored sandstone, shale, and limestone beds, is the youngest formation in the deep-water clastic wedge sequence (Richards et al., 2002). The Late Pennsylvanian Atoka Formation is also evident in the Ouachitas but represents shallower deposition in a shelf-delta system (Richards et al., 2002). All of the syn-orogenic units tend to thicken towards the south, because the continental shelf was southward-dipping (Blythe et al., 1988).

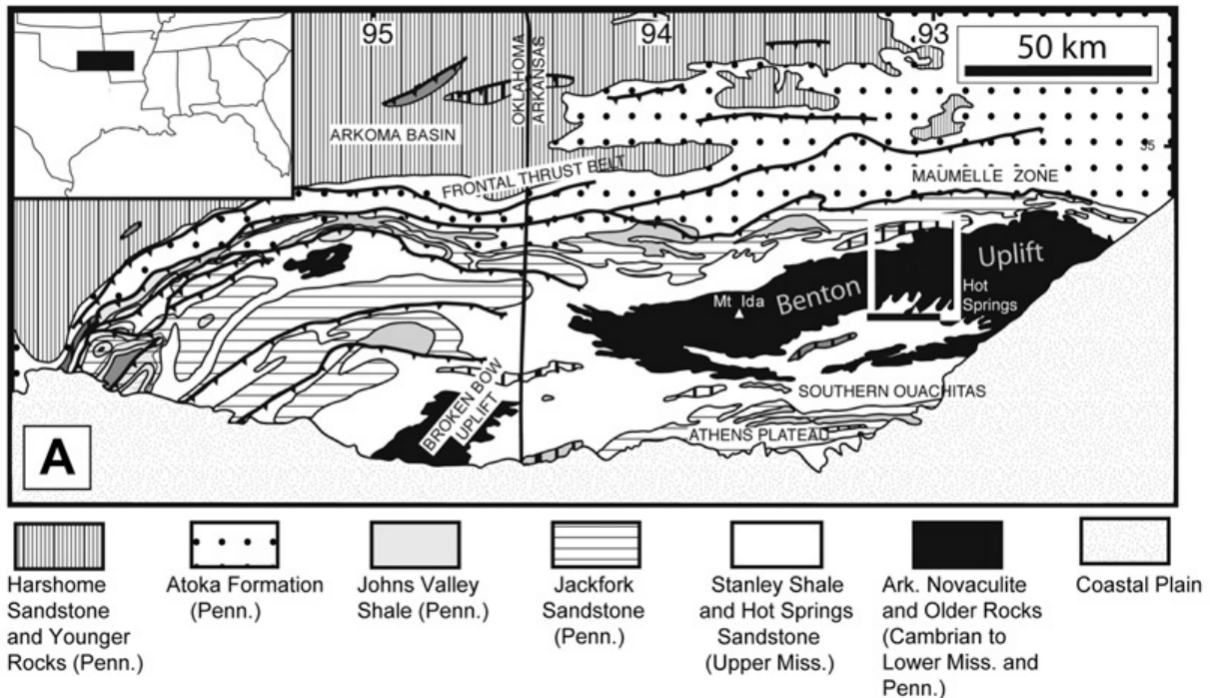


Figure 6: This map shows the location of the Ouachita Range in relation to the contiguous United States and the provinces of the Ouachitas: the Arkoma basin, frontal thrust belt, and the Benton and Broken Bow uplifts. The stratigraphic setting is also shown. (From Cervantes and Wiltschko, 2010).

The Ouachitas have several distinct structural provinces, shown in Figure 6. Beginning in the north, the Arkoma Basin is composed of the syn-orogenic flysch sequence (Blythe et al., 1988). To the south of the basin, a series of anticlines and synclines make up the frontal thrust zone. The northern limbs of the anticlines dip more steeply than the southern limbs (Blythe et al., 1988). North-verging thrust faults, which emerge along the crests of the anticlines, are apparent. The Jackfork Belt (also known as the Maumelle Chaotic Zone), characterized by east-west trending thrust faults, lies to the south of the frontal thrust zone (Blythe et al., 1988). The Benton-Broken Bow uplift makes up the core of the Ouachita Range. This anticlinorium exposes many of the older pre-orogenic rocks, which have been metamorphosed to lower greenschist facies (Blythe et al., 1988). Thrust faults and overturned folds are other features found in the anticlinorium.

Quartz veins are abundant in the vein-quartz belt, which runs parallel to the uplift from Little Rock, AR, to Broken Bow, OK. The veins occur in all rock types, and are highly concentrated towards the center of the uplift (Richards et al., 2002). The veins range from <1 centimeter to >20 meters in width and contain many varieties of quartz. The veins cut across folded beds, following fractures, faults, and bedding planes. The veins themselves are not folded, but are often fractured (Richards et al., 2002). In addition to quartz, other minerals such as calcite, adularia (which can be used for radiometric dating), chlorite, and dickite are commonly found in veins (Richards et al., 2002; Cervantes and Wiltschko, 2010).

The Early-Middle Paleozoic rocks found in the Ouachita Mountains record the rifting along the southern margin of the North American craton, the beginnings of a complete Wilson cycle (ocean opening and closing). The passive margin sedimentation provides evidence for the tropical conditions inherent to the paleoenvironment. In the Late Paleozoic, the closing of the ocean basin began, starting with collision in the east (Appalachian Orogeny) between the North American craton and the African plate (Gutschick and Sandberg, 1981). Proceeding eastward along an irregular margin, the craton collided with a microcontinent (Sabine terrane) at ~350 Ma, and deposition of the Stanley Shale began. During this convergence, the incipient orogenic belt formed as an accretionary wedge as south-dipping subduction started (Houseknecht and Matthews, 1985). As the collision continued, the accretionary wedge was thrust on top of the subducting plate, causing extensive faulting and folding (Houseknecht and Matthews, 1985). Figure 7 details this evolution of the accretionary wedge over time.

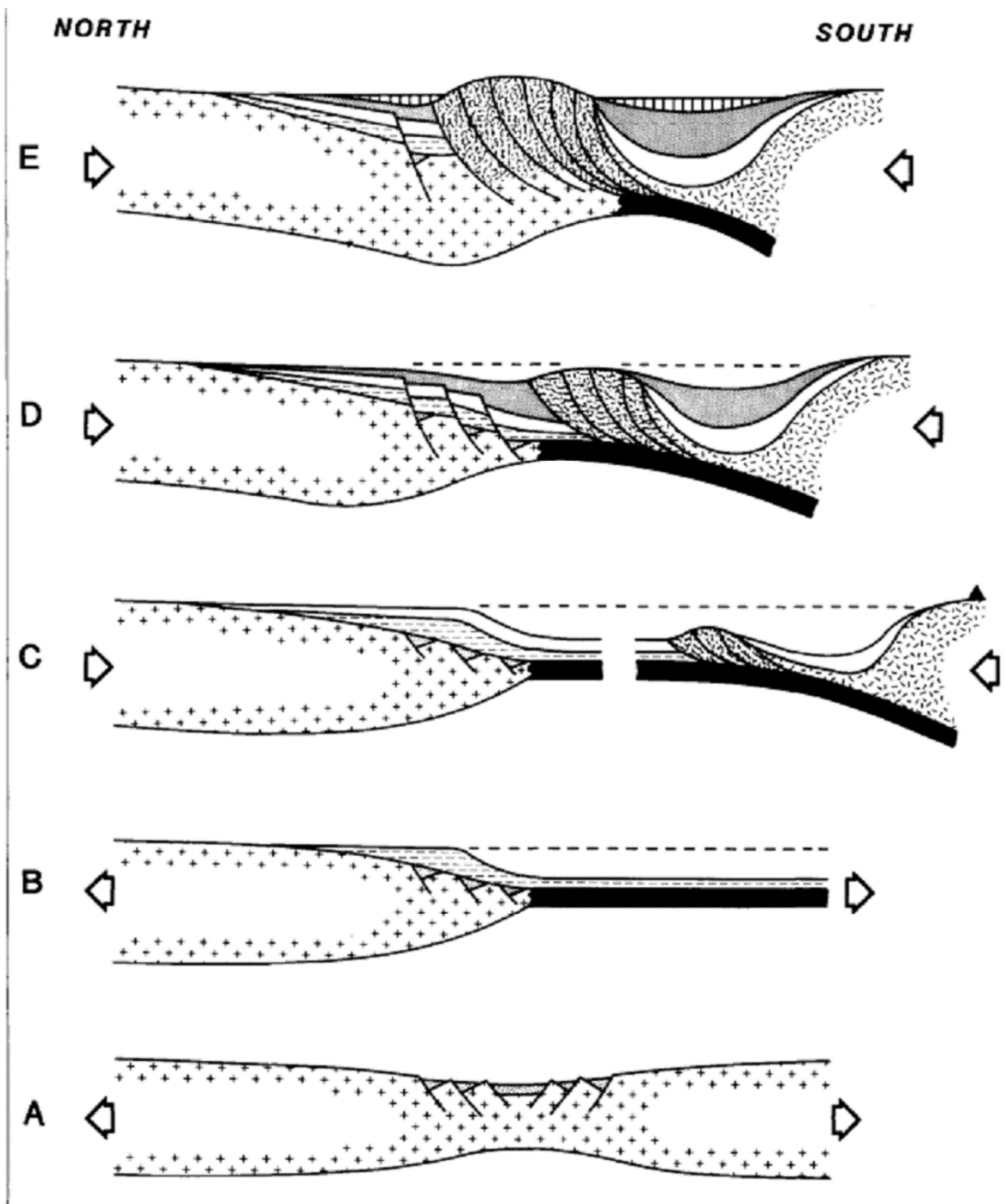


Figure 2—Hypothetical cross sections depicting tectonic evolution of southern margin of North America during (A) late Precambrian-earliest Paleozoic, (B) late Cambrian-earliest Mississippian, (C) early Mississippian-earliest Atokan, (D) early-middle Atokan, and (E) late Atokan-Desmoinesian.

Key to patterns: crosses = continental crust (undifferentiated in A, North American in B-E); straw hachures = "Llanorian" crust; black = oceanic crust; stippling = earliest Paleozoic strata; horizontal hachures = late Cambrian-earliest Mississippian strata; white = Mississippian-earliest Atokan strata; shaded = early-middle Atokan strata; vertical lines = late Atokan-Desmoinesian strata; mottled = imbricated Paleozoic strata forming subduction complex (Ouachitas); black triangle = magmatic arc volcanoes.

Figure 7: These theoretical cross-sections illustrate the evolution of the Ouachita system and paleo-accretionary wedge over time. Note that subduction is directed to the south. (From Houseknecht and Matthews, 1985).

An accretionary wedge develops when material is scraped off of a subducting slab. The wedge deforms internally in response to frontal accretion or tectonic underplating (Platt, 1986). In the Ouachita example, the rocks deposited in the passive margin setting are being added to the wedge as the collision occurs. In response to the addition of material, significant thrust faulting occurs to shorten the wedge and maintain its stable state, according to Critical Taper Theory (Dahlen, 1990). These thrust faults are evident in the frontal thrust zone of the Ouachita Mountains (Blythe et al., 1988). The deformation and fracturing provided the means of transport for mineralized veins to form throughout the area, with radiometric dating of adularia confirming that precipitation occurred near the end of the orogeny (Late Pennsylvanian to Early Permian) (Richards et al., 2002).

The abundance of sediment deposited on the Gulf Coastal plain has hidden many aspects of the Ouachita orogeny from researchers, most notably the nature of the Sabine terrane, the overriding microcontinent that should have evidence of arc magmatism associated with subduction (Blythe et al., 1988). To better understand the subsurface, gravity and seismic reflection surveys have been conducted to image cross-sections of the Ouachitas. The Consortium for Continental Reflection Profiling (COCORP) recorded the most complete deep seismic reflection profiles of the Ouachita region (Lillie et al., 1983). Five profiles were taken, extending from the coastal plain sediments in the south to the Arkoma basin. The compiled profiles and potential interpretations of the data are shown in Figure 8. The profiles uncover the potential position of the crystalline basement and deep thrust faults from the accretionary wedge (Lillie et al., 1983).

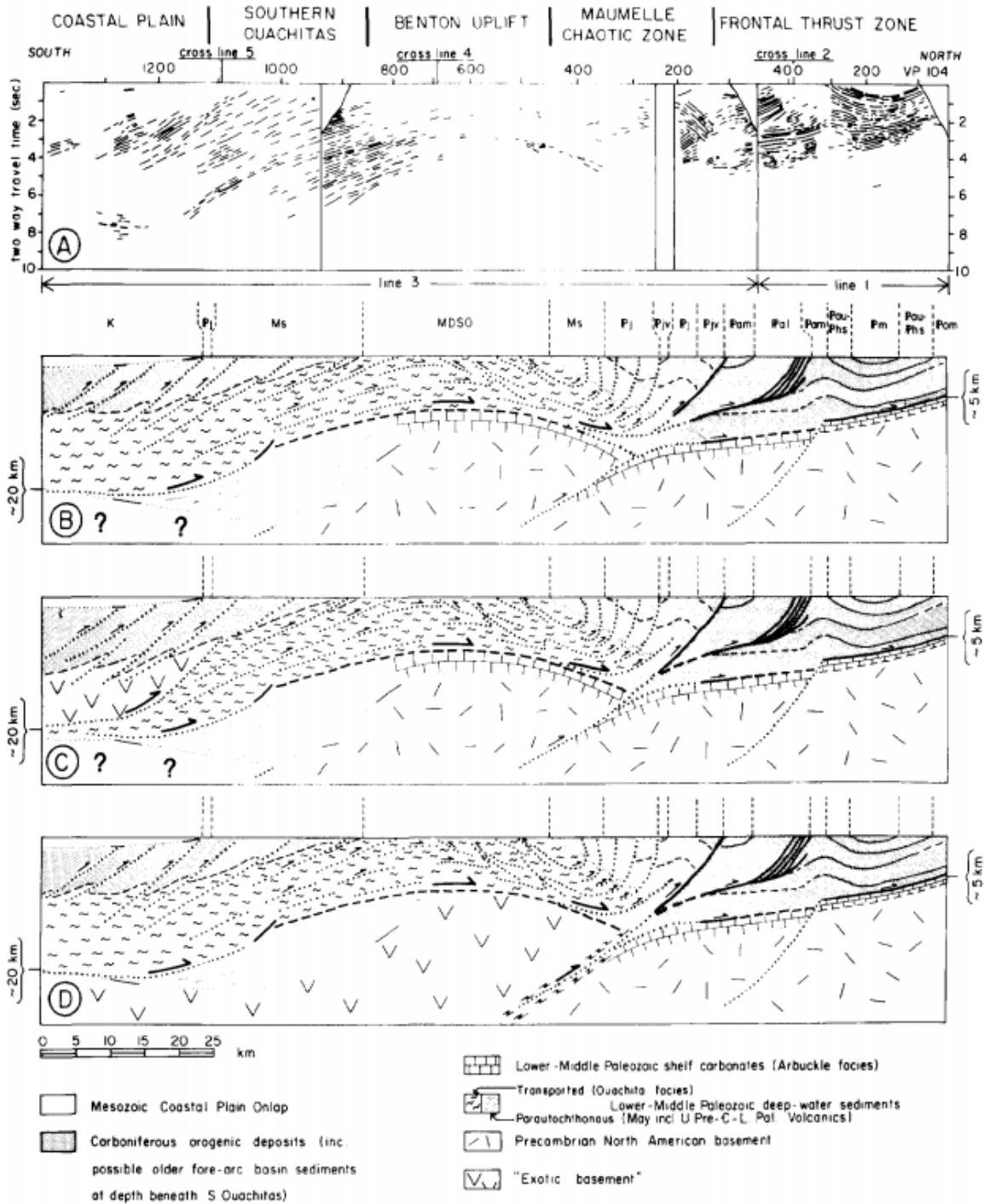


Figure 8: A: Major seismic reflection events. B: Interpretation of A. C: Alternative interpretation, showing crystalline basement to the north. D: Alternative interpretation of an "exotic" basement source. (From Lillie et al., 1983).

Seismic reflection data proved an excellent starting point for gravity-related studies (Mickus and Keller, 1992). The lithospheric transect model of Mickus and Keller (1992) integrates previous seismic data, geological evidence, and gravity anomaly data to visualize the subsurface features of the Ouachita Range. The thick sedimentary units making up the Arkoma basin correspond with low gravity values, while the metamorphosed rocks in the core of the uplift have higher values (Mickus and Keller, 1992). The data also indicate a region of thick continental crust, which likely was the microcontinent involved in the collision. The wedge shape of the Ouachita facies rocks is also clearly visible in the model. The gravity data and the interpreted subsurface is shown in Figure 9.

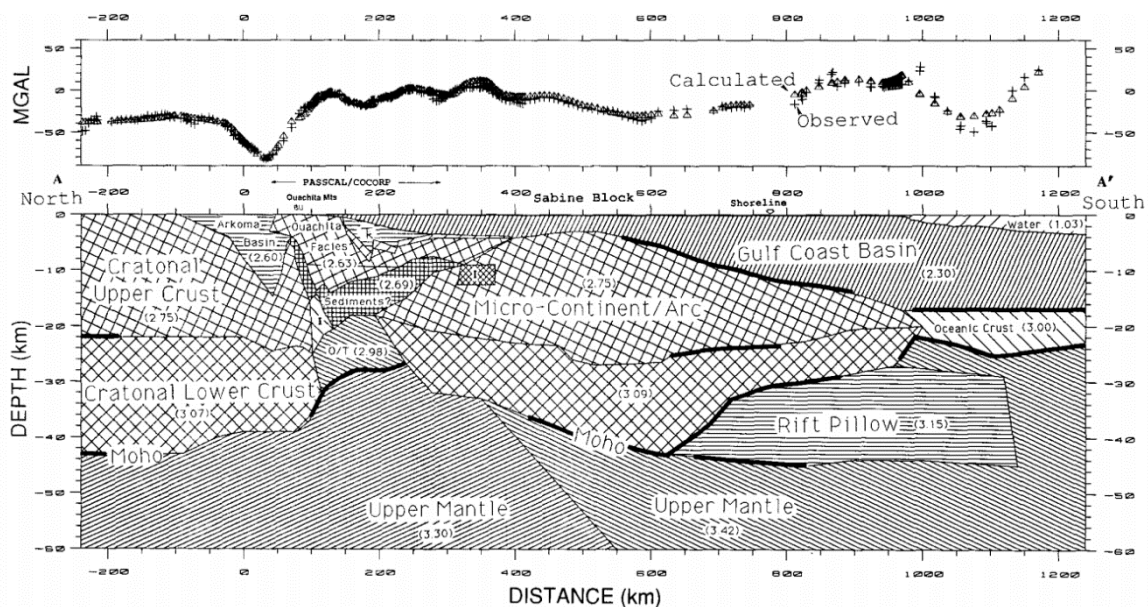


Figure 9: This integrated model combines seismic data, gravity data, and geological observation to model the subsurface of the Ouachita Orogeny. The microcontinent is named the Sabine Terrane. The wedge shape of the Ouachita rocks is apparent. (From Mickus and Keller, 1992).

In a subduction zone setting, metamorphic rocks associated with high pressures would be expected to be found due to the pressure-temperature conditions of a subducting slab. However, any remnants of such rocks, if they exist in the Ouachitas, are buried beneath kilometers of coastal plain sediment along with the potential arc. Instead, the metamorphic rocks found in the

Ouachitas are from the accretionary wedge and represent a lower-pressure environment (Johnson et al., 2019). The maximum temperature conditions have been constrained to be slightly above 300°C from vitrinite reflectance and thermal maturation data (Johnson et al., 2019). Paleothermal gradients suggest that peak metamorphic conditions occurred at the same time as thrusting within the wedge (Cervantes and Wiltschko, 2010). There is no evidence of high heat flow from igneous intrusions (Johnson et al., 2019).

The rocks with the highest metamorphic grade lie close to the core of the Ouachitas and also contain the most veins (Cervantes and Wiltschko, 2010). The mineralization of the veins occurs in two ways: the diffusion of wall-rock components into fractures or direct precipitation from a transporting fluid (Richards et al., 2002). The veins of the Ouachitas likely formed from a combination of these mechanisms, as evidenced by stable isotope studies (Richards et al., 2002). Veining within this system is analogous to the Chilean Coastal Range, where prograde internal fluid production and subsequent high pore-fluid pressures caused veining to occur in a metamorphosed paleo-accretionary wedge (Munoz-Montecinos et al., 2020).

The deformation of sedimentary strata caused by the Ouachita Orogeny provided the pathways for mineralizing fluids to travel in the subsurface. The convergence between the North American craton and the Sabine Terrane caused southward subduction and the formation of an accretionary wedge. The Mona Lisa Mine is located along a ridge of folded and fractured Arkansas Novaculite that was deformed as the wedge evolved. Thus, the tectonic activity during the Ouachita Orogeny provides the background for all future geologic events that allowed phosphates to mineralize in western Arkansas.



## Chapter 3: Literature Review

### *3.1 Turquoise History and Value*

#### *3.1.1 Global*

Turquoise has been desired since ancient times due to its distinctive appearance in addition to beliefs in its healing and mythical properties. The earliest uses of ornamental turquoise, identified by archaeological excavations, include beads dating back to 5000 BCE from Mesopotamia (Bonewitz, 2013). The ancient Egyptians also treasured this stone, evidenced by its appearance in jewelry discovered in the tombs of Egyptian royalty (Lowry and Lowry, 2018). The oldest known turquoise mining sites are located on the Sinai Peninsula, where nomadic groups briefly camped at mineralized sites, seeking turquoise, malachite, and copper for trade. Archaeological studies conducted by Sir Flinders Petrie identified two areas of mining: Wadi Maghara (in the Sinai) and Serabit el-Khadim (Lowry and Lowry, 2018). As the Early Dynastic Period of Egypt began, the mining of those materials took on increased importance. Hieroglyphic and pre-Canaanite inscriptions in the Wadi Maghara area recount ore production and describe the area as the “Terraces of the Turquoise” (Pogue, 1915). The pharaohs of the time would often sanction expeditions to these mining areas to increase the supply of turquoise to their kingdom. The word *mfkzt* in inscriptions translates to malachite, copper, and turquoise. *Mfkzt*, or mefkat, also meant “joy”. In Egypt, turquoise had an important connection with the deity Hathor, a goddess worshipped for love and motherhood (Lowry and Lowry, 2018). Turquoise maintained its status as a valuable gemstone in Egyptian culture over multiple millennia. The Nile River provided the ability to transport turquoise for trade over a wide area of Egypt while new ports and overland routes were established. These routes would eventually connect Egypt with the Mediterranean, Mesopotamia, and western Asia (Lowry and Lowry, 2018). Perhaps the most

famous Egyptian turquoise artifacts are those which were preserved in the tomb of Tutankhamun excavated in the 1920s. The mines of the Sinai Peninsula have been inactive for over a century and the turquoise reserves have likely been exhausted (Pogue, 1915). Early examples of turquoise simulants have also been identified; Steatite beads would be shaped and heated, then glazed with faience to attain a turquoise-like color (Lowry and Lowry, 2018).

Persian turquoise is famed for its hardness and valued for its clarity. The Iranian plateau has the conditions required for many mineral resources, including turquoise, copper, and marble. Its adjacency to the people of Sumeria and central location between budding ancient civilizations allowed Persian turquoise to be distributed across the civilized world (Lowry and Lowry, 2018). The Persians established new cutting styles and grading methods for their turquoise. Stonecutters first developed the cabochon shape with Persian material, and the stones were valued for their purity (lack of matrix material within the stone). Turquoise was valued in ancient Persian culture as protection; the stone was said to change color to warn of danger. Turquoise was also used in the construction of palaces, because the sky-blue color was associated with heaven (American Gem Society, 2022). Known as *pirezeh* or *pirouzeh* (meaning victory), Persian turquoise was mined at sites located in Khorasan Province near the town of Neyshabur (Lowry and Lowry, 2018). Neyshabur's access to trade routes opened Persian turquoise into new markets. Turquoise and related mining in this region were documented by noted historical figures Pliny the Elder and Marco Polo (Pogue, 1915). Along the Silk Road in the 13<sup>th</sup> century, Persian turquoise reached European markets through Turkey. Through this association with Turkish traders, the name turquoise developed from the French term *pierre tourques*, meaning "Turkish stone" (American Gem Society, 2022). To this day, "Persian" turquoise is considered the most valuable turquoise material on the market due to its purity, color, and hardness.

Despite jade's prominence as the symbolic gemstone of China and East Asia, turquoise has also been mined, inlaid, and carved into figurines for thousands of years across the region (Figure 10). Artifacts with turquoise insets in China date back to 1500 BCE (Lowry and Lowry, 2018). Mining of turquoise in China has been largely focused around the deposits in the highlands of Hubei Province. The local economies have longstanding traditions in the extraction, cutting, and setting of the gem. Marco Polo described turquoise production in central China as well as in Persia during his travels through Asia along the Silk Road in the 13<sup>th</sup> century (Pogue, 1915). However, the first accepted Chinese word specifically for turquoise, "*tien-tse*", was not in literary use until the 1366 text *Cho Keng Lu*. This text describes the production of turquoise in China and a comparison with turquoise material which was traded from Persia (Pogue, 1915). Because of active trade routes throughout much of Asia, surrounding countries also discovered turquoise and began to mine their own deposits when possible. Tibet, Nepal, Afghanistan, Mongolia, and India all traded for turquoise and developed their own jewelry and ornamentation styles using the gemstone. The earliest description of turquoise in Hindu literature is attributed to the physician Narahari in the 15<sup>th</sup> Century (Pogue, 1915).



Figure 10: Chinese turquoise carving dating to the Qing dynasty. (Photo courtesy of T. Paradise).

In Western scholarly writings, the first mentions of turquoise are likely from the writings of Pliny in AD 77, who used the terms *callaina*, *callais*, and *callaica* to refer to “pale green”, “water-tinted”, and “clouded” stones, respectively. Though most agree that *callais* did refer to turquoise, the *callaina* and *callaica* have disputed meanings, based on their descriptions (Pogue,

1915). Pliny also described many types of jasper, including a “sky-blue” jasper with a Persian origin, which potentially was Persian turquoise from Neyshabur (Pogue, 1915). Mineralogical study over the following centuries was restricted to physicians, who described the quality of Neyshabur turquoise and identified the stone often in the “ears of Orientals” (Pogue, 1915). The name “turquoise” found its first use in the 13<sup>th</sup> century (Kunz, 1913). However, the earliest uses of the term referred to a stone of yellow color from Turkey. Ahmed Teifascite, an Arabian scholar, produced a description of true turquoise (called “*fairuz*” in Arabic) formation, properties, and value that remained superior to all European accounts until Agricola and Anselmus de Boodt’s works in the 16<sup>th</sup> and 17<sup>th</sup> centuries (Pogue, 1915). De Boodt, physician and alchemist of Holy Roman Emperor Rudolf II, published his crowning work, *Gemmarum et Lapidum Historia*, in 1608. His chapters on turquoise identify the types of turquoise, important localities, and physical properties, while also expounding upon the mystical virtues of the stones, as confirmed or discredited by personal experiments (Pogue, 1915; Kunz, 1913). Subsequent accounts over the course of several centuries debated the differences between “bone turquoise” (odontolite) and true turquoise (known as Oriental turquoise). The differentiation between these two materials was only fully established and accepted in the early 19<sup>th</sup> century (Pogue, 1915). European access to southwestern American turquoise, catered and marketed widely by the Tiffany Company, led to a rebound in the popularity of the stone in Europe in the 20<sup>th</sup> century (Lowry and Lowry, 2018).

Ancient global turquoise production was centered on the Egyptian, Persian, and Chinese cultures. The supply of turquoise from the Sinai Peninsula, Neyshabur region, and Hubei Province dictated its market value, as did the preferences of wealthy pharaohs, kings, and emperors. Trade networks, especially the Silk Road, transported turquoise material to the rest of

the civilized world over many centuries. The study of turquoise by Arabian and European physicians led to the first mineralogical descriptions of turquoise and many other important gemstones. Although the landscape of the global turquoise market has shifted dramatically in recent years, Persian and Chinese turquoise remain highly profitable and influential sources. The clarity and color of Persian material continues to elevate prices, and is still seen as the standard for high quality turquoise. The affordability and supply of Chinese turquoise have led to China becoming currently the largest source of global turquoise (Lowry and Lowry, 2002). Lower labor costs and fewer mining restrictions allow Chinese turquoise to be sold at lower prices than Persian or American turquoise. This has led to frequent misrepresentation of gem origin to make unethical profit. Chinese turquoise is often fashioned into more valuable styles of jewelry in an attempt to simulate a more valuable location and may be enhanced to match more notable locale colors (Lowry and Lowry, 2002). Throughout ancient history and even today, the market for turquoise is not only driven by aesthetics, but by the mythical powers and benefits that the stone is said to possess.

Varying myths about the origins and spiritual abilities of turquoise developed across the ancient world. The stone represented femininity, motherhood, and love in Ancient Egypt. In the Middle East, turquoise is auspicious and can be used as a talisman to ward off sickness from the Evil Eye. In contrast to the Egyptians, turquoise was worn more prominently by kings who claimed it removed them from danger (Lowry and Lowry, 2018). Early Asian texts established even wider medicinal properties, including safety from snakes, scorpions, lightning, and drowning. Applying turquoise over the eyes or through ingestion with wine would cure many illnesses. One myth which persisted through many years across many cultures is the protection that turquoise provides a rider on horseback. A turquoise talisman would help the rider avoid

injury in a fall, and maintain the horse's strength (Kunz, 1913). Anselmus de Boodt described personal experiences with this magical property; he experienced one fall and one overexertion, which each resulted in the turquoise he was wearing cracking into pieces, while preserving his body from injury (Kunz, 1913). From de Boodt's observations, turquoise jewelry was desired almost exclusively by men as adornment (Kunz, 1913).

In the 21<sup>st</sup> century, turquoise has retained added significance through its supposed metaphysical properties. Crystal healing shops describe the protection that turquoise provides, and its use in healing throat-related ailments. In Western culture, turquoise's position as the birthstone of December increases its popularity to the typical consumer. The concept of birthstones was first developed in reference to the twelve stones of the high-priest's breastplate (Kunz, 1913). However, the wearing of the suitable birthstone did not become a tradition until 18<sup>th</sup> century Poland (Kunz, 1913). Until the 20<sup>th</sup> century, turquoise was considered the birthstone of July in most lists. The switch of turquoise and ruby (July-December) in 1912-13 was a return to the original Polish ordering of the stones to standardize the list (Kunz, 1913). This standardization and the myths surrounding turquoise have contributed to the lasting value of turquoise as a gemstone across the globe.

### *3.1.2 North, Central, and South America*

Many regions in North, Central, and South America are located at high elevations with arid climates, allowing for the precipitation and accretion of turquoise. Consequently, turquoise has been an important historical and mythical gemstone of American cultures for thousands of years. In South America, pre-Incan artifacts dating to between 100 and 700 AD were discovered in the tombs of royalty (Lowry and Lowry, 2018). Mining areas in Peru, Chile, and Argentina are considered the major sources of turquoise for both pre-Incan cultures and the Incans. The

Spanish later recorded the turquoise inlays, beads, and mosaics of South American civilizations during their forced colonization of South America (Pogue, 1915). Relatively little South American turquoise is currently being marketed, but there is likely an abundance of old sites yet to be rediscovered and deposits that may have been lost through the preferential mining of copper and other metal resources.

The Mayan (Figure 11) and Aztec Mesoamerican civilizations held the gemstone they called *chalchihuitl* in high regard for ceremonial and protective purposes (Pogue, 1915). The term referred to green gemstones of special power, as documented by the Spanish. The mineralogical identity of the *chalchihuitl* is difficult to constrain and may have had different meanings in certain regions. Modern blue turquoise stones do not fit the description, and the Aztecs used the terms *xiuhitl* or *teoxiuitl* to refer to blue turquoise (Pogue, 1915). Emerald, nephrite, jadeite, and greener shades of turquoise are considered possible identities, although emerald is unlikely because the Spanish would have recognized it. Turquoise and *chalchihuitl* were both stones that were gifted to Spanish conquerors by Moctezuma II of the Aztecs (Kunz, 1892). Conquests between neighboring tribes resulted in the losers submitting turquoise and the green stones as required tribute to the victors. Turquoise in Central America originated from ancient mines in northern Mexico and present-day New Mexico (Lowry and Lowry, 2018). Mesoamerican trade routes distributed the precious material to the civilizations of the region (Carpenter, 2020). In recent years, the majority of mined Mesoamerican turquoise is imported quickly into the United States and sold as American turquoise, to increase its value and marketability.





Figure 11: Turquoise-inlaid Mayan mask, dating from 1400 - 1600 AD. (Photo courtesy of T. Paradise).

Much of the history of turquoise in North America has been deduced by the archaeological discoveries of ancient turquoise artifacts combined with the oral histories of existing Native American tribes. A map of southwestern turquoise sites is shown in Figure 12. At Pueblo Bonito in Chaco Canyon, NM, a tremendous amount of turquoise-inlaid artifacts that have been attributed to a multitude of origins (Hull et al., 2014) were found, indicating widespread trade between tribes further east and further west. Trade of turquoise between Native American groups extended into East Texas and south into Mesoamerica (Carpenter, 2020). These extensive networks cause difficulties in evaluating the earliest turquoise sources, which were previously often attributed to the Cerrillos Hills localities in New Mexico (Kunz, 1892). Before Spanish intrusion, turquoise would have been one of the valuable currencies enabling trade between multiple thriving ancient Native American cultures. Cabeza de Vaca described the presence of turquoise with several tribes in the 1530s as he journeyed across the Southwest (Pogue, 1915). As he neared the Pacific, he was gifted turquoise by a local tribe, who indicated that they had traded for it using parrot plumes (Pogue, 1915). The term *chalchihuitl* in North America is used by some tribes (Navajo and Zuni) to denote turquoise specifically, not the mineralogically ambiguous green stone of the Aztecs (Pogue, 1915). These tribes, along with the Hopi and the Pueblo, are traditionally considered the people bestowing highest cultural and mystical value to turquoise in North America, even in present times (Pogue, 1915). In the 19th century, American westward expansion led to increased popularity and exports of American turquoise, largely driven by the Tiffany and Company's catering of American turquoise to Europeans (Lowry and Lowry, 2018) as well as Fred Harvey's popularization of the sky-blue stone and Native American jewelry through his network of Harvey Houses across the American West (Fried, 2010). Although turquoise has been reported in several states outside of the

Southwest, these deposits are small in number, scale, and value. Reports of turquoise from Alabama, New Jersey, and Virginia indicate isolated mineralization related to localized copper sources. Specimens from Lynch Station, Virginia are unique in their crystallinity and occur in similar silica-dominant rock as the Mona Lisa Mine (Pogue, 1915).

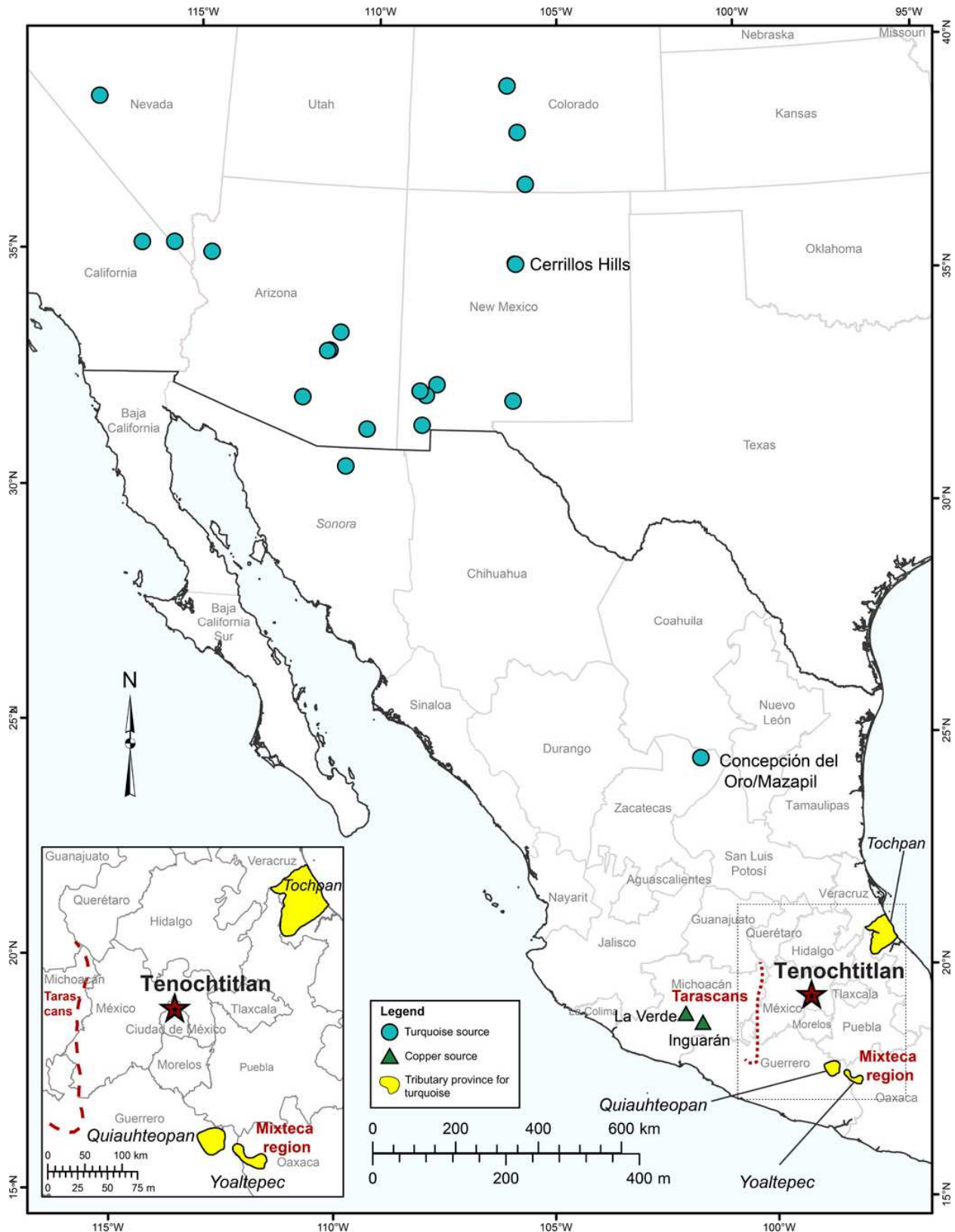


Figure 12: Turquoise and copper sources in the southwestern U.S.A. and Mexico. (From Thibodeau et al., 2018).

The abundance of turquoise artifacts at Native American burial sites demonstrates the importance of turquoise to spiritual ceremonies in those cultures. Carved turquoise pendants often resemble southwestern animals, purposefully designed to entrain guardian spirits into the stone (Kunz, 1913). Turquoise affixed to a bow or firearm was said to ensure the accuracy of shots taken by warriors or hunters (Kunz, 1913). While most Native American tribes historically ascribe to the belief that turquoise is a sign for good luck and happiness, legends about turquoise vary greatly with the diverse cultures. For example, a tale from a Santa Domingo Pueblo elder describes the formation of turquoise as the result of sweat from a great chief from within the Earth (Lowry and Lowry, 2018). Comparisons of turquoise with the color of the sky are common, as are the relationships between turquoise and certain deities. Turquoise amulets and powders have been used by medicine men to soothe ailments and gather strength (Lowry and Lowry, 2018). American “New Age” crystal shops advertise numerous powers of turquoise: the stone’s communication powers reduce the fear of public speaking and it opens all chakras, especially the 8<sup>th</sup> (heart) chakra, signifying universal love (Lowry and Lowry, 2018).

### ***3.2 Turquoise Mineralogy***

#### ***3.2.1 Turquoise Group***

In the field of archaeology, the term “cultural turquoise” is sometimes used by field researchers in order to quickly classify similarly colored blue-green geologic material (Weigand and Harbottle, 1993). This classification is solely based on the observation of apparent physical properties at the archaeological sites. However, for an intensive mineralogical and geological evaluation of the Mona Lisa Mine, it was vital to distinguish between the multiple species which may share many properties, and to define the word “turquoise” as precisely as mineralogically possible. Scanning electron microscopy (SEM), thermogravimetric analysis (TGA), Mössbauer

spectroscopy, x-ray diffraction (XRD), electron microprobe analysis (EMPA), Fourier transform infrared spectroscopy (FTIR), and Raman spectroscopy all represent various instruments of an ever-growing list of analytical techniques used to study the crystallography and chemistry of turquoise (Foord and Taggart, 1998; Frost et al., 2006; Abdu et al., 2011). Close investigation of turquoise and other phosphate minerals led to the establishment of the turquoise group; a set of turquoise and 5 similar minerals with minor chemical differences (Foord and Taggart, 1998).

Turquoise, planerite, chalcociderite, faustite, aheylite, and an unnamed iron-bearing endmember comprise the turquoise group. These mineral species are isostructural, with limited differences in unit cell dimensions. The general formula for turquoise group minerals is commonly expressed as  $A_{0-1}B_6(PO_4)_4(OH)_8 \cdot 4H_2O$  (Abdu et al., 2011). The A chemical site is occupied by divalent cations, typically Cu and Fe, while the B site houses the trivalent cations of Al or Fe. The range in metal compositions at the A and B sites is responsible for variation in color in turquoise group minerals (Abdu et al., 2011). All members of the turquoise group are in the triclinic crystal system, representing the space group  $P\bar{1}$ , with the only symmetrical element being a point of inversion. Focusing on the crystallography of turquoise group minerals requires additional nomenclature to describe the structural relationships between the chemical components. Therefore, the turquoise group formula that better represents the crystal structure of the unit cell is  $X(M1_2M2_2M3_2)_{\Sigma=6}(PO_4)_4(OH)_8 \cdot 4H_2O$ . The structural formula differentiates the positions of the four octahedrally coordinated cation sites. The X, M1, M2, and M3 sites are coordinated by oxygen and hydroxyl anions. The tetrahedral anionic phosphate groups, characteristic of all phosphate minerals, share corners with the M1 and M2 sites, extending in the crystallographic *b* direction (Abdu et al., 2011). The X octahedra shares an edge with the M1 and M2, while shared corners between the tetrahedral phosphate and the M3 site extends the motif in

the *a* and *c* directions. An illustration of this structure is shown in Figure 13, with the phosphate groups abbreviated as T1 and T2. The structure is additionally strengthened by hydrogen bonds between (OH) groups (Abdu et al., 2011). Resulting from this structure, the X site and the M3 site's differences in spatial arrangement from the M1 and M2 sites allow certain elements to preferentially substitute in particular locations; the X site accepts divalent cations with intermediate ionic radii, as the M sites accept trivalent cations with smaller radii, with M3 preferring more frequent substitutions (Abdu et al., 2011).

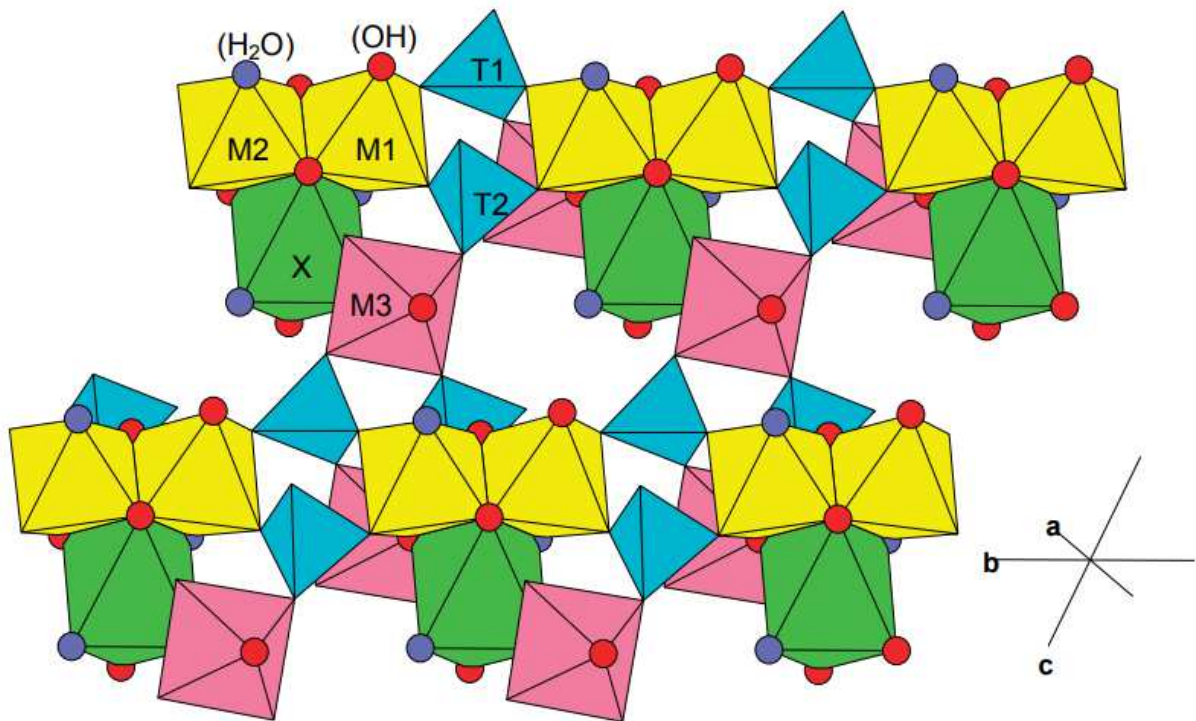
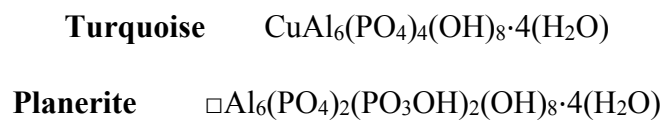


Figure 13: The triclinic crystallographic structure of turquoise is illustrated in this diagram. Site nomenclature corresponds with description in the preceding section. (From Abdu et al., 2011).

The six mineral members of the turquoise group and their respective chemical formulas are as follows:



**Chalcosiderite**       $\text{CuFe}^{3+}_6(\text{PO}_4)_4(\text{OH})_8 \cdot 4(\text{H}_2\text{O})$

**Aheylite**       $\text{Fe}^{2+}\text{Al}_6(\text{PO}_4)_4(\text{OH})_8 \cdot 4(\text{H}_2\text{O})$

**Faustite**       $\text{ZnAl}_6(\text{PO}_4)_4(\text{OH})_8 \cdot 4(\text{H}_2\text{O})$

**Unnamed (UM1981-32-PO:FeH)**       $\text{Fe}^{2+}\text{Fe}^{3+}_6(\text{PO}_4)_4(\text{OH})_8 \cdot 4(\text{H}_2\text{O})$

The iron analogue member of the group was accepted as a mineral, but not with the proposed name (Foord and Taggart, 1998). The possibility of a  $\text{Ca}^{2+}$ -bearing member is deemed unlikely (Foord and Taggart, 1998), despite some reports of the mineral (under the name coeruleoactite). The turquoise group mineral species represent endmember compositions, with intermediate compositions from partial substitution overwhelmingly common. The solid-solution series between turquoise and planerite, and turquoise and chalcosiderite will be explored in-depth in the following sections.

### *3.2.2 Turquoise-planerite solid-solution*

The distinction between turquoise and planerite has unique importance in Arkansas, because planerite has been identified in Arkansas phosphate mineral assemblages with wavellite and variscite for decades. Planerite is distinguished from turquoise by the vacancy in the X site of the crystal structure, instead of an octahedrally coordinated  $\text{Cu}^{2+}$  cation. This vacancy is accommodated in the chemical formula through the protonation of two phosphate groups into  $(\text{PO}_3\text{OH})$  groups (Foord and Taggart, 1998). Therefore, planerite will form in secondary environments similar to turquoise, but from solutions deficient in copper. Such environments are common in the Ouachita Mountains of Arkansas, with abundant phosphate and aluminum a result of the weathering of deep-water sedimentary strata. Absence of concentrated and widespread copper sources in the area led many to categorically dismiss all light-blue phosphates as planerite, not turquoise (Laney, 2020). More detailed analysis has shown the complexities of



the turquoise-planerite solid solution relationship. Rarely is the X site fully occupied or fully vacant; instead, intermediate copper contents are exceedingly common. Stoichiometric calculations indicate that ideal turquoise would have 9.78 wt.% copper, while planerite would have none (Hotujec, 2011). A consistent determination for what weight percent is required to define a mineral as turquoise does not exist, but typically intermediate compositions are classified as turquoise because they do contain some copper and it is a more recognized name. There is an additional positive correlation between X site vacancy and water content (Foord and Taggart, 1998). Ideal planerite maintains a weight percent H<sub>2</sub>O roughly three percent higher than ideal turquoise (fully occupied X site), as illustrated in Figure 14. Chemical analysis is required to discern the difference between planerite and turquoise, especially regarding reports of turquoise in the south-eastern United States.

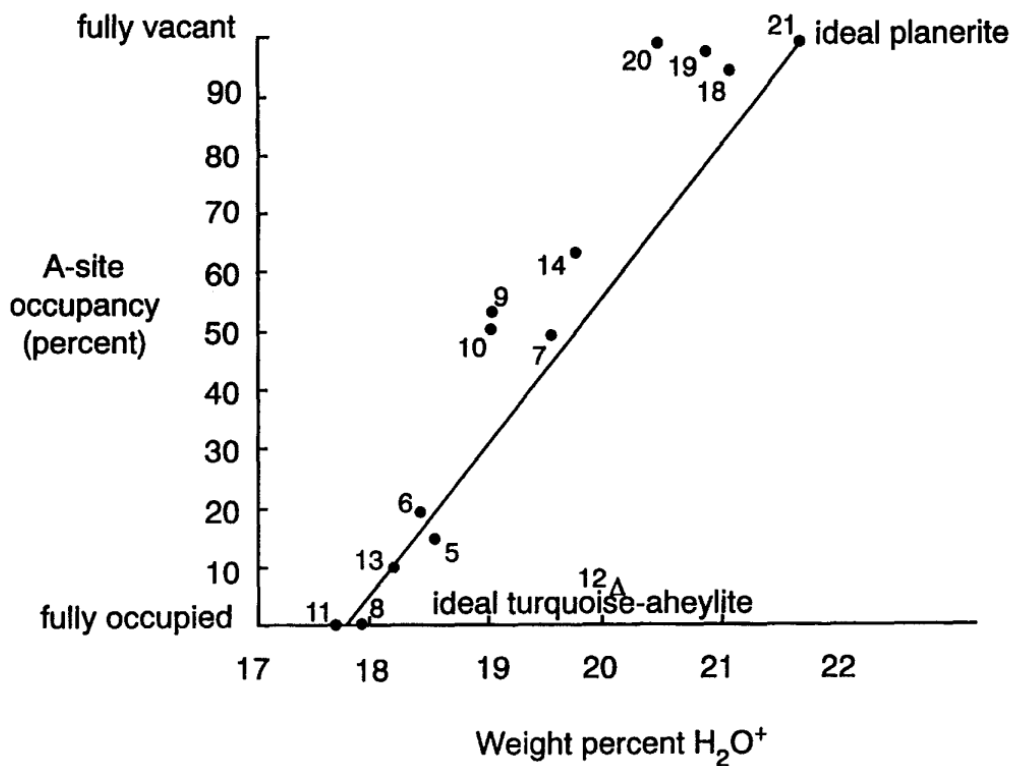


Figure 14: The solid-solution relationship between planerite and turquoise, defined by water content and vacancy in the X crystallographic site (here named the A-site). Numbered datapoints represent analyses by Foord and Taggart (1998) and ideal endmembers.

### 3.2.3 Turquoise-chalcosiderite solid-solution

Turquoise and chalcosiderite differ in the trivalent cations that fill the M1, M2, and M3 sites. Turquoise has  $\text{Al}^{3+}$  filling those sites, while chalcosiderite's M sites are occupied by ferric iron ( $\text{Fe}^{3+}$ ). Single-crystal structure refinement (SREF) and Mössbauer spectroscopy have further demonstrated that 36% of the  $\text{Fe}^{3+}$  is found at the M3 site, more than the 1/3 that would be expected (Giuseppetti et al., 1989; Abdu et al., 2011). The M3 site's lesser degree of covalency and increased octahedral volume to accept the larger radii cation are reasons potentially responsible for this preference (Abdu et al., 2011). However, differences between individual source locations could suggest that the preferential M3 substitution is dependent upon the conditions of mineralization. Ideal wt.% concentrations in chalcosiderite are 48.6 wt.%  $\text{Fe}^{3+}$  and 8.06 wt.% Cu (Hotujec, 2011). The mineral variety rashleighite refers to an intermediate member along the turquoise-chalcosiderite solid-solution series.

Crystallographic discrimination between turquoise and chalcosiderite is also possible, because the presence of ferric iron increases the unit cell volume to 502 Å from 460 Å for Al-bearing turquoise group minerals (Foord and Taggart, 1998). The expansion of the unit cell is primarily in the *b* crystallographic direction. Studies suggest that the presence of iron also greatly impacts the color of the material, as SEM analysis found that darker green colors were associated with higher iron concentrations, and purer blue associated with higher copper concentrations (Foord and Taggart, 1998). The presence of trace amounts of vanadium, chromium, or other chromophores could also be responsible for color changes. Confirmation of the importance of the  $\text{Cu}^{2+}/\text{Fe}^{3+}$  ratio in color determination was attained through the use of Raman spectroscopy, though the effect of trace elements and local crystallographic symmetry were also proven to be of consequence (Dumanska-Slowik et al., 2019).

Throughout history, reports of turquoise changing its color with exposure and age have been prevalent (Kunz, 1913). These observations do have scientific foundations, because the water content of turquoise group minerals influences the richness of color. Increases in temperature do slowly dehydrate the minerals, causing color to fade and tend towards greyish-green (Dumanska-Slowik et al., 2019). Although the other turquoise group minerals (aheylite, faustite, unnamed iron analogue) likely represent further solid-solution endmembers with turquoise, their rarity has obstructed detailed analysis. The relationships between turquoise, chalcocite, and planerite will be further discussed in specific reference to mined material from the Mona Lisa Mine.

#### *3.2.4 Mineralization*

The occurrence of turquoise is typically defined as secondary, supergene mineralization in hydrothermally altered igneous rocks, with close association to copper porphyry deposits (Nesse, 2017). The majority of turquoise deposits in the American Southwest fit this description, although many discoveries have proven that the host rock for a deposit need not be volcanic in origin. In fact, many deposits have been found in sedimentary and metamorphic environments in the United States. A range of host rock compositions is inherent to secondary, supergene mineralization. “Secondary” refers to the deposit’s derivation from the weathering of some primary copper-bearing minerals (often chalcopyrite). Whereas these primary deposits formed from high-temperature fluids, the secondary minerals form at much lower temperatures from the weathered elemental components in solution. There are lower temperatures because of the supergene environment, denoting mineralization near the Earth’s surface, as opposed to hypogene mineralization at great depths beneath the surface. Meteoric waters containing the required elements Cu, Al, and P percolate into the shallow subsurface through fractures and

porous strata, and turquoise precipitates (King, 2002). Turquoise is generally mined within 30 meters of the surface, and is usually fine-grained or massive, filling pre-existing fractures and voids. However, it has also been found as natural encrustations, disseminated grains, stalactitic forms, and reniform habits (Nesse, 2017).

The geochemistry of turquoise-precipitating solutions can vary and is often difficult to interpret. Mineral assemblages are vital in constraining the properties of these solutions. Interaction between water, oxygen, and the sulfide chalcopyrite and pyrite produces divalent Cu cations, iron oxide compounds, and sulfuric acid (Anderson, 1982). The  $\text{Cu}^{2+}$  is mobilized under oxidizing conditions with  $\text{pH} < 3.5$ . The acidic solutions leach phosphate from apatite, xenotime, or deep-water sedimentary sequences (Crook and Lueth, 2014), and aluminum from local country rock.

Comprehensive analysis of phosphate mineral assemblages in the Nuba Mountains of Sudan provided clarity on the stages of phosphate mineralization. The alteration of apatite corresponds to an increase in the aluminum oxide to calcium oxide ratio of the Nuba Mountains system (Dill et al., 1991). This shows that the system was continually changing from Ca-phosphate precipitation to Ca-Al-phosphate precipitation. With this understanding, it is possible to sort the mineral assemblages into stages representative of the time of mineralization. Stage 1 consists of an apatite-quartz-illite assemblage, and stage 2 is marked by the first appearance of a crandallite-goethite-kaolinite assemblage. The addition of wavellite and variscite and the disappearance of goethite characterizes stage 3, while stage 4 replaces the wavellite and variscite with turquoise as the phosphates continue to increase in Al content (Dill et al., 1991).

In order to continually increase the aluminum to calcium oxide ratio at the Nuba Mountains site, increasingly acidic solutions were required. When constrained to the activity

conditions of the study area, the discovered stages of mineralization can be observed. The pH of the mineral solution must have changed from about 8 during illite mineralization to less than 4 to accommodate crandallite, kaolinite, and turquoise (Dill et al., 1991). Although this represents a case study, not an overarching statement on the mineralization of turquoise in any setting, the study illustrates the importance of determining mineral assemblages in tracing the geochemical history of a deposit.

Overall, the mineralization of turquoise depends on the geochemical conditions of the mineralizing fluid, the pathways for the fluid to travel, and the presence of copper, aluminum, and phosphate in the fluid. By describing mineral assemblages, it is possible to reconstruct the petrogenesis of a turquoise deposit. As a cryptocrystalline phosphate mineral, a turquoise deposit will alter readily when weathered. Therefore, studying the petrogenesis of turquoise requires the use of methodologies which are not greatly affected by weathering processes. The carefully chosen mineralogical techniques in this study provide insights into the composition and geologic source of Mona Lisa turquoise, while giving an extensive geologic description of the Mona Lisa Mine itself.

## Chapter 4: Methodology

### *4.1 Mapping*

#### *4.1.1 Isohypsometry*

The first step towards understanding the Mona Lisa Mine was to map the exposed features at the surface. Currently, the mine consists of one trench of ~100 meter length, and depths not exceeding 20 meters. Because the area is densely forested, aerial photography and existing geologic and topographic maps were unable to provide the necessary precision for mapping the mine. Therefore, we had to carefully preserve the spatial relationships between surface features while mapping in the field. On March 26 and 27<sup>th</sup>, 2021, we constructed an isohypsometric map using a false datum on the southwestern side of the mine trench. An isohypsometric map measures the relative elevation changes of an area, with reference to a datum instead of existing topographic data. This map, along with images of each side of the Mona Lisa Mine, expresses the extent of the mine and serves as a reference frame for identifying the mineralized area within the trench. The mapping was conducted by Dr. T. R. Paradise and the author using tape measures, Abney and laser levels, and a stadia rod to determine changes in distance and elevation. As the Mona Lisa Mine remains active under the ownership of Avant Mining as of 2022, the site can be expected to change as miners work to follow the mineralization paths of turquoise.

#### *4.1.2 Seam diagrams*

The most productive area of the trench is in the deepest part of the mine, where the turquoise seams were found in white-tan weathered novaculite. Seam diagrams represent an important mining tool for indicating areas of expansion, especially with a surface mine. They have been used extensively for mapping gold mineralization in vertical sections (Derry, 1939).

Patterns and orientations of ore mineralization can be tracked into the subsurface and future yield can be estimated with evaluation of the surrounding geologic environment. Visits to the mine site have occurred during inactive mining seasons, and only small amounts of turquoise have been exposed. The orientations of turquoise-filled fractures were measured using Brunton™ compasses and the StereonetMobile app (Allmendinger et al., 2017). This limited field data was supplemented by turquoise seams shown in Avant Mining social media videos. These exposed seams were digitized in Adobe Creative Suite (CS) to show how more mineralized areas of the trench appeared.

#### *4.1.3 Structural Orientations*

A solution containing the chemical components Cu, Al, and P mineralizes turquoise in pre-existing fractures and voids in a host rock to form a deposit. Therefore, the existing structural features in the host novaculite represent the most efficient passages for the transport and mineralization of Cu-rich fluids. The Arkansas Novaculite is a pre-orogenic formation that experienced significant deformation as the Ouachita orogeny began. Brecciation, thrust faulting, and folding are all identified from novaculite outcrops in the Ouachita Mountains. To quantifiably demonstrate the possible extent of further turquoise mineralization at the Mona Lisa Mine, we measured the orientations of the bedding and fractures at various points across Little Porter Mountain. Dr. Gregory Dumond and the author took >200 strike and dip measurements of bedding and fracture planes within the Mona Lisa Mine trench and of the surrounding Stanley Shale, Arkansas Novaculite, and Missouri Mountain Shale formations. These planar orientations were recorded using the right-hand rule, with planes dipping towards the right of the strike azimuth. Measurements made with Brunton™ compasses and with the StereonetMobile app were directly entered into Microsoft Excel. The data were plotted on stereonet using the

Stereonet v. 11 software (Allmendinger et al., 2012; Cardozo and Allmendinger, 2013).

Stereonet diagrams are displayed with reference to previous work completed on structural orientations found in the area (Keng, 2011), that used comparable methodology over a broader scale.

## ***4.2 Mineralogy***

### *4.2.1 Physical properties*

The general characteristics of the mineral turquoise are widely known, due to its common appearance in decoration and jewelry. The value of turquoise is directly related to its color, texture, and matrix color and pattern. Although the mineral turquoise is most commonly associated with the color turquoise, the mineral can be many different hues and shades, ranging from a light blue-green to a deep sky blue. The varying amounts of iron and copper in the mineral are most often the cause of coloration (Foord and Taggart, 1998). Turquoise has a hardness of 5-6, but this varies with surface exposure and/or addition of silica. Turquoise is in the triclinic crystal system and typically forms as cryptocrystalline masses in veins. Even within the Mona Lisa Mine trench, turquoise mineralogy varied. Chalky, weathered turquoise was common throughout the trench. This material must be stabilized (epoxy injection) before it can be rounded into cabochons for jewelry. However, in the deepest part of the trench, turquoise is found with a hardness of >6 while maintaining desirable color. Hardnesses of a variety of Mona Lisa turquoise specimens have been determined using hardness picks with values between 4 and 7 on the Mohs Hardness Scale. These same specimens were color matched using a Pantone™ Bridge set to identify the precise CMYK values of Mona Lisa material. Using this qualitative matching method allowed the color of turquoise to be accurately compared with many different mines with standardization. Previous analysis of the appearance identified similarities between



Mona Lisa turquoise and turquoise from the famous Sleeping Beauty site in Arizona (Laney, 2020). Using these techniques, we have expanded upon the physical description of Mona Lisa turquoise.

#### *4.2.2 X-ray diffraction*

To analyze the crystal structure and chemical composition of the Mona Lisa turquoise, samples were cut into small slabs and analyzed by Dr. Andrian V. Kuchuk from the University of Arkansas Nanocenter for x-ray diffraction patterns. The 10 samples represented the compositional variability inherent in the Mona Lisa Mine and the material was donated by Avant Mining for use in this research. Pictures and descriptions of these samples are found in Appendix B. The samples were labelled with the preface “TQ” followed by sample letter and number, if needed. Sample slabs (not powdered samples) were able to be analyzed directly due to the cryptocrystalline nature of the turquoise and matrix material. X-ray diffraction is a quick and useful tool to identify minerals based on their crystal structures. This technique has been used by many turquoise studies, because of what the crystal structure can tell us about chemical composition and the unit cell (Foord and Taggart, 1998). For analysis, the samples were scanned between the  $5.04^\circ$  to  $50.96^\circ$   $2\theta$  angles with a step sizes of  $0.015^\circ$  every 0.6 seconds. The radiation was sourced from a Cu anode with a wavelength of  $1.5406 \text{ \AA}$ . The PANalytical X’Pert HighScore™ mineral software was used at the University of Arkansas Nanocenter to process the data and identify the mineral phases.

Results from this software indicated that the highly altered nature of the matrix material and presence of clay-sized particles made the sample phases difficult to identify. Often, the identifiable peaks do not correspond to one mineral, rather a suite of possible mineral identities. Because of the complexity of many of the samples, the diffraction patterns collected from the

Nanocenter were additionally processed using the QUALX2.0™ diffraction software (Altomare et al., 2008; Altomare et al., 2015). Plotted spectra were compared with the collection of crystal structures within the POW\_COD publicly available database. Peaks were matched with the dominant crystal phases after background correction based on figure of merit of the database entries.

#### *4.2.3 Raman spectroscopy*

Raman spectroscopy is a non-destructive technique that causes vibrations within molecules and measures those vibrations. The strength and nature of bonds and the molecules themselves within a mineral give a unique spectrum when analyzed. Raman spectroscopy is less commonly used than x-ray diffraction for turquoise samples but has high value in gem research because it preserves the sample. Raman analysis was conducted by the author at the Baylor University Igneous Petrology Lab using a Thermo Scientific DXR™ Raman Microscope fitted with a 10X objective, 532 nm laser, 25 µm pinhole, and 1800 lines/mm grating. Analyses were conducted at room temperature (~25° C) with a spot size of 2.1 µm. Although fluorescence correction was applied, laser power was also adjusted from 8.0 to 1.0 mW to account for peak saturation and to limit disturbances, as documented in other Raman studies of turquoise (Dumanska-Slowik et al., 2020).

The Raman signature of turquoise has been mapped by Dumanska-Slowik et al. (2020), Cejka et al. (2015), and Frost et al. (2006). From their work, each vibrational mode can be labelled and attributed to types of bonding within the turquoise sample. For matrix and mineral identification, the RRUFF library was queried for reference spectra. Sample spectra were automatically baseline corrected and smoothed to reflect the lack of a perfect polish on the gem surfaces. The analyzed samples were the identical slabs used for x-ray diffraction analysis. For

each sample, at least two different spot locations were analyzed to identify the phosphate material and the matrix composition of the samples.

### **4.3 Geochemistry**

#### *4.3.1 Elemental concentrations*

Select major and trace element concentrations were analyzed for 14 Mona Lisa samples, with one replicate analysis carried out on one sample (MLI 02-R). Sample preparation began with the processing of chunks of rough turquoise-bearing material from the Mona Lisa Mine provided by Avant Mining. Eight of these whole rock samples, denoted by a “TQ” label, were also analyzed for x-ray diffraction and Raman spectroscopy, although the slabs themselves were not used to preserve those specimens. The remainder six samples and the replicate were collected from new Mona Lisa material and are denoted by an “MLI” label. Samples were first described and photographed, then wrapped in aluminum foil and paper towels. A sledgehammer was used to crush the samples and the freshest, unexposed chips of turquoise material were removed and placed into Ziploc bags. The MLI M sample represented the white chalky matrix material common at the mine, not turquoise. The Ziploc samples were moved into the University of Arkansas Radiogenic Isotope Class 100 Clean Laboratory. The fresh chips were rinsed with 3.5 N HNO<sub>3</sub> and triple distilled water and allowed to dry. Around 250 mg of each sample (when possible) was removed, and the exact weights were recorded (Appendix C). Weighed samples were digested in 2 mL of double distilled HCl and 2 mL of double distilled HNO<sub>3</sub>. Samples that did not fully digest because of small amounts of silicate matter were centrifuged at 3000 rpm for three minutes and the undigested material was discarded. Samples TQ-A and MLI M had significant amounts of silica and were therefore digested in 2 mL HF and 2mL 7N HNO<sub>3</sub>. Following this step, the samples were dried down on a hot plate. The digestion process was

repeated with only 2 mL double distilled HNO<sub>3</sub>. 2 mL of 2% HNO<sub>3</sub> were added to the redigested and dried samples. Different dilutions are required to analyze for minor and major elements in the material. For measuring trace elements, including Pb and Sr concentrations, 0.1 mL of the sample solution and 2.9 mL of pure 2% HNO<sub>3</sub> were added into acid-cleaned 5 mL centrifuge tubes for analysis. Multiple dilutions were required to collect major element (Cu, Fe, Zn) concentrations. First, 2  $\mu$ L of each sample was diluted with 9.998 mL of 2% HNO<sub>3</sub>. 100  $\mu$ L of this dilution was then diluted with an additional 4.9 mL 2% HNO<sub>3</sub>. The dilution calculations were based on the elemental concentrations of Mona Lisa turquoise determined by Laney (2020) and the assumption that the current samples would be in a comparable compositional range.

The samples were analyzed by a Thermo Scientific™ iCAP Q quadrupole mass spectrometer at the University of Arkansas on September 27, 2021. Raw results were attained in counts per second and ppb for each element. To determine the actual concentrations of the material, the ppb values were used as the final concentrations in dilution equation calculations, while the sample weights (~250 mg) were the initial masses. It was then possible to solve for the initial concentration of the material based on the dilution factors applied to the minor element and major element samples. The results are presented in Table 2 and the detailed results in Appendix D.

#### 4.3.2 *Lead and strontium isotope ratios*

Strontium isotope ratios capture variations in age, source, and chemistry of igneous deposits (Thibodeau et al., 2015). Although the Mona Lisa Mine is hosted by sedimentary strata, the Sr isotope ratios will indicate the composition of the rock that might have sourced the copper. Lead isotope ratios in ore minerals can give information about the source of metals, the timing of ore deposition, and the regional isotopic variations on a crustal scale (Tosdal et al., 1999). The

behavior of lead, thorium, and uranium in solution is dependent upon the geologic environment and the chemistry of the solution. U/Pb and Th/U ratios record the geochemical interactions that a sample has undergone, which can be correlated with the geologic history of the sample (Tosdal et al., 1999). Lead and Sr isotopes have been used to determine provenance of turquoise archaeological artifacts (Thibodeau et al., 2015), and similar techniques have been applied to the Mona Lisa samples to gain insight into the geologic setting, the source of the metal ions, and how it relates to the sources of turquoise in the American Southwest.

The fractions of the Mona Lisa sample solutions that were not subjected to the dilution treatment for concentration analysis were processed using column chemistry to separate the Pb and Sr for isotope analysis. The methodology for column chemistry is detailed in Pin et al. (2014) and involves the addition of extraction chromatography materials Sr Spec and TRU Spec resins, column pre-cleaning, pre-conditioning, sample wash, and Sr and Pb collection. The Sr Spec and TRU Spec resins separate Sr and Pb from the samples, respectively. The Ln Spec procedure was not conducted due to the yet unknown value of neodymium isotopes for turquoise research. When columns are separated, this results in a collected Sr and Pb fraction for each sample. The post-column concentration samples were processed at the same time as the pre-column concentration samples in order to provide an accurate dilution factor for the samples to be analyzed for isotopic ratios. The Pb and Sr isotope analyses were carried out on a Nu Plasma MC-ICP-MS by Dr. John R. Samuelsen at the University of Arkansas on February 17th and 22nd of 2022, respectively. All samples were diluted in 2% HNO<sub>3</sub> prior to analysis, and a thallium (Tl) spike (internal standard) was added to each Pb sample to correct for mass-dependent fractionation in mixed Pb-Tl solutions (Kamenov et al., 2004). The Pb isotope data denote the average of 60 ratios per sample, corrected to the NBS 981 Pb standard. The Sr isotope results are

presented in Table 4, Pb isotope results in Table 5, and the detailed combined results in Appendix E.

## Chapter 5: Results

### *5.1 Maps and Stereonets*

The isohypse map constructed of the Mona Lisa trench in March of 2021 is shown in Figure 15. A shaded depth model is included as an inset, showing the increasing depth of the trench towards the geographic center point. The false datum on the southwestern rim of the trench used to build the isohypses is illustrated as well. Although only very small in situ turquoise seams were exposed during the study, mineralized areas were uncovered in a 2019 Avant Mining social media video. From this video, the patterns of two seams were digitized (Figure 16). The pattern shows preferential mineralization along vertical fractures, with some horizontal connectivity. These seams occur in highly altered zones, with a light colored and chalky host rock. The manganese oxide dark-colored zones occur with variable correlation to the turquoise seams.

Comprehensive mapping of structural orientations was completed with the aid of Dr. Gregory Dumond at the Mona Lisa Mine on November 11 and 12, 2021. 39 strike and dip measurements of bedding planes were made using Brunton™ compasses and the StereonetMobile app. Stanley Shale orientations were measured along Polk County Road 402 (FS 176) at the base of Little Porter Mountain, next to the mine road entrance. Novaculite bedding orientations were taken along the mine road, at exposed outcrops on the ridge of Little Porter Mountain, and within the Mona Lisa trench. The combined bedding measurements are illustrated in Figure 17 (displayed as poles), showing steeply dipping beds (49-89°), with 8 measurements dipping towards the north and 31 measurements dipping to the south. The strike of the bedding runs consistently in an E-W direction, with the 31 measurements striking close to directly east and the other bedding planes striking west. The Mona Lisa trench lies along strike

of the local bedding. Joint surface orientations (211 measurements) were collected using the same methods and are plotted as poles on a stereonet in Figure 18. The orientations can be split into four populations: steeply westward-dipping, steeply eastward-dipping, shallowly northward-dipping, and steeply northward-dipping surfaces. Apart from the 8 orientations that are steeply northward-dipping, the rest of the surfaces are oriented orthogonally to the bedding. The sets of steeply E-W dipping surfaces and shallowly northward-dipping surfaces are also perpendicular to each other.

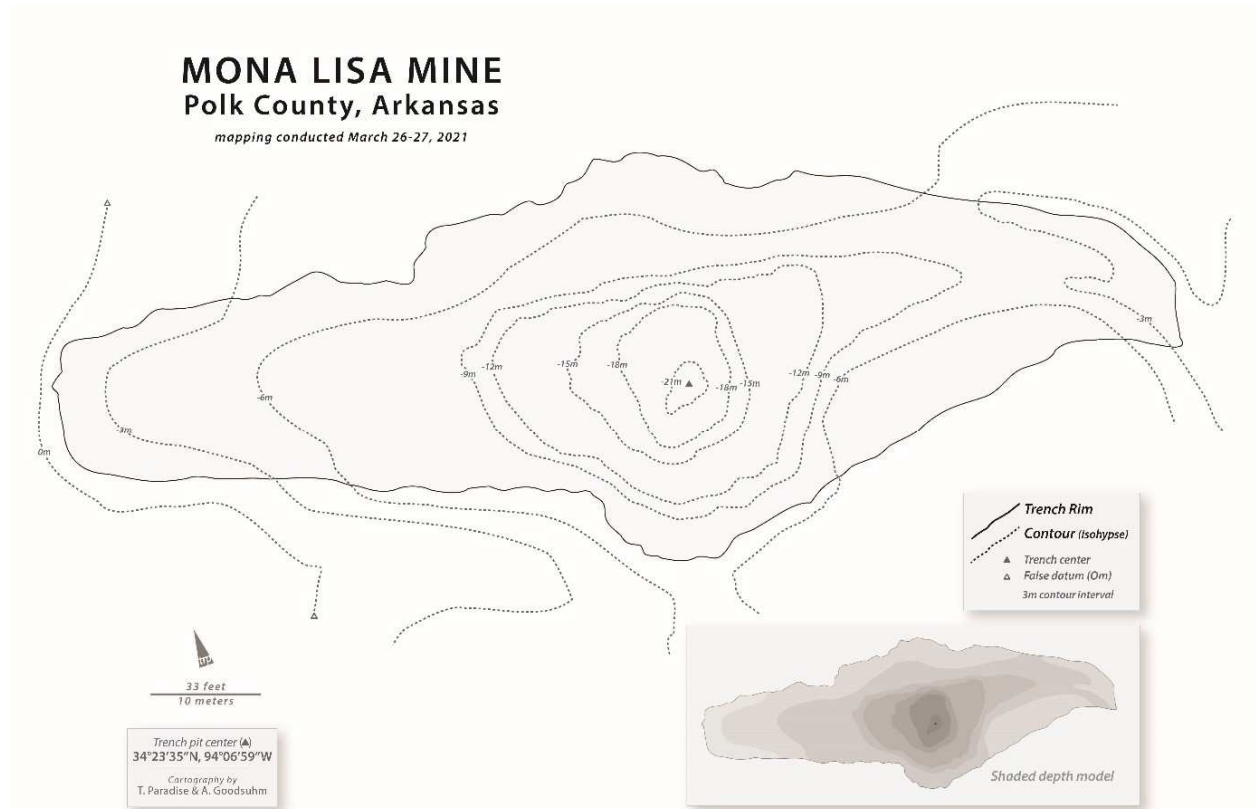


Figure 15: Field mapping conducted on March 26-27, 2021. Isohypse map constructed by T. Paradise and A. Goodsuhm.



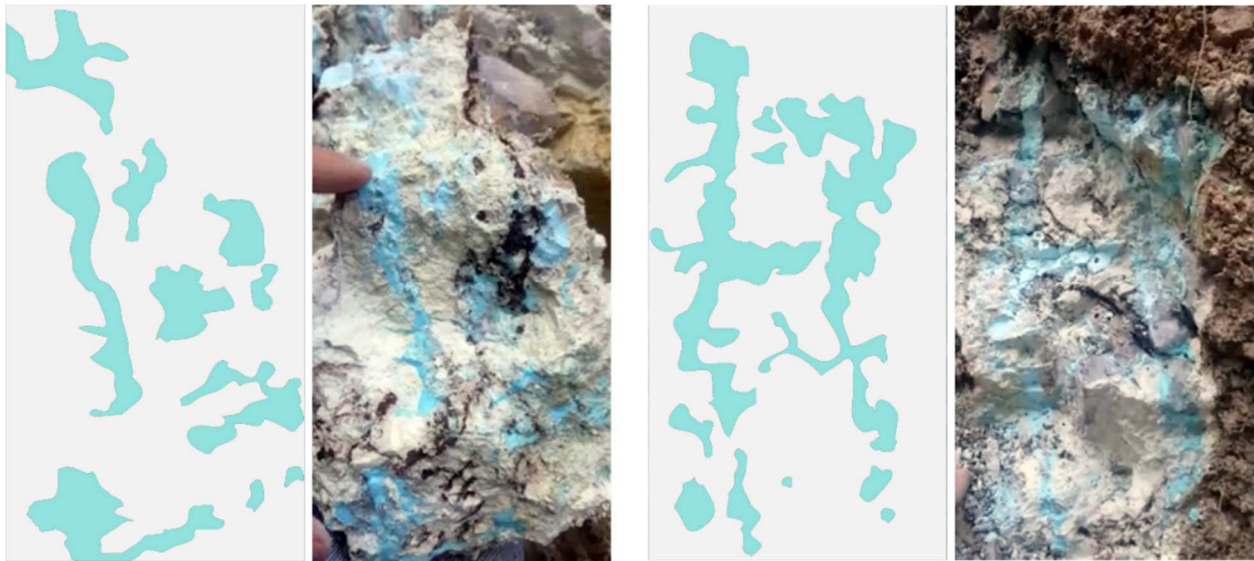


Figure 16: Seam diagrams of Mona Lisa turquoise precipitating within the white chalky matrix. Pictures taken as screen capture from an Avant Mining LLC video from September 23, 2019. The video is taken from the deepest part of the trench looking at the sides. Digitization by T. Paradise.

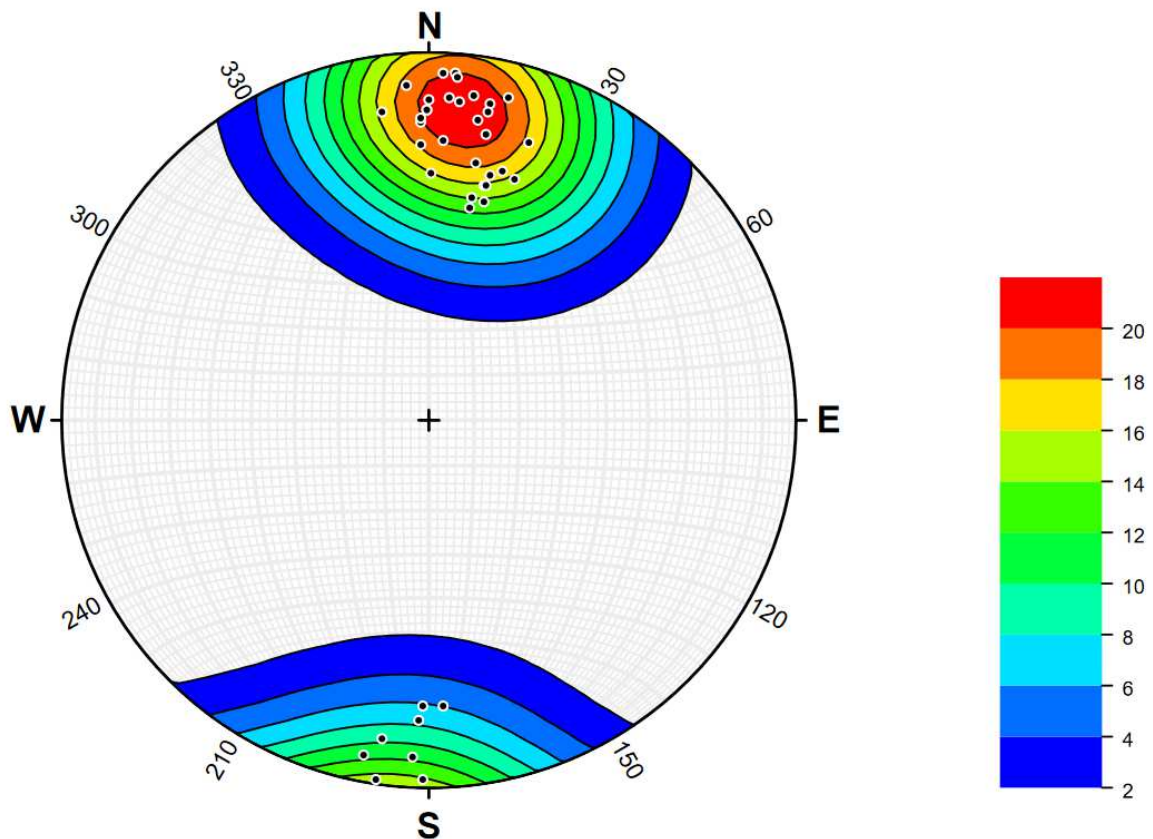


Figure 17: Contoured stereonet of 39 bedding plane orientations on Little Porter Mountain constructed on Stereonet v. 11 software. Contours represent the number of datapoints, displayed as poles. Measurements taken on the Stanley Shale and Arkansas Novaculite formations, both on the south side of the mountain and within the Mona Lisa trench.

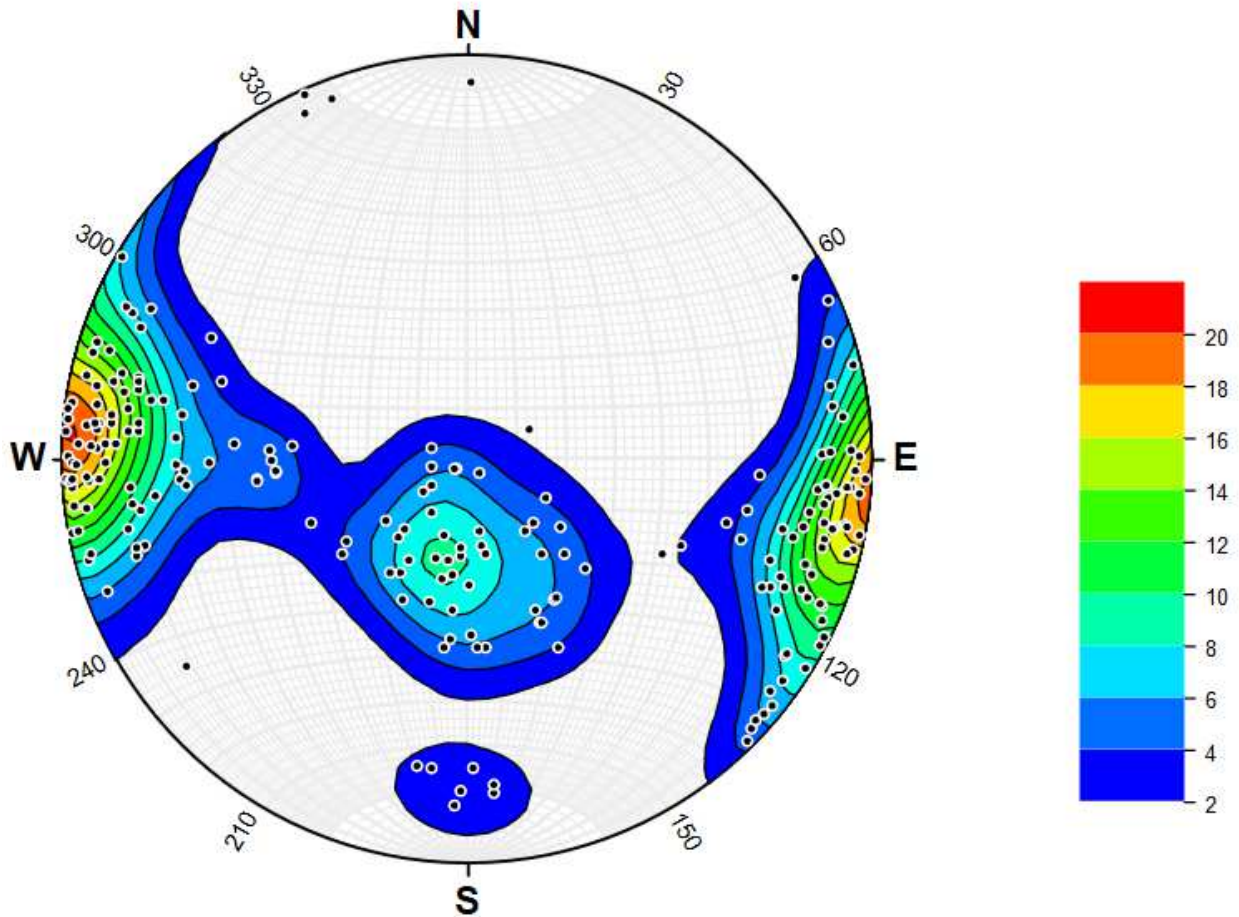


Figure 18: Contoured stereonet of 211 measured joint surface orientations within the Mona Lisa trench. Mineralization along fracture surfaces is not considered. Contours represent the number of datapoints, displayed as poles.

### 5.2 Color and Hardness

The color range of 17 Mona Lisa turquoise samples is expressed in CMYK values in Table 1. An example comparison between Pantone™ color ranges and Mona Lisa turquoise is shown in Figure 19. The cyan component ranges from 30 to 100, while only sample “MLI 02 Light” has any magenta added. A narrow range of yellow (10-30) and black (0-15) color components also characterized the material. The use of CMYK values was selected because of its advantage over the RGB scale on printed mediums that can be used to compare with turquoise specimens. The sample labelled “Polished Slab” was donated to the study for purely non-

destructive analysis and is therefore not present in analytical results. A photo of this sample and the suite of analyzed samples are included in the Appendix B. Hardness values of the material were determined using hardness picks that were calibrated to every 0.5 change on Mohs Hardness Scale. Samples with hardness below 4 were then tested by a fingernail scratch. The hardness of turquoise is generally considered 5-6.

Table 1: CMYK color values and hardness of the Mona Lisa turquoise samples. Color values determined through matching with a Pantone bridge set. Hardness determined by hardness picks calibrated to each 0.5 step on Mohs Hardness Scale.

<b>Sample ID</b>	<b>Cyan (C)</b>	<b>Magenta (M)</b>	<b>Yellow (Y)</b>	<b>Key Black (K)</b>	<b>Hardness</b>
<b>TQ-A1</b>	80	0	25	0	5.5-6.0
<b>TQ-A2</b>	65	0	20	0	4.5-5.0
<b>TQ-B1</b>	65	0	20	5	6.0
<b>TQ-B2</b>	95	0	25	0	6.0
<b>TQ-C1</b>	75	0	15	0	5.0-6.0
<b>TQ-C2</b>	75	0	15	0	4.5-5.0
<b>TQ-D1</b>	65	0	20	5	6.0
<b>TQ-F1</b>	75	0	25	0	6.0
<b>TQ-I1</b>	65	0	25	0	<2.5
<b>TQ-J1</b>	50	0	25	0	6.0
<b>Polished Slab</b>	100	0	25	0	6.0
<b>MLI 01</b>	70	0	30	0	4.5-5.0
<b>MLI 02 Dark</b>	70	0	30	0	<2.5
<b>MLI 02 Light</b>	30	5	15	0	<2.5
<b>MLI 03</b>	50	0	10	15	6.0
<b>MLI 04</b>	70	0	30	0	5.5-6.0
<b>MLI 05</b>	50	0	10	0	<2.5

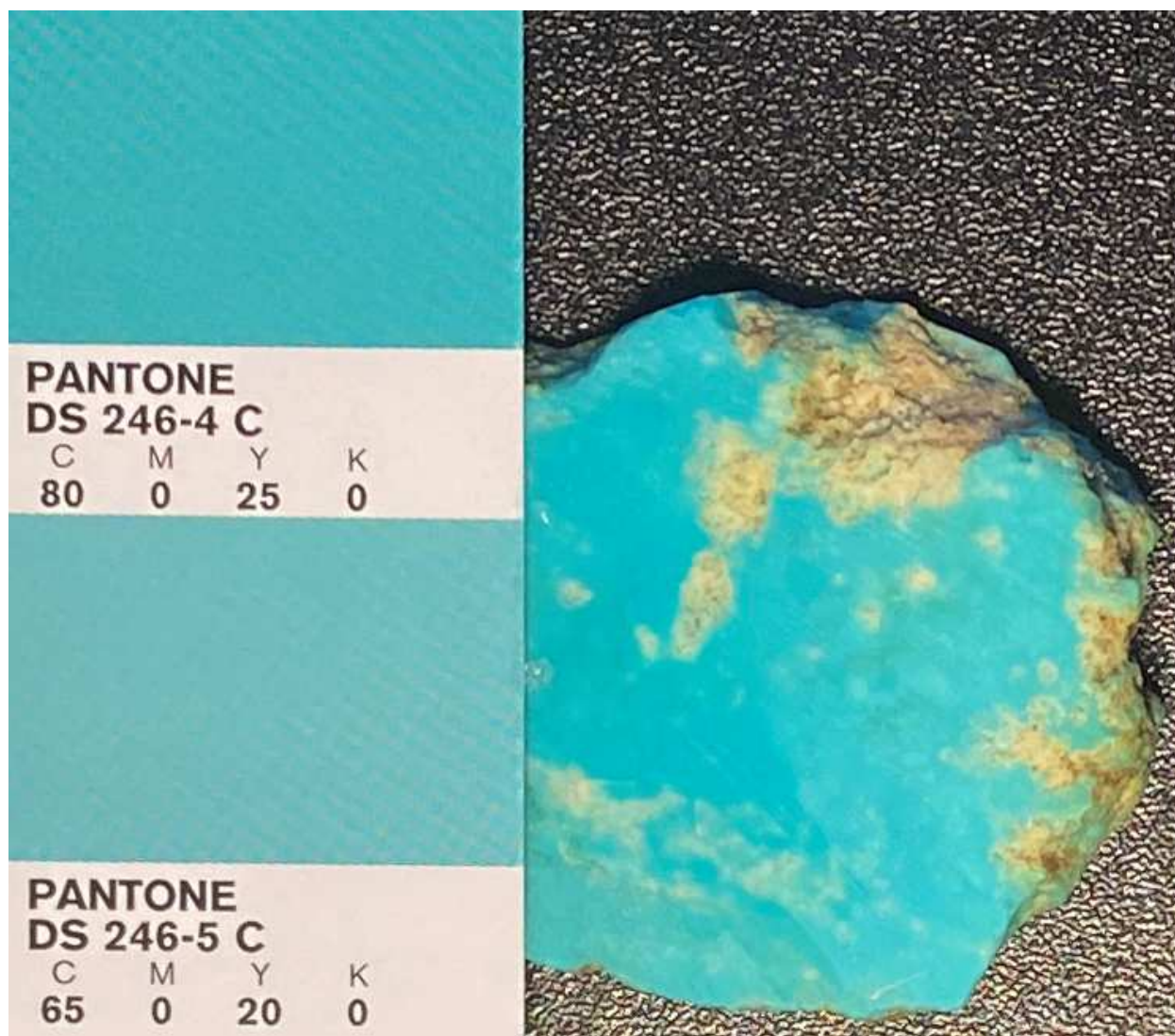
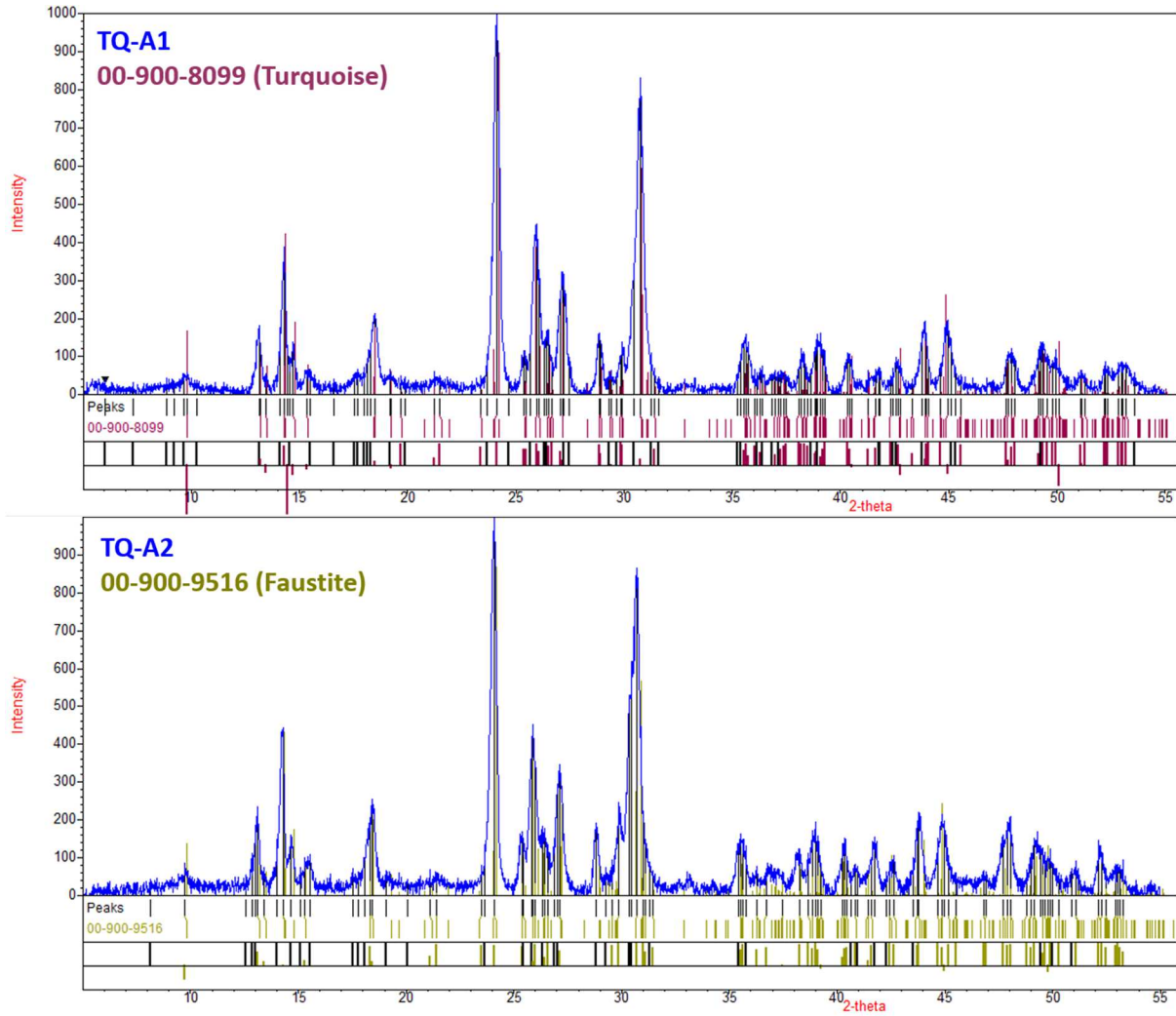


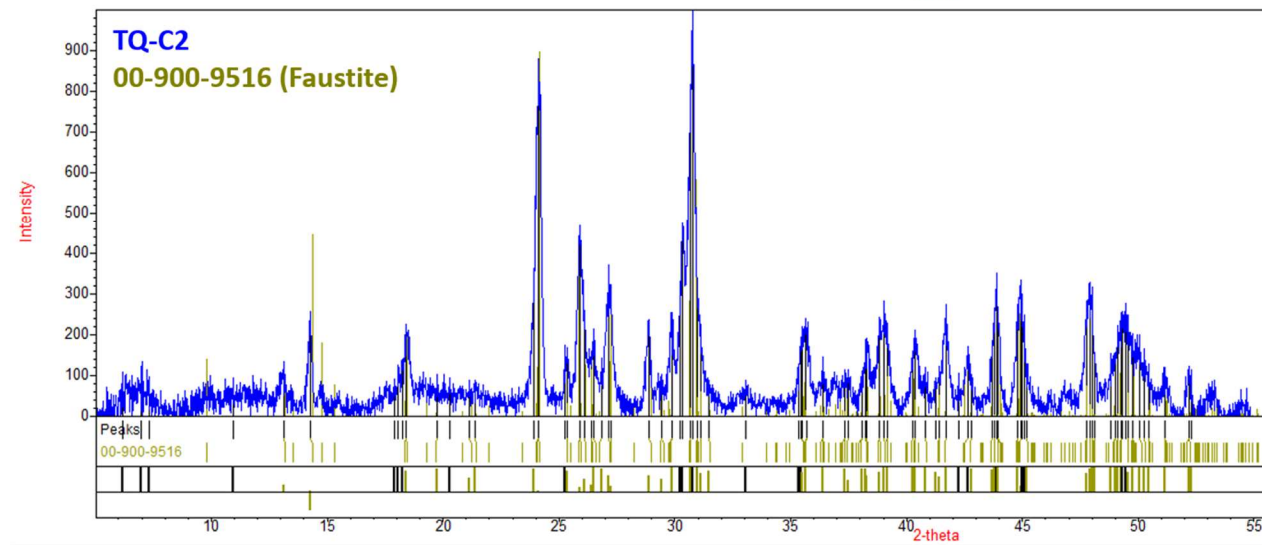
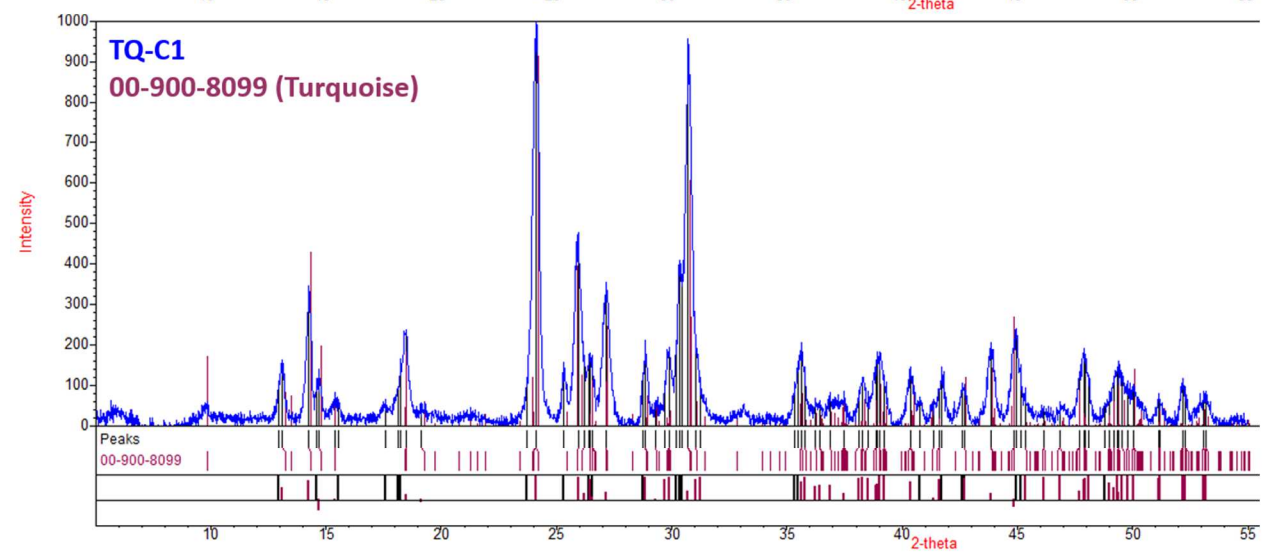
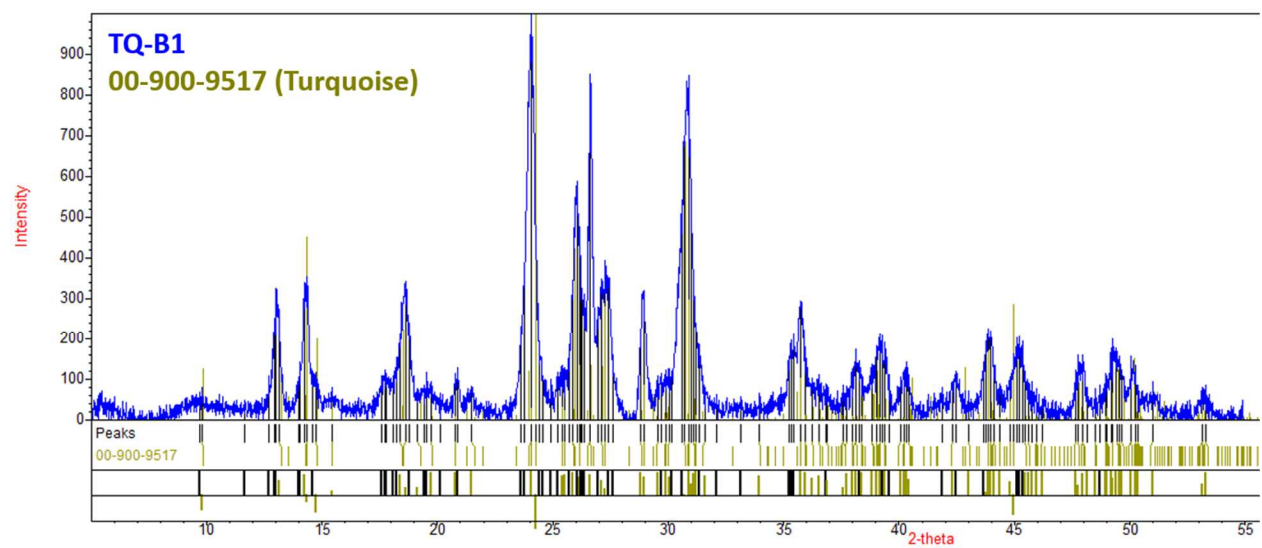
Figure 19: This image shows the process of matching CMYK colors from a Pantone™ Bridge set with turquoise samples from the Mona Lisa Mine. (Photo by T. Paradise).

### ***5.3 X-ray Diffraction***

X-ray diffraction analysis was performed on 10 Mona Lisa samples of varying physical properties at the University of Arkansas Nanocenter by Dr. Andrian V. Kuchuk. Seven of the sample diffraction patterns that align with turquoise group reference patterns are displayed in Figure 20. These patterns were matched with the POW\_COD database on QUALX2.0™ software. On the QUALX2.0™ window, background was subtracted and peaks were listed prior to use of the “Search-Match” function querying the database. Sample TQ-J did not match with

any reasonable reference patterns on QUALX2.0™ and was not included, while samples TQ-I1 and TQ-B2 had signatures influenced by the matrix material within the slabs (Figure 21). TQ-J did have potential matches of chalcociderite and planerite using X'Pert Highscore™ software.





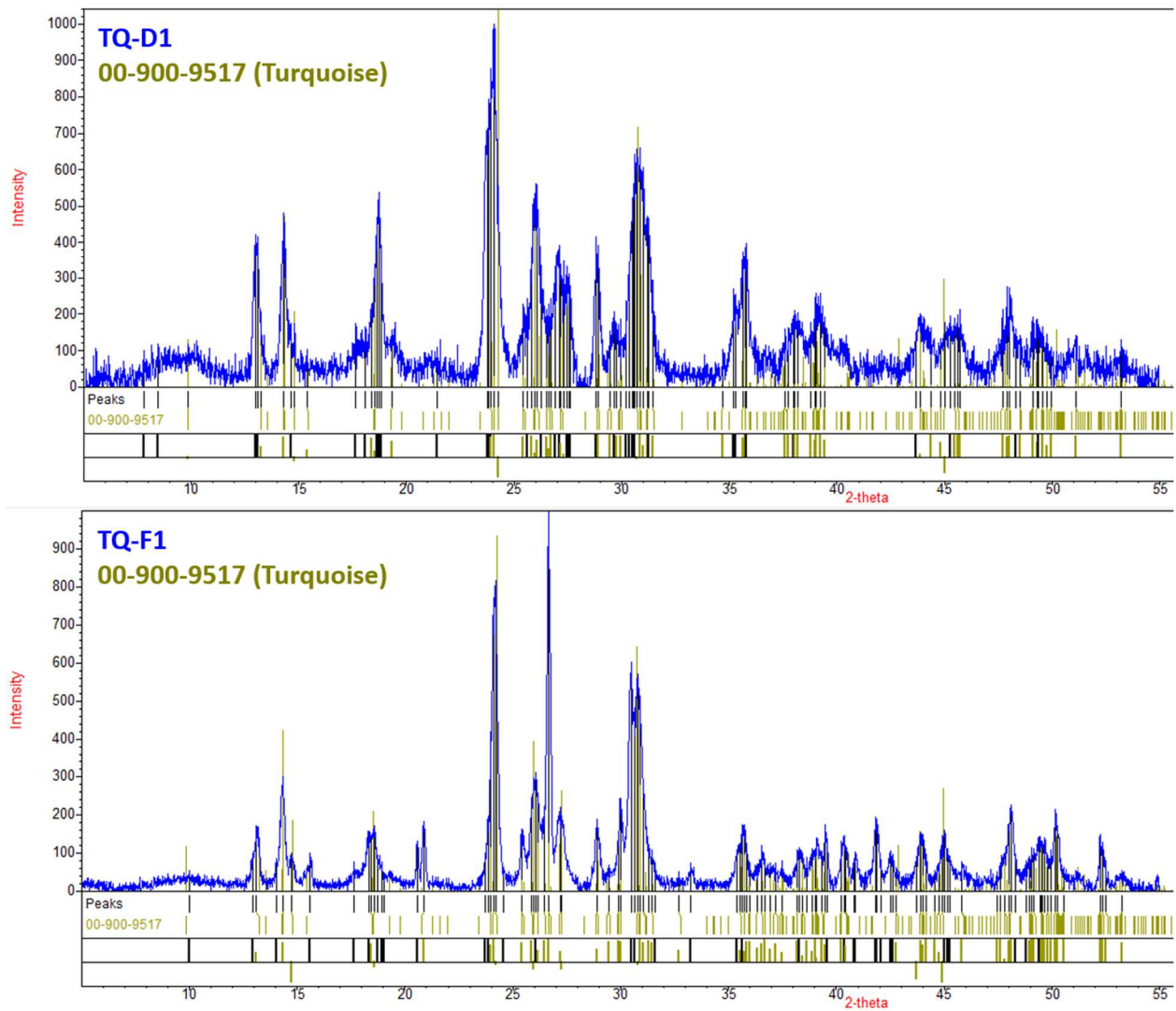


Figure 20: Mona Lisa sample diffraction patterns, referenced to the best mineralogical match using the POW\_COD database on QUALX2.0™ diffraction software. These select 7 samples match closely with turquoise or faustite reference patterns.

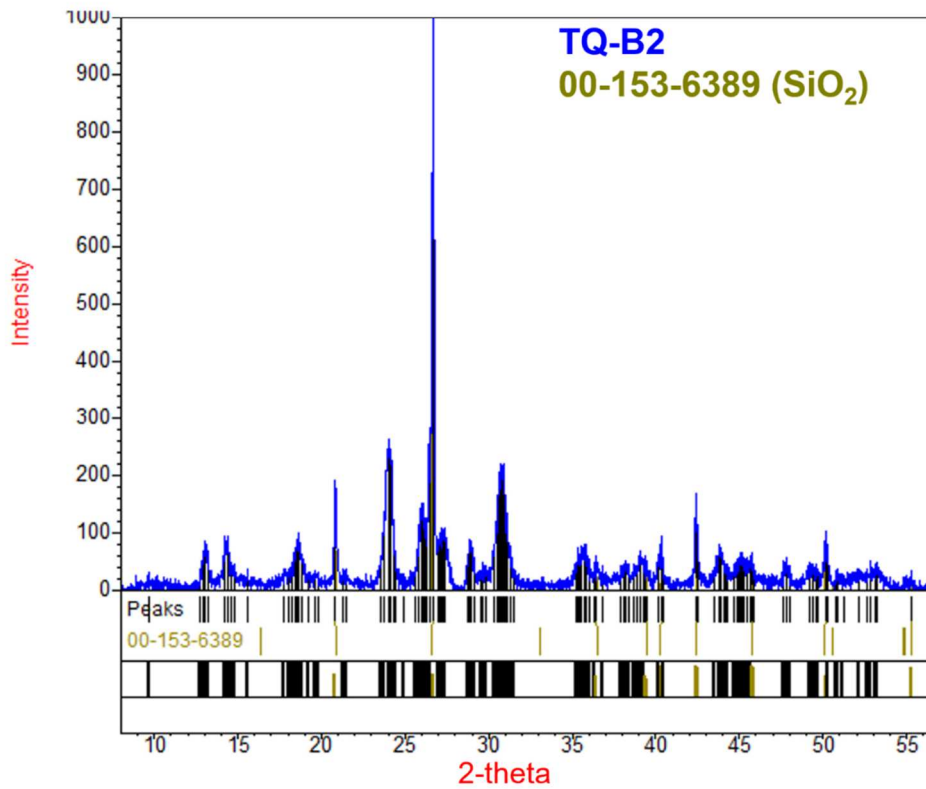
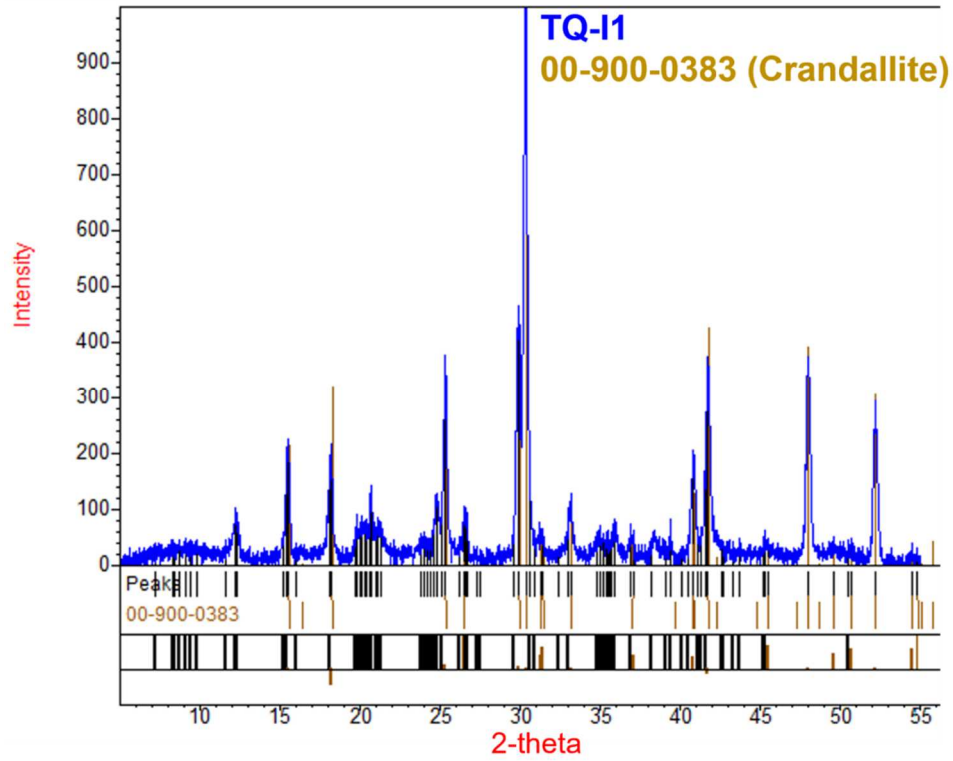


Figure 21: Sample diffraction patterns of Mona Lisa matrix material. TQ-B2 matched with quartz reference, and TQ-11 matched with the rare phosphate mineral crandallite.



### 5.4 Raman Spectra

Raman spectroscopy is another method used to identify minerals. Raman spectra for the 10 Mona Lisa samples were analyzed, both for gem material and matrix identification. A Thermo Scientific™ DXR Raman microscope at the Baylor University Igneous Petrology Laboratory was used by the author with the permission of Dr. Kenneth S. Befus for Raman analysis. TQ-A1, TQ-A2, TQ-B1, TQ-B2, TQ-C1, TQ-C2, TQ-D1, and TQ-F1 all matched closely with the turquoise reference spectrum from the RRUFF mineralogical database. An example comparison (for TQ-A1) is displayed in Figure 22. Anatase, quartz, and planerite were found to be mineral phases present in certain Mona Lisa samples (TQ-B2, TQ-D1, TQ-J1, shown in Figure 23).

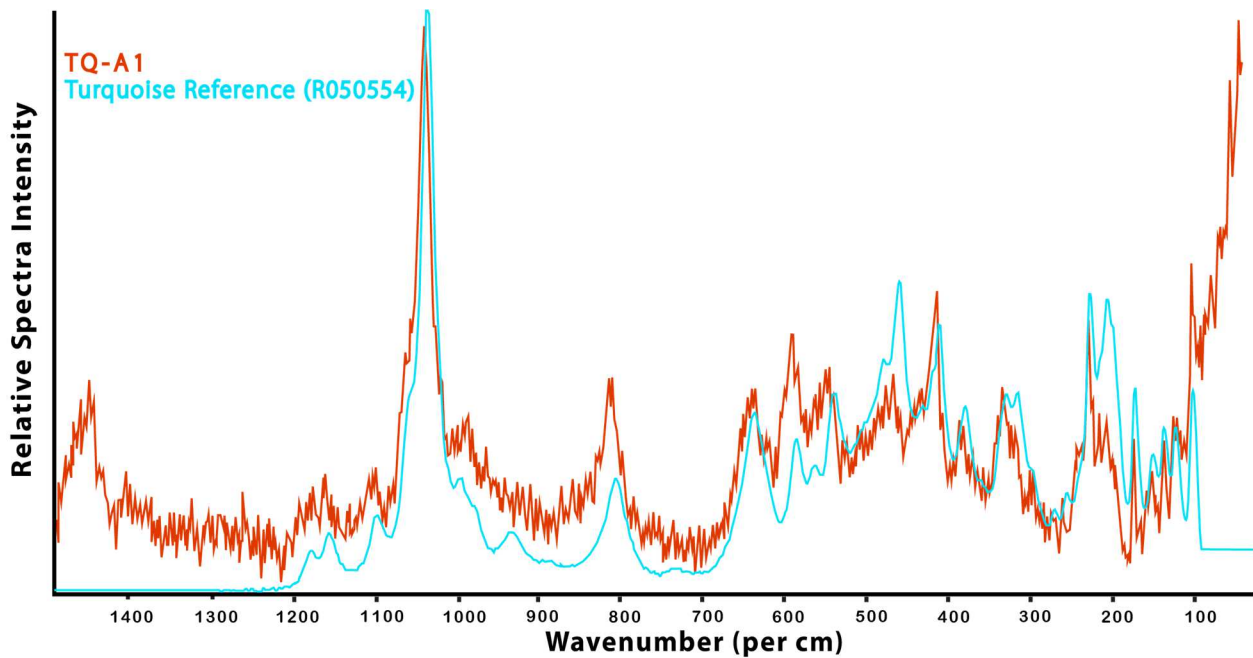


Figure 22: Comparison between an RRUFF database turquoise reference Raman spectrum with the measured spectrum of Mona Lisa sample TQ-A1.

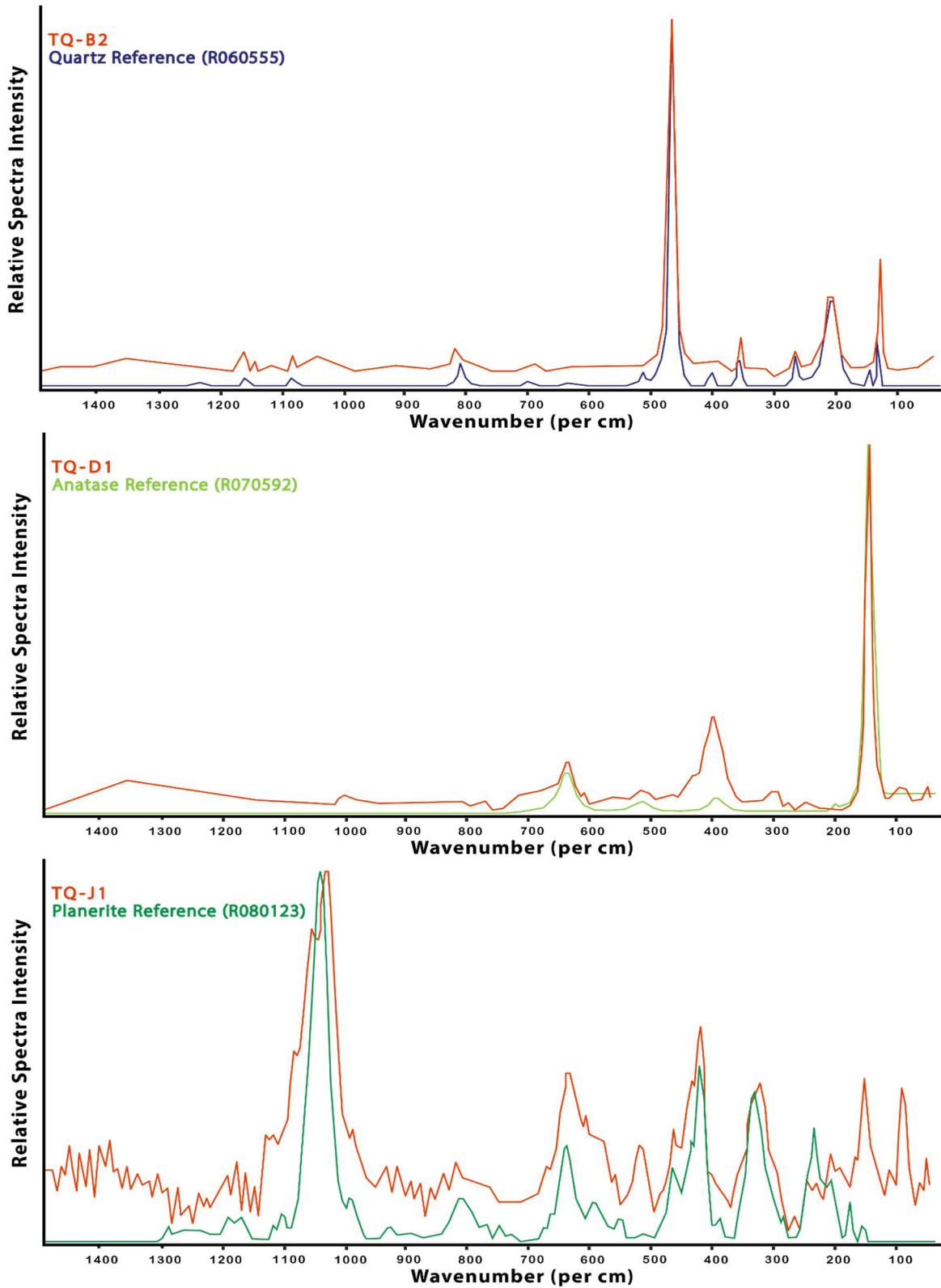


Figure 23: Mineral phase comparisons of Raman spectra references with Mona Lisa samples TQ-B2, TQ-D1, and TQ-J1. Identifiable are the minerals quartz, anatase, and planerite, respectively.

### ***5.5 Elemental Concentrations***

The concentrations of Cu, Zn, Fe, Pb, and Sr of Mona Lisa material analyzed at the University of Arkansas (14 samples and 1 replicate) are listed in Table 2. The table displays all recorded concentration data from the Mona Lisa locality, along with available data collected by Attard's Minerals (Laney, 2020). Sample MLI 02-R represents the replicate sample, which was analyzed to evaluate the precision (reproducibility) of the data. Blanks were run throughout the analyses, yielding very low values that account for negligible external contamination. Copper, Zn, and Fe concentrations of the currently analyzed samples ranged from 0.14 to 5.82 wt.%, 0.12 to 1.49 wt.%, and 1.40 to 8.93 wt.%, respectively. Lead and Sr concentrations are listed in ppm because they are not major elements in any turquoise group minerals and therefore occur in low concentrations. The concentration results of the entire suite of analyzed elements, including REE values, are found in Appendix D. Table 3 lists the elemental concentrations of the Arkansas Novaculite analyzed at the University of Arkansas in 2016 by John B.S. Philbrick and 2019 by Julie M. Cains. Philbrick analyzed 19 samples with one duplicate, and Cains collected concentration data from 10 novaculite samples. The novaculite samples were recovered from the Caddo Gap outcrop, an extensive exposure of both upper and lower novaculite. Values are listed in parts per million (ppm). The concentration ranges of select elements in the novaculites are as follows: 0.33-102.38 ppm Cu, 0.38-72.26 ppm Zn, 69.66-3554.83 ppm Fe, 0.03-33.19 ppm Pb, and 0.67-35.62 ppm Sr.

Table 2: Cu, Zn, Fe, Pb, and Sr concentrations of Mona Lisa samples. Samples L-1 through L-12 are from Laney (2020).

<i>Sample ID</i>	<i>wt.% Cu</i>	<i>wt.% Zn</i>	<i>wt.% Fe</i>	<i>ppm Pb</i>	<i>ppm Sr</i>
TQ-A	N/A	N/A	N/A	0.05	36.91
TQ-B	N/A	N/A	N/A	2.52	129.74
TQ-C	4.55	0.53	2.15	0.05	220.54
TQ-D	N/A	N/A	N/A	3.54	99.59
TQ-E	N/A	N/A	N/A	0.41	2.96
TQ-F	N/A	N/A	N/A	2.59	62.11
TQ-H	N/A	N/A	N/A	0.12	266.48
TQ-J	0.14	0.12	1.49	0.86	0.27
MLI 01	5.43	0.23	8.93	0.03	192.27
MLI 02	1.40	0.20	1.91	0.50	11.66
MLI 02-R	5.82	0.17	3.11	N/A	N/A
MLI 03	0.23	0.12	1.40	0.01	0.38
MLI 04	N/A	N/A	N/A	0.18	11.75
MLI 05	3.17	1.49	2.32	0.02	701.62
MLI M	N/A	N/A	N/A	1.47	55.76
L-1 MLM	4.33	0.03	2.72	N/A	N/A
L-2 MLM	3.63	0.00	1.34	N/A	N/A
L-3 MLM	5.47	0.74	1.91	N/A	N/A
L-4 MLM	6.89	0.02	1.59	N/A	N/A
L-5 MLM	6.87	0.70	1.46	N/A	N/A
L-6 MLM	6.40	0.03	1.57	N/A	N/A
L-10 MLM	5.72	N/A	7.23	N/A	N/A
L-11 MLM	6.98	N/A	4.19	N/A	N/A
L-12 MLM	5.88	N/A	7.24	N/A	N/A

Table 3: Cu, Zn, Fe, Pb, and Sr concentrations of Arkansas Novaculite from Philbrick (2016) and Cains (2019). Samples analyzed by Cains are denoted by an \*.

<i>Sample ID</i>	<i>ppm Cu</i>	<i>ppm Zn</i>	<i>ppm Fe</i>	<i>ppm Pb</i>	<i>ppm Sr</i>
<b>CG8</b>	3.32	5.4	N/A	6.19	N/A
<b>CG23</b>	1.31	2.39	N/A	2.28	N/A
<b>CG6</b>	14.22	6.54	N/A	5.70	N/A
<b>CG13</b>	1.97	3.21	N/A	3.47	N/A
<b>CG2</b>	22.14	9.04	N/A	7.97	N/A
<b>CG26</b>	1.79	3.5	N/A	2.43	N/A
<b>CG67</b>	23.18	17.81	N/A	18.17	N/A
<b>CG86</b>	8.81	25.73	N/A	7.21	N/A
<b>CG35</b>	4.85	11.93	N/A	6.02	N/A
<b>CG60</b>	41.84	12.34	N/A	18.31	N/A
<b>CG69</b>	58.57	72.26	N/A	19.82	N/A
<b>CG50A</b>	102.38	26.91	N/A	28.66	N/A
<b>CG66</b>	23.55	14.94	N/A	16.92	N/A
<b>CG52</b>	53.17	16.64	N/A	19.79	N/A
<b>CG50B</b>	27.89	17.01	N/A	33.19	N/A
<b>CG18</b>	35.65	17.94	N/A	8.99	N/A
<b>CG39</b>	6.41	7.82	N/A	7.53	N/A
<b>CG77</b>	3.86	6.49	N/A	2.28	N/A
<b>CG85</b>	5.9	10.8	N/A	8.60	N/A
<b>CG13-D</b>	3	6.67	N/A	3.68	N/A
<b>CG6*</b>	17.45	7.75	2843.33	3.43	31.18
<b>CG8*</b>	0.86	0.67	555.62	1.35	16.44
<b>CG18*</b>	22.19	3.34	144.05	0.52	11.88
<b>CG39*</b>	0.33	0.52	75.45	0.10	9.81
<b>CG52*</b>	33.54	1.82	3554.83	2.97	35.62
<b>CG71*</b>	9.90	46.56	989.16	1.07	23.56
<b>CG77*</b>	1.20	0.38	69.66	0.03	0.67
<b>CG82*</b>	3.75	2.35	480.43	1.01	7.76
<b>CG85*</b>	1.74	1.15	365.93	0.23	1.79
<b>CG86*</b>	6.30	26.79	1966.34	1.60	31.04

### ***5.6 Strontium Isotope Ratios***

Measured Sr isotope ratios of 13 samples and one duplicate (TQ-D2) analysis of Mona Lisa material are displayed in Table 4. The samples fall within a narrow range of  $^{87}\text{Sr}/^{86}\text{Sr}$  ratios, between 0.71229 and 0.71916. The Sr isotope ratios are not age corrected due to the unknown age of the turquoise deposit. Figure 24 shows the range of these ratios in comparison with those

of the Arkansas Novaculite samples (Cains, 2019) and turquoise deposits of the American Southwest (Thibodeau et al., 2015).

Table 4: Present day  $^{87}\text{Sr}/^{86}\text{Sr}$  ratios from select Mona Lisa samples.

<i>Sample ID</i>	<i><math>^{87}\text{Sr}/^{86}\text{Sr}</math></i>
TQ-A	0.71234
TQ-B	0.71456
TQ-C	0.71230
TQ-D1	0.71496
TQ-D2	0.71498
TQ-E	0.71713
TQ-F	0.71749
TQ-H	0.71229
TQ-J	0.71916
MLI 01	0.71256
MLI 02	0.71648
MLI 04	0.71341
MLI 05	0.71230
MLI M	0.71280

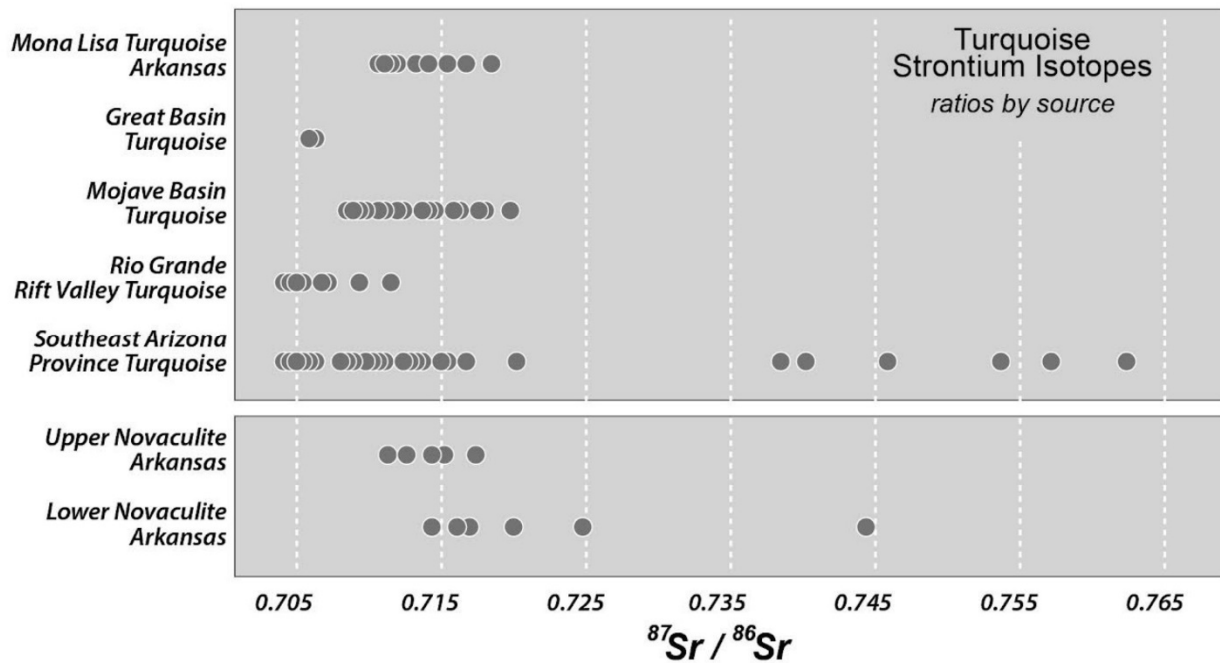


Figure 24: The  $^{87}\text{Sr}/^{86}\text{Sr}$  ratios of the Mona Lisa turquoise, the Arkansas Novaculite (Cains, 2019), and various southwestern United States turquoise sites (Thibodeau et al., 2015).

### 5.7 Lead Isotope Ratios

Lead isotope values (Table 5) are presented as ratios between  $^{208}\text{Pb}$  and  $^{204}\text{Pb}$ ,  $^{207}\text{Pb}$  and  $^{204}\text{Pb}$ , and  $^{206}\text{Pb}$  and  $^{204}\text{Pb}$ . The data reflect the ratios collected from 12 Mona Lisa samples and 1 duplicate. These ratios range between 38.4897 and 39.2655 ( $^{208}\text{Pb}/^{204}\text{Pb}$ ), 15.6797 and 15.8571 ( $^{207}\text{Pb}/^{204}\text{Pb}$ ), and between 19.3089 and 22.7770 ( $^{206}\text{Pb}/^{204}\text{Pb}$ ). The values represent present-day ratios. Detailed tables with the Pb and Sr isotope results and uncertainties can be found in Appendix E. Lead isotope data from the Mona Lisa Mine, adjacent strata, and southern Ozark MVT ore districts are represented on covariate thorogenic and uranogenic diagrams in Figure 25. Figure 26 displays the Mona Lisa Pb isotope data along with fields representing published data (Thibodeau et al., 2015) for southwestern US turquoise. For archaeological purposes, the  $^{208}\text{Pb}/^{204}\text{Pb}$  ratios have additionally been plotted against the  $^{207}\text{Pb}/^{204}\text{Pb}$  ratios in Figure 27 to further differentiate between turquoise deposits.

Table 5: Present day Pb isotope ratios of Mona Lisa samples.

<b>Sample ID</b>	<b><math>^{208}\text{Pb}/^{204}\text{Pb}</math></b>	<b><math>^{207}\text{Pb}/^{204}\text{Pb}</math></b>	<b><math>^{206}\text{Pb}/^{204}\text{Pb}</math></b>
<b>TQ-A</b>	38.5129	15.7077	20.7344
<b>TQ-B</b>	38.5858	15.7120	19.8953
<b>TQ-C</b>	38.9758	15.8571	23.1794
<b>TQ-D1</b>	38.4916	15.6797	19.3089
<b>TQ-D2</b>	38.4897	15.6803	19.3094
<b>TQ-E</b>	39.0764	15.7962	21.6647
<b>TQ-F</b>	38.9101	15.7949	21.3226
<b>TQ-H</b>	38.8510	15.7733	22.7770
<b>TQ-J</b>	38.9307	15.7896	21.2573
<b>MLI 01</b>	38.7570	15.7895	21.7871
<b>MLI 02</b>	38.9598	15.7877	21.4767
<b>MLI 04</b>	38.9712	15.7633	21.3593
<b>MLI M</b>	39.2655	15.8273	21.9286

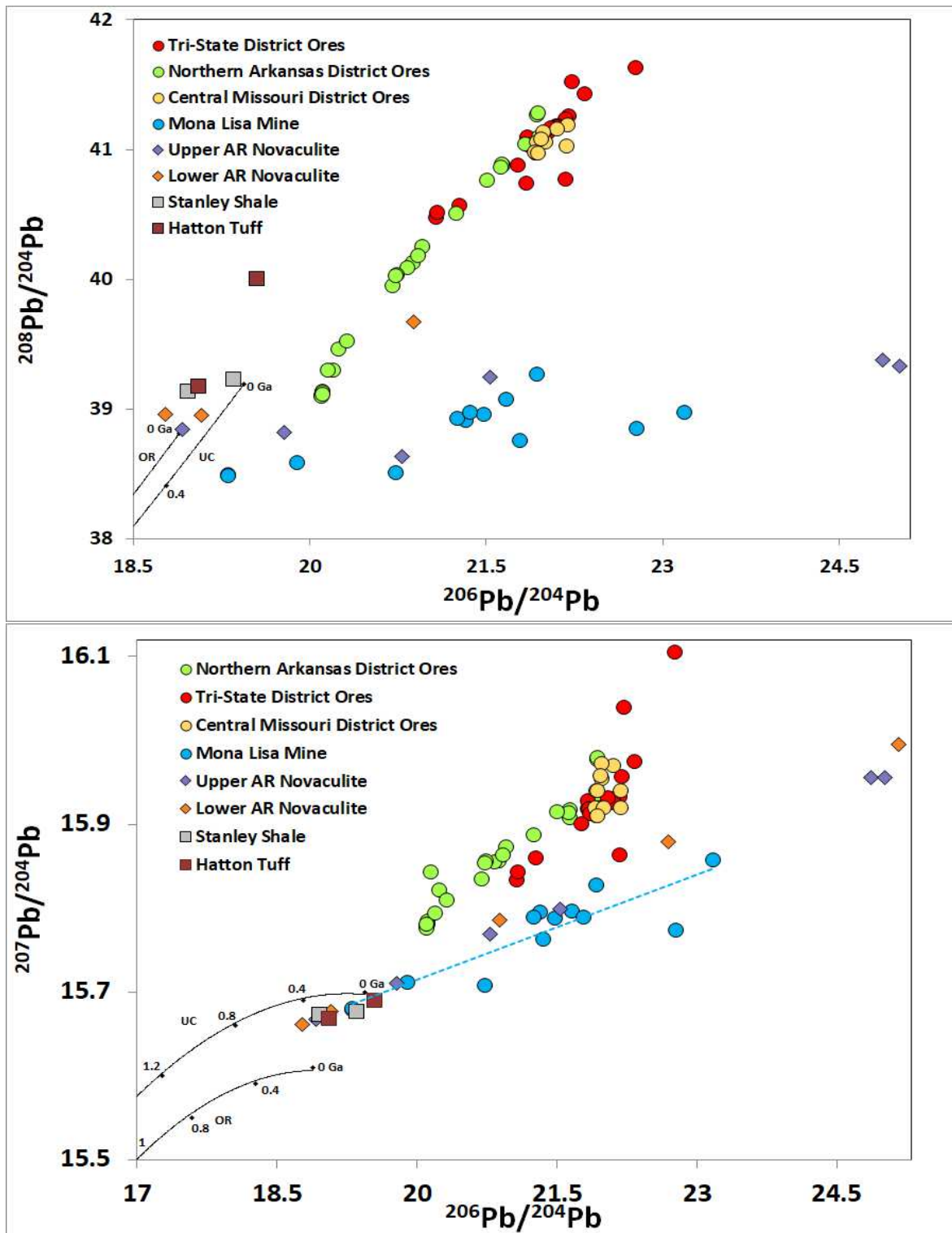


Figure 25: Covariate thorogenic (top) and uranogenic (bottom) Pb isotope plots of Mona Lisa samples, regional ore districts (Potra et al., 2018; Bottoms et al., 2019), and local strata (Cains, 2019). The linear trendline for Mona Lisa samples on the uranogenic diagram has a slope of 0.0418. Lead growth curve models for orogene (OR) and upper crust (UC) conditions are also included (Zartman and Doe, 1981).



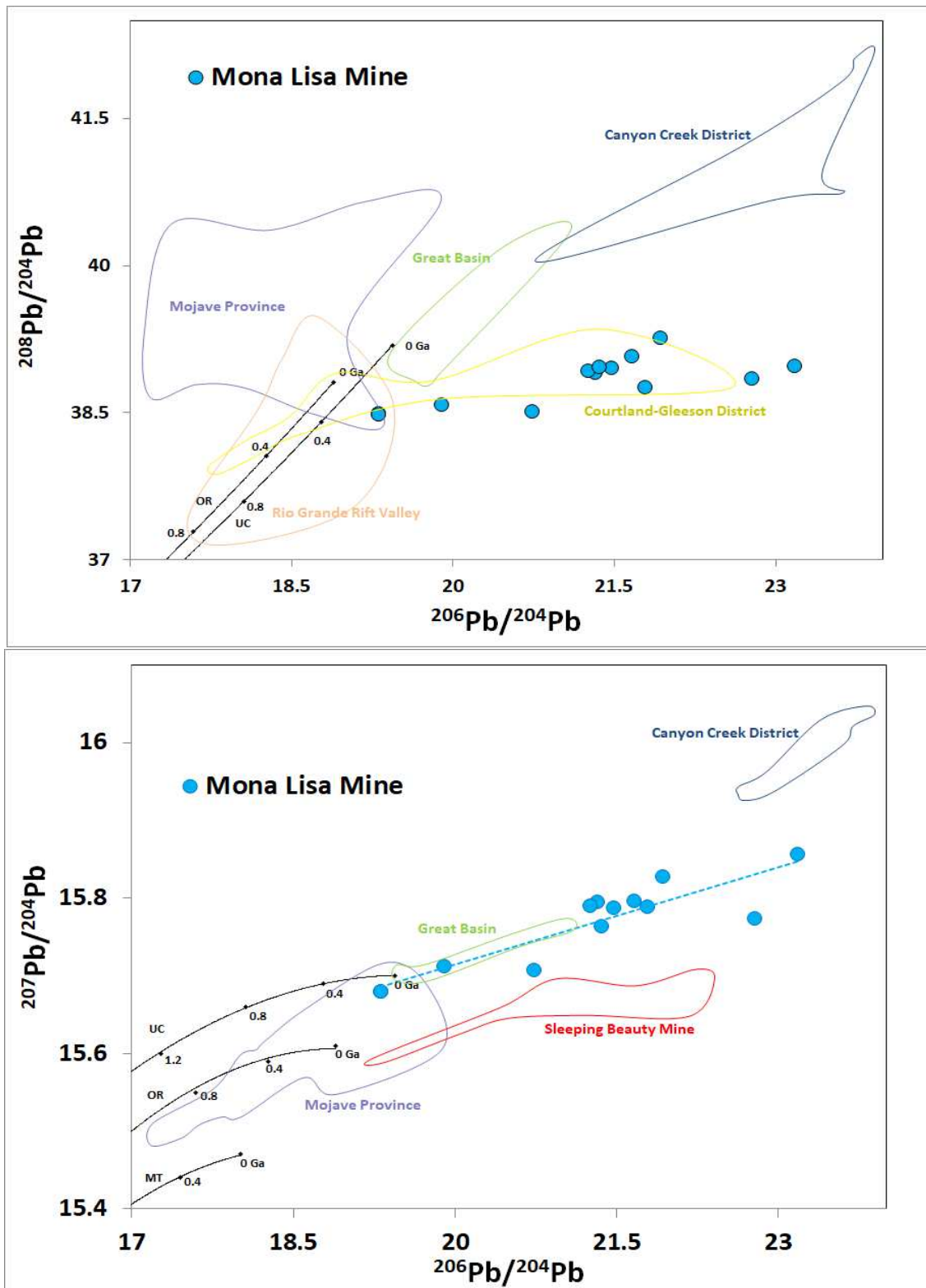


Figure 26: Thorogenic (top) and uranogenic (bottom) Pb isotope covariate plots comparing Mona Lisa material with turquoise deposits in the American Southwest. Fields constructed from Thibodeau et al (2015) data. Pb model growth curves for upper crust (UC), orogene (OR), and mantle (MT) from Zartman and Doe (1981) included.

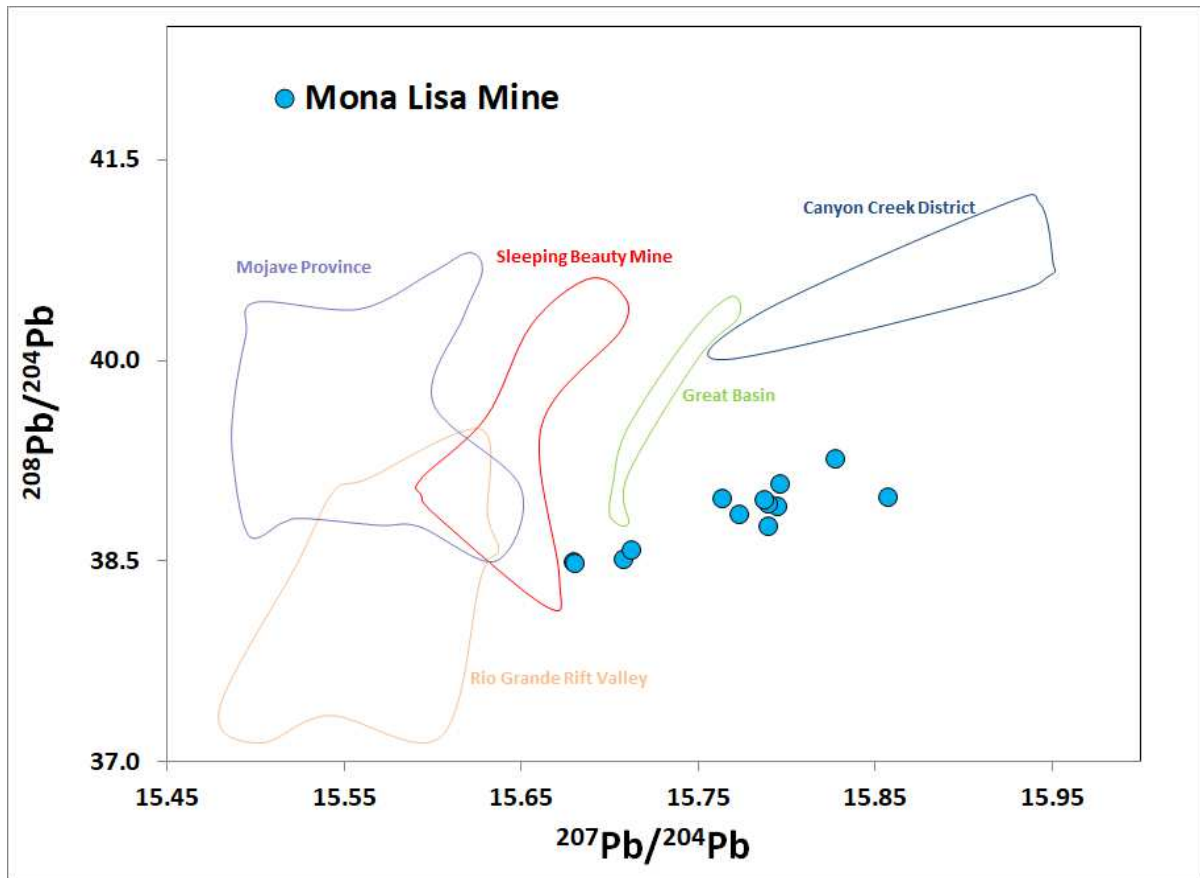


Figure 27: Pb isotope composition chart of  $^{208}\text{Pb}/^{204}\text{Pb}$  vs  $^{207}\text{Pb}/^{204}\text{Pb}$ , comparing Mona Lisa samples with fields reflecting turquoise deposit locations in the American Southwest.

## Chapter 6: Discussion

### *6.1 Local Geology*

The Mona Lisa Mine consists of a trench along the ridge of Little Porter Mountain in Polk County, Arkansas. The trench extends East to West, with the deepest pit in the center. In this central zone, turquoise has mineralized in seams within a white, chalky matrix material. This material was analyzed using X-ray diffraction and Raman spectroscopic techniques to identify mineral phases. Although not all of the analyses were conclusive, clear signatures for quartz and crandallite phases were apparent. Crandallite, a calcium phosphate mineral, has been identified in assemblage with turquoise (Dill et al., 1991). Because phosphate minerals like turquoise weather so readily, additional phosphate mineral phases can be expected as the turquoise itself weathers. The presence of quartz in the matrix material was to be expected, with the mine hosted in Arkansas Novaculite, a formation composed of high-purity silica. The novaculite must have been exposed to significant weathering processes to be changed to such a soft, chalky state. The novaculite ranges in character throughout the trench, with turquoise seams visible in hard, less weathered novaculite fractures as well. However, the area with the most extensive phosphate mineralization, producing the most notable gem-quality turquoise, was in the highly weathered novaculite. Turquoise's formation as a secondary, supergene mineral requires the weathering of rock components to mobilize nutrient-rich fluids. These fluids, likely derived from meteoric waters, percolated through pre-existing fractures in the novaculite and mineralized turquoise and other phosphate minerals. The pre-existing fractures in the novaculite provided the pathways for Cu-, Al-, and P-bearing fluids to travel.

Deformation of the Arkansas Novaculite occurred during the Ouachita Orogeny. Both brittle and ductile deformation is apparent in Arkansas Novaculite at various outcrops in western

Arkansas and the steeply north and south-dipping novaculite, Missouri Mountain Shale, and Stanley Shale beds exposed at Little Porter Mountain and in the Mona Lisa trench have comparable orientations to other ridges in this area of the Ouachita Mountains (Keng, 2011). To create the geologic pattern at the Mona Lisa Mine, there must be an overturned, tilted anticline structure forming the ridge. This causes the older Missouri Mountain Shale to outcrop along the ridge, with younger novaculite and Stanley Shale on the slopes of Little Porter Mountain. The abundance of steeply dipping conjugate fractures striking N-S agree with prior joint measurements in the area and could indicate shortening in the N-S direction and extension in the WNW-ESE direction as the orogeny progressed (Figure 28). Although a sample size of joint measurements from within the Mona Lisa trench is insufficient to make any overarching claims about the orogenic system, the data supports the interpretation of Keng (2011) of late-stage extension parallel to the orogen caused by the thinning and spreading of the accretionary wedge above the south-subducting North American craton. At a more localized scale, the fracture orientations do provide evidence that turquoise mineralization could extend north and/or south along the joint surfaces. However, the seam diagrams from the most productive parts of the trench show that the seams do follow more complex patterns, when the novaculite has experienced substantial weathering.

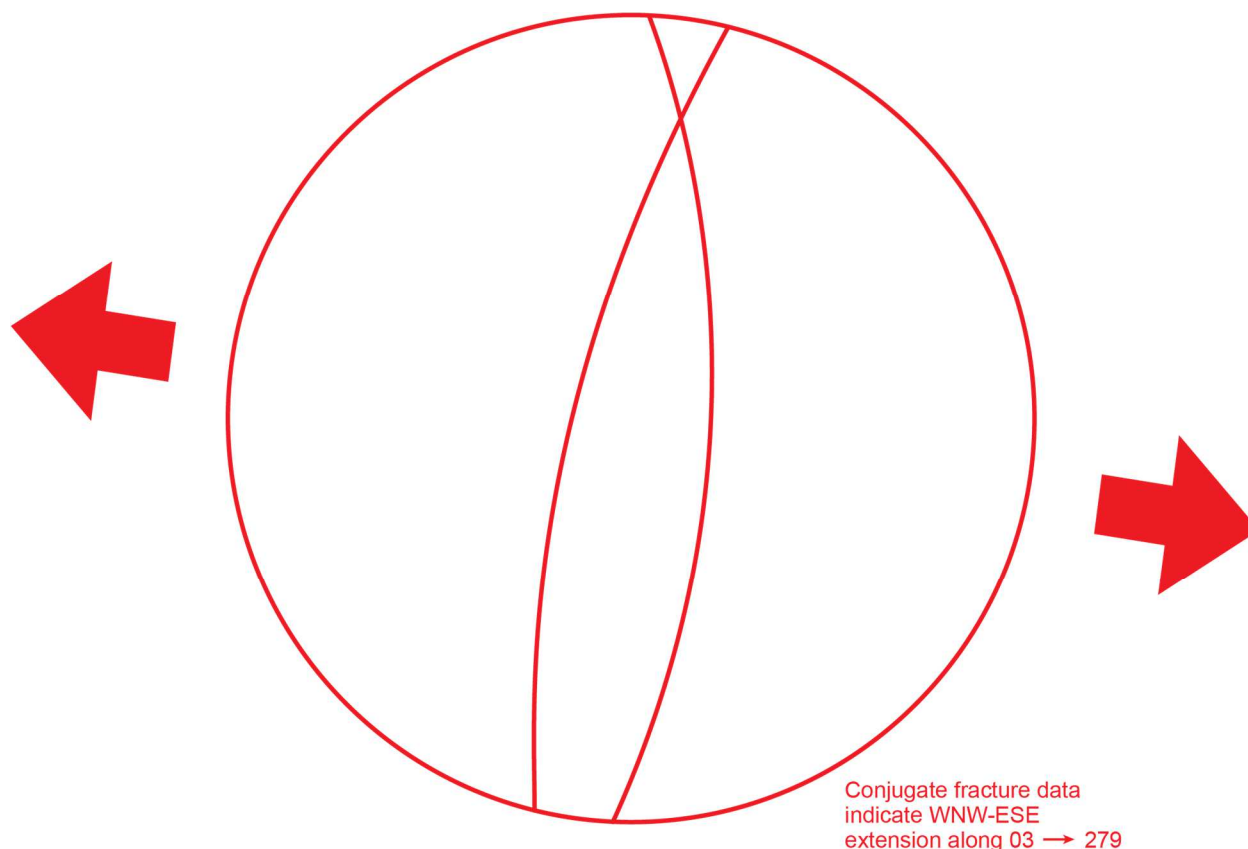


Figure 28: Averaged W- and E-dipping conjugate fracture orientations from the Mona Lisa Mine plotted as planes (great circles) on a stereonet. (Digitized by G. Dumond).

## 6.2 Gemological Value

As a gemstone, the value of turquoise is dictated by the color, matrix color and pattern, hardness, and administered treatments. Mona Lisa material ranks highly in several of these categories, but confirmation of its mineralogical nature was first required to ascribe value to the stones. X-ray diffraction, Raman spectroscopy, and mass spectrometer concentration data were all used in this study to verify the mineralogical identity of the phosphate material in the Mona Lisa Mine. Out of 10 Mona Lisa samples, 7 samples had conclusive matches with x-ray diffraction reference patterns for turquoise. The other 3 analyses revealed the minerals crandallite and quartz as present in the matrix material, and found the “white turquoise” sample slab (TQ-J1) to be the turquoise group mineral planerite. 8 of the 10 Mona Lisa samples were

identified conclusively as turquoise through comparison with the RRUFF database reference spectra. TQ-J1 was again confirmed to be planerite with this method, and the dominance of quartz in the matrix material was demonstrated once more. Despite these results, the most compelling evidence is the Cu content of Mona Lisa samples. Out of 7 samples diluted and analyzed specifically for major elements Cu, Fe, and Zn, 5 samples had >1 wt.% turquoise, with whole sample TQ-J again being one of those exceptions. The presence of Cu as major elemental component differentiates turquoise from all other turquoise group minerals, which have similar crystallographic dimensions. In conjunction with the EMPA concentration data from Laney (2020), there are now 14 Mona Lisa samples that have known Cu concentrations above 1 wt.%.

With the establishment that the Mona Lisa Mine does contain turquoise (Figure 29), the value of the material is enhanced. The color, hardness, and location of the turquoise are favorable to add economic value as well. Because of the compositional variability of turquoise at even small scales, the color of Mona Lisa turquoise ranges from green to light blue. The color differences are likely caused by alteration and the presence of Fe. Mona Lisa turquoise varies significantly in hardness, with some samples able to be cut and polished without stabilization. In the process of sample preparation for concentration and isotope data, several samples did not dissolve in HCl and HNO<sub>3</sub>. This suggests a high silica content within certain samples, especially those with even blue color and high hardness (TQ-A for example). An abundance of silica would have been in the mineralizing system due to the composition of the Arkansas Novaculite. The correlation between the Pb and Sr isotope ratios of Mona Lisa material and the Arkansas Novaculite demonstrates that the host rock did have a major influence on the turquoise composition. Applying this correlation to the presence of silica in the turquoise allows the

interpretation that Si leached from the host novaculite inundated areas of mineralized turquoise at the Mona Lisa Mine.

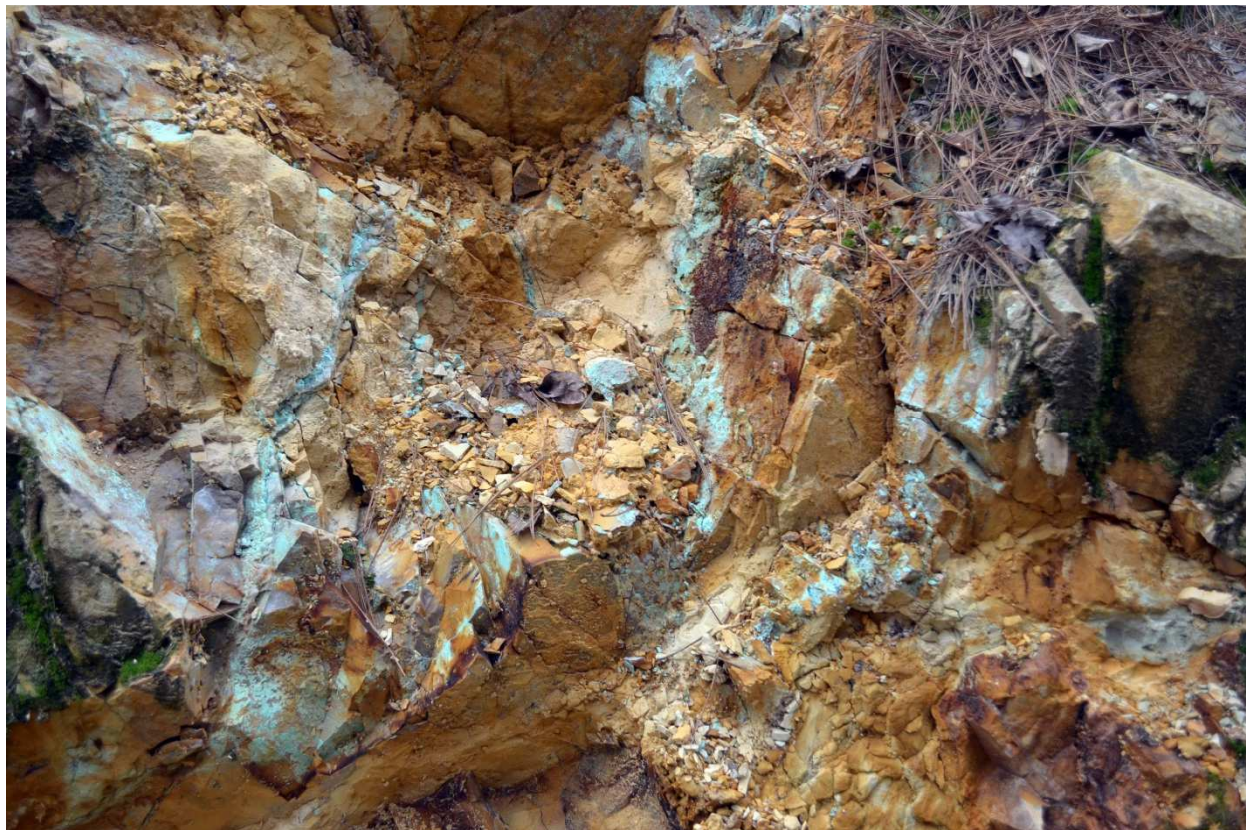


Figure 29: Turquoise mineralization at the Mona Lisa Mine in host novaculite. This view is looking south from the center of the trench. (Photo by T. Paradise).

The matrix pattern of Mona Lisa turquoise is also a distinguishing characteristic. In cut and polished stones, the matrix appeared light tan, with some patches of white and brown. The matrix is visible in stabilized and polished cabochons in Figure 30 and in a polished necklace in Figure 31. The stones lack the distinctive “spiderweb” pattern that can add value to certain samples, but the nondescript appearance of the Mona Lisa matrix promotes focus on the color of the turquoise itself. With all gemstones, the provenance of the stone has an impact on its inherent value. For turquoise, American-sourced turquoise commands higher prices than Chinese material, although Persian turquoise is currently considered the standard for turquoise. Pb isotope

analysis does provide evidence that the Mona Lisa turquoise can be distinguished from sources in the American Southwest, albeit with a destructive analytical technique. The location of the Mona Lisa Mine increases the rarity and value of the material, because turquoise from Arkansas has been hitherto unconfirmed or passed off as economically insignificant. However, the value of Mona Lisa turquoise will depend heavily on increased marketing, as the site currently remains relatively unknown. Until this Arkansas turquoise becomes a known and respected locality for turquoise collectors and dealers, the demand and subsequent worth of the material will remain lower than well-known sources, despite its rarity and peculiarity. The Mona Lisa turquoise specimens with the highest value per carat are those that are hard enough to be cut and polished directly from the mine. A large amount of the turquoise extracted from the mine, however, was soft and required stabilization. The stabilization of turquoise allows the softer material to attain value as a gemstone, but stabilized turquoise's prevalence on the turquoise market decreases the rarity of the material, location notwithstanding.





Figure 30: Stabilized and polished cabochons of Mona Lisa turquoise, demonstrating the range in color and matrix appearance. (Photo by T. Paradise).



Figure 31: Mona Lisa turquoise necklace with a matched suite of large turquoise beads. (Photo by T. Paradise).

### ***6.3 Solid Solution Relationships***

In the turquoise group, solid-solution relationships between mineral endmembers are common. The substitution of the elements copper (Cu) and zinc (Zn) in the X crystallographic site causes the turquoise-planerite solid-solution series and the probable turquoise-faustite solid-solution series. Concentration data from this study indicated the presence of Cu and Zn as major elements, with Cu having higher average concentrations. Thus, the mineralogical character of the material can more precisely be described as a potential intermediate member of the turquoise-

faustite series. The concentrations of both Zn and Cu in the material, however, fell well short of their idealized concentrations. These lower concentrations indicate that vacancies fill many octahedrally coordinated X crystallographic sites in Mona Lisa material. Ideal planerite has only vacancies in its X site, with no Cu or Zn. The presence of vacancies in Mona Lisa samples provides evidence that the samples are intermediate members in the turquoise-planerite series. Fe concentrations were also analyzed, but these concentrations do not distinguish between  $\text{Fe}^{2+}$  and  $\text{Fe}^{3+}$ . Because Fe can fill the X site ( $\text{Fe}^{2+}$ , aheylite) or the M1-3 sites ( $\text{Fe}^{3+}$ , chalcosiderite) the valence state of the Fe is important to consider when evaluating solid-solution relationships between turquoise and Fe-bearing turquoise group minerals. The major elemental concentrations of Fe can still be interpreted as an indicator of further substitution within the crystal structure.

#### ***6.4 Lead and Strontium Isotopic Signatures***

The Sr isotope ratios for Mona Lisa material fall within a narrow range (0.71229-0.71916) and are similar to those from multiple southwestern turquoise localities, especially those within the Mojave Province at the California, Arizona, and Nevada border. The ratios match those from the Upper Arkansas Novaculite closely, implying that the Sr in the turquoise was leached from the novaculite host. The absence of very high  $^{87}\text{Sr}/^{86}\text{Sr}$  ratios ( $>0.730$ ) indicates that the source rock does not exhibit high Rb/Sr ratios (Thibodeau et al., 2015), as there were in some Arizona sites (Sleeping Beauty Mine).

In both thorogenic and uranogenic (Figure 25) diagrams, the Pb isotope ratios of Mona Lisa material follow a linear trend, which correlates with the trend of Arkansas Novaculite samples, especially those of the upper novaculite. The Stanley Shale, which outcrops along the slopes of Little Porter Mountain, has a different slope on the thorogenic diagram. Additionally, the Mississippi Valley-type (MVT) ores from the Northern Arkansas, Central Missouri, and Tri-

State districts do not follow the Mona Lisa trend. This eliminates the possibility that the Pb in the Mona Lisa samples was sourced from the same reservoir as the MVT-type deposits. The strong correlation between the Pb isotope signatures of the novaculite and Mona Lisa samples suggests that the Pb in the Mona Lisa phosphate material was heavily influenced by the host novaculite. It is likely that some Pb within the Mona Lisa samples was leached directly from the upper novaculite as hydrothermal fluids mineralized turquoise within fractures. The Arkansas Novaculite thus affected the isotopic signatures of the turquoise.

The linear nature of the Mona Lisa samples on the uranogenic diagram suggests two possibilities. First, the slope of the trend on a uranogenic diagram can serve as a pseudo-isochron that could provide a model age for the Pb (Stacey and Kramers, 1975). The slope of the Mona Lisa samples, 0.0418 (Figure 25 bottom), would correspond to a model age projected in the future, which cannot be a reasonable value for the age of the Pb. Consequently, the linear trend appears to be the result of mixing of two Pb components with different Pb isotope ratios. Because the novaculite also displays a linear trend, it is possible that the ore Pb is sourced from the novaculite host rock, which contains Pb from two endmember compositions.

Lead isotopes can be used as a proxy for determining the source of other metals, including Cu, because of their similar behavior in hydrothermal systems (Tosdal et al., 1987). Concentrations of Pb and Cu in the host novaculite do suggest that some Cu and Pb in the turquoise is a result of direct leaching of metals from the novaculite. Although this is a reasonable assumption, the concentrations of Cu in the novaculite host are much too low for the novaculite to be the sole source in the mineralization of turquoise, with Cu as a major chemical component. Regionally, there are limited potential sources of Cu that have been discovered. Chalcopyrite and manganese minerals have been discovered in the Arkansas Novaculite and

Stanley Shale formations as vein fillings (Erickson et al., 1983). The Mona Lisa Mine lies along strike of the novaculite-hosted abandoned manganese mines of Polk County, and the Cu concentrations in the manganese ore have sometimes exceeded 1.0 wt% (Stroud, 1972). It is thus feasible that localized manganese ores and chalcopyrite precipitating within fractures of novaculite were weathered, providing the necessary Cu for secondary turquoise mineralization.

The Pb isotope ratios illustrated in Figures 26 and 27 reflect the archaeological significance of using Pb isotopes to differentiate between the origins of turquoise artifacts. Even from a relatively small batch of Mona Lisa samples, it is apparent that their isotopic signatures distinguish them from any of the turquoise provinces of the American Southwest. The current data can now be used to determine whether turquoise from Arkansas was ever mined by indigenous groups, or if extended trade networks moved Arkansas turquoise to various sites in Mesoamerica or the southwestern USA (Carpenter, 2020). The Pb isotopic signatures also provide data for the origin determination of gemstones. The popularity of American gems, including turquoise, leads to imitations from other sources, especially China. Although the methodology used in this study is a destructive technique, it would provide confirmation of turquoise sourced from Arkansas.

## **Chapter 7: Conclusions and Implications**

### ***7.1 Geologic History***

Understanding the geologic setting of the turquoise-bearing Mona Lisa Mine was the first step in a comprehensive evaluation of the locality. By applying the methodologies of isohypsometry, seam mineralization diagramming, and by measuring the orientations of the joint surfaces and bedding planes, the geologic history of the Mona Lisa Mine location, beginning with the deposition of the Arkansas Novaculite, was synthesized in this study. It may be speculated that the novaculite formation was deposited in a deep-water environment, with the silica potentially sourced from both micro-organisms and volcanic ash. The novaculite was deformed during the Ouachita Orogeny, a southward-subducting tectonic convergence between the North American craton and a volcanic arc or microplate (Sabine Terrane). The beds in this location were tilted to  $>60^\circ$  from horizontal, and joints perpendicular to bedding developed pervasively. Based on the orientations and positions of the Stanley Shale, Arkansas Novaculite, and Missouri Mountain Shale, the geologic structure at Little Porter Mountain is an overturned and tilted anticline. The orientation of the dominant joint direction indicates N-S shortening and E-W extension in the area. Cu-bearing ores, likely either localized chalcopyrite or Cu-bearing Mn oxides were later weathered by meteoric water during surface or near-surface exposure. The deep-water sedimentary facies provided the necessary P and Al to this mineralizing solution. The solution followed the existing joint surfaces to travel in the shallow subsurface. Turquoise thus mineralized as cryptocrystalline masses from this fluid along fracture planes and in void spaces. After turquoise mineralization, the turquoise and host novaculite have continued to weather because of their shallow, vadose and phreatic zone depths. The weathering of silica-rich rock allowed some Si, Pb, and Sr to be leached from the country rock and permeate the phosphate

material. On record, this site was only discovered by humans in the 1950s. Since then, the mine has operated sporadically under various owners, with limited attention from outside of western Arkansas.

### ***7.2 Copper Source***

While lack of marketing and understanding was important in the mine's relative obscurity since its discovery, skepticism of turquoise from Arkansas stemmed from the lack of an igneous copper source nearby and the similarities between turquoise and planerite. This research demonstrates that the material does have major elemental concentrations of Cu, differentiating the material from the planerite endmember. The question as to where such high concentrations of Cu come from, however, remains unanswered. The Pb isotope ratios of Mona Lisa samples match almost perfectly with the ratios in Arkansas Novaculite. This indicates that the Pb in the turquoise is sourced from the host novaculite or synchronous in deposition. But the novaculite does not contain enough Cu to be the source of the Cu as well. We can therefore restrict the search for a copper source to Cu-rich ores with low Pb concentrations. The source must have negligible Pb, because it did not affect the Pb isotope signature. From known ore occurrences in Polk County, the potential Cu source can be predicted to be either localized chalcopyrite mineralization in association with quartz veining or Cu-rich Mn ores which have been recorded at multiple locations along strike of novaculite ridges in the area – a possible answer to the missing Cu source.

### ***7.3 Further Exploration and Economics***

The confirmation of the mineralogical identity of turquoise from Arkansas could have a substantial impact on the prices on Mona Lisa turquoise. The prices for Mona Lisa raw turquoise material currently range from \$1.50 to \$5.00 per gram for samples requiring stabilization.

Nuggets with high hardness (not requiring stabilization) are priced individually at higher rates. Stabilized and polished samples range from \$10 to \$20 per gram for cabochons at typical jewelry sizes. These prices represent wholesale value, with Mona Lisa material retailing at significantly higher prices. Based on price observations at the 2022 Tucson Gem and Mineral Show, turquoise from recognized localities in the American Southwest are valued at many times higher value than Mona Lisa turquoise. Name recognition and the historical importance of these mines increases their value. However, the rarity of turquoise from Arkansas or any other southeastern state could distinguish Mona Lisa turquoise from any other turquoise mine. If mining at the Mona Lisa continues, the fame and value of the material will rise according to its academic establishment as turquoise and a focus on increasing public awareness of Arkansas turquoise.

One major question arises: Could there be more turquoise mineralization in this area of the Ouachitas? Initially, at the mine, the possibility of turquoise mineralization at greater depths or outside the boundaries of the current trench must be considered. Fractures trending orthogonally to the longest trench direction suggests that mineralizing fluids could have travelled along those fractures. Observations within the trench, however, tend to demonstrate more sporadic, arbitrary, and unpredictable phosphate mineralization on the far north and south sides. At a regional scale, abandoned Mn mines along similarly striking novaculite ridges in Polk County could have been Cu reservoirs. Closer in-depth inspection of these old mine sites and reports of chalcopyrite mineralization is needed to constrain the probability of further turquoise deposits.

#### ***7.4 Future Directions***

The lack of geologic research about the Mona Lisa Mine offers many opportunities for ongoing study. Investigating this deposit has both economic and academic importance. Future



coring or trench expansion would give more insight into the Mona Lisa system, and provide further clarity on the quality and quantity of turquoise possibly yielded by the mine. Future discoveries about inclusions within Mona Lisa turquoise, trace elemental concentrations, matrix patterns, and isotope data from a range of isotope systems would all give scientific context to the site and serve as signatures for determining the possible origin of material as Mona Lisa turquoise. Using electron microscopes, the microfeatures within Mona Lisa turquoise could be observed, and microscale accessory minerals could be analyzed. With the mineral assemblage defined with this method, geochemical techniques could reconstruct the pH and temperature conditions of the mineralizing solution that formed Mona Lisa turquoise. This study has provided the necessary background in mapping, geology, mineralogy, geochemistry, and economics to serve as a foundation for a multitude of mining and academic projects in the future. One day, Arkansas turquoise may become notable as its American Southwest counterpart through continued geologic research and marketing strategies – a goal of this study of the Mona Lisa Mine turquoise of Arkansas.

## Chapter 8: References

- Abdu, Y. A., Hull, S. K., Fayek, M., & Hawthorne, F. C., 2011. "The turquoise-chalcosiderite  $\text{Cu}(\text{Al},\text{Fe}^{3+})_6(\text{PO}_4)_4(\text{OH})_8 \cdot 4\text{H}_2\text{O}$  solid-solution series: A Mössbauer spectroscopy, XRD, EMPA, and FTIR study." *American Mineralogist*, vol. 96, 1433-1442.
- Allmendinger, R. W., Cardozo, N., & Fisher, D. M., 2012. *Structural Geology Algorithms: Vectors and Tensors*, Cambridge University Press.
- Allmendinger, R. W., Siron, C. R., & Scott, C. P., 2017. Structural data collection with mobile devices: Accuracy, redundancy, and best practices." *Journal of Structural Geology*, vol. 102, 98-112.
- Altomare, A., Corriero, N., Cuocci, C., Falcicchio, A., Moliterni, A., and Rizzi, R., 2015. "QUALX2.0: a qualitative phase analysis software using the freely available database POW\_COD." *Journal of Applied Crystallography*, vol. 48, 598-603.
- Altomare, A., Cuocci, C., Giacobozzo, C., Moliterni, A., & Rizzi, R., 2008. "QUALX: A computer program for qualitative analysis using powder diffraction data." *Journal of Applied Crystallography*, vol. 41, no. 4, 815-817.
- American Gem Society, 2022. December Birthstones: History of Turquoise. American Gem Society.
- Anderson, J. A., 1982. Characteristics of leached capping and techniques of appraisal, in Titley, S.R., ed. *Advances in geology of the porphyry copper deposits south-western North America*: Tucson, University of Arizona Press, 275–295.
- Archuleta, J. L. & Renfro, N., 2018. "Turquoise from western Arkansas." *Gem News International*, Tucson 2018, 86.
- Avant Mining LLC, 2018. @avantmining, Jessieville. AR.
- Barwood, H. L. & DeLinde, H., 1989. "Arkansas Phosphate Minerals: A review and update." *Rocks & Minerals*, vol. 64, no. 4, 294-299.
- Blythe, A. E., Sugar, A., & Phipps, S. P., 1988. "Structural Profiles of Ouachita Mountains, Western Arkansas." *AAPG Bulletin*, vol. 72, no. 7, 810-819.
- Bonewitz, R. L., 2013. "Smithsonian NatureGuide: Gems." Dorling Kindersly. 86-87.
- Bottoms, B., Potra, A., Samuelsen, J. R., and Schutter, S. R., 2019. Geochemical investigations of the Woodford-Chattanooga and Fayetteville Shales: Implications for genesis of the Mississippi Valley-type zinc-lead ores in the southern Ozark Region and hydrocarbon exploration. *AAPG Bulletin*, vol. 103, no. 7, 1745-1768.

- Cains, J. M., 2019. Geochemical Analysis of Mississippian Cherts and Devonian-Mississippian Novaculites, Southern Midcontinent Region. MS Thesis, University of Arkansas, 1-58.
- Cardozo, N. & Allmendinger, R. W., 2013. "Spherical projections with OSXStereonet." *Computer and Geosciences*, vol. 51, 193-205.
- Carpenter, S. M., 2020. "Mesoamerican-Mississippian interaction across the far Southern Plains by long-range Toyah intermediaries." *Plains Anthropologist*, vol. 65, no. 256, 325-356.
- Čejka, J., Sejkora, J., Macek, I., Malíková, R., Wang, L., Scholz, R., Xi, Y., & Frost, R. L., 2015. Raman and infrared spectroscopic study of turquoise minerals. *Spectrochimica Acta Part A: Molecular and Biomolecular Spectroscopy*, vol. 149, 173–182.
- Cervantes, P. & Wiltschko, D. V., 2010. "Tip to Midpoint Observations on Syntectonic Veins, Ouachita Orogen, Arkansas: Trading Space for Time." *Journal of Structural Geology*, vol. 32, no. 8, 1085-1100.
- Chen, Q., Yin, Z., Qi, L., & Xiong, Y., 2012. "Turquoise from Zhushan County, Hubei Province, China." *Gems and Gemology*, vol. 48, no. 3, 198-204.
- Chester, A. H., 1877. "On the identity of the so called peganite of Arkansas with the variscite of Breithaupt and Callanite of Damour." *Amer. Jour. of Science and Arts*, vol. 13, no. 3, 295-296.
- Crook, J. C. & Lueth, V. W., 2014. "A geological and geochemical study of a sedimentary-hosted turquoise deposit at the Iron Mask Mine, Orogrande, New Mexico." *NMGS Guidebook, 65<sup>th</sup> Field Conference, Geology of the Sacramento Mountains Region*, 227-233.
- Dahlen, F. A., 1990. "Critical Taper Model of Fold-And-Thrust Belts and Accretionary Wedges." *Annual Review of Earth and Planetary Sciences*, vol. 18, no. 1, 55-99.
- Derry, D. R., 1939. "The geology of the Canadian Malartic gold mine, N. Quebec." *Economic Geology*, vol. 34, no. 5, 495-523.
- Dill, H. G., Busch, K., & Blum, N., 1991. "Chemistry and origin of vein-like phosphate mineralization, Nuba Mountains (Sudan)." *Ore Geology Reviews*, vol. 6, no. 1, 9-24.
- Dumańska-Słowik, M., Wesełucha-Birczyńska, A., Natkaniec-Nowak, L., Gaweł, A., Włodek, A., & Kulmaczewska, K., 2020. "Blue or green? Turquoise–planerite species from Carico Lake Valley in Nevada, the United States: Evidence from Raman spectroscopy." *Journal of Raman Spectroscopy*, vol. 51, no. 2, 346–356.
- Erickson, G.E., Patterson, S.H., Dunn Jr., M.L., & Harrison, D.K., 1983. "Mineral Resources of the Caney Creek Wilderness, Polk County, Arkansas." *Studies Related to Wilderness. Geological Survey Bulletin 1551*, 1-41.
- Foord, E. & Taggart J. E., 1998. "A Reexamination of the Turquoise Group: The Mineral Aheylite, Planerite (Redefined), Turquoise and Coeruleolactite." *Mineralogical Magazine*,

vol. 62, no. 1, 93-111.

Fried, S., 2010. "Appetite for America: Fred Harvey and the Business of Civilizing the Wild West." Bantam Press. 544.

Frost, R. L., Reddy, B. J., Martens, W. N., & Weier, M., 2006. The molecular structure of the phosphate mineral turquoise—A Raman spectroscopic study. *Journal of Molecular Structure*, vol. 788, no. 1, 224–231.

Giuseppetti, G., Mazzi, F., and Tadini, C., 1989. "The crystal structure of chalcosiderite,  $\text{CuFe}_6\text{3}+(\text{PO})_4(\text{OH})_8\cdot 4\text{H}_2\text{O}$ ." *Neues Jahrbuch für Mineralogie Monatshefte*, 227–239.

Goldstein Jr., A., 1959. "Cherts and novaculites of Ouachita facies." *Silica in Sediments*, Society of Economic Paleontologists and Mineralogists, Special Publication No. 7, 135-149.

Gutschick, R. C. and Sandberg, C. A., 1981. "Mississippian Continental Margins of Conterminous United States: ABSTRACT." *AAPG Bulletin*, vol. 65.

Harry, D. L. & Mickus, K. L., 1998. "Gravity constraints on lithosphere flexure and the structure of the late Paleozoic Ouachita orogen in Arkansas and Oklahoma, south central North America." *Tectonics*, vol. 17, no. 2, 187-202.

Hotujec, C., 2011. "Mineralogical and compositional analysis of turquoise artifacts linked to prehistoric mines in New Mexico, USA." University of Georgia. MS Thesis.

Houseknecht, D. W., & Matthews, S. M., 1985. "Thermal Maturity of Carboniferous Strata, Ouachita Mountains." *AAPG Bulletin*, vol. 69, no. 3, 335-345.

Hull, S., Fayek, M., Mathien, F. J., and Roberts, H., 2014. "Turquoise trade of the Ancestral Puebloan: Chaco and beyond." *Journal of Archaeological Science*, vol. 45, 187–195.

Johnson II, H. E., Wiltschko, D. V., & Harris, J. P., 2019. "Diagenetic to Incipient Metamorphic Zones of the Benton Uplift, Ouachita Orogen, Arkansas, USA." *GSA Bulletin*, vol. 132, no. 5-6, 977-986.

Kamenov, G. D., Mueller, P. A., and Perfit, M. R., 2004. Optimization of mixed Pb-Tl solutions for high precision isotopic analyses by MC-ICP-MS. *Journal of Analytical Atomic Spectrometry*, vol. 19, 1262-1267.

Keller, W. D., Stone, C. G., & Hoersch, A. L., 1985. "Textures of Paleozoic Chert and Novaculite in the Ouachita Mountains of Arkansas and Oklahoma and Their Geological Significance." *Geological Society of America Bulletin*, vol. 96, no. 11, 1353-1363.

Keng, R. V., 2011. "Field-based constraints on the origin of the Benton Uplift, Ouachita Mountains." University of Arkansas. MS Thesis.

- King, R. J., 2002. "Minerals Explained 36: Turquoise." Blackwell Science Ltd., *Geology Today*, vol. 18, no. 3, 110-114.
- Kunz, G. F., 1883. "Perofskite and wavellite from Arkansas." *Transactions, New York Academy of Science*, vol. 3, 17-18.
- Kunz, G. F., 1892. "Gems & Precious Stones of North America." Dover Publications, Inc. 54-65.
- Kunz, G. F., 1913. "The Curious Lore of Precious Stones." Dover Publications, Inc. 108-114.
- Laney, S. E., 2020. "Turquoise in the Ouachita Mountains." *Mineral News*, vol. 36, no. 9, 1-14.
- Leach, D. L., and E. L. Rowan, 1986. "Genetic link between Ouachita foldbelt tectonism and the Mississippi Valley-type lead-zinc deposits of the Ozarks." *Geology*, vol. 14, no. 11, 931-935.
- Lillie, R. J., Nelson, K. D., De Voogd, B., Brewer, J. A., Oliver, J. E., Brown, L. D., Kaufman, S., & Viele, G. W., 1983. "Crustal Structure of Ouachita Mountains, Arkansas: A Model Based on Integration of COCORP Reflection Profiles and Regional Geophysical Data." *AAPG Bulletin*, vol. 67, no. 6, 907-931.
- Lowry, J. D. & Lowry, J. P., 2002. *Turquoise Unearthed*. Rio Nuevo Publishers. 1-21.
- Lowry, J. D. & Lowry, J. P., 2018. *Turquoise: the World Story of a Fascinating Gemstone*. Gibbs Smith. 43-121.
- Malvern Minerals Company, 2013. Celebrating 65 years supplying lamellar ground silica quartz. Retrieved Jan. 18, 2022 from [www.malvernminerals.com](http://www.malvernminerals.com).
- Mickus, K. L., & Keller, G. R., 1992. "Lithospheric Structure of the South-Central United States." *Geology*, vol. 20, 335-338.
- Muñoz-Montecinos, J., Angiboust, S., Cambeses, A., & Garcia-Casco, A., 2020. "Multiple Veining in a Paleo-Accretionary Wedge: The Metamorphic Rock Record of Prograde Dehydration and Transient High Pore-Fluid Pressures along the Subduction Interface (Western Series, Central Chile)." *Geosphere*, vol. 16, no. 3, 765-786.
- National Climatic Data Center, 2009. *Climatology: eastern Oklahoma/northwest Arkansas*.
- Nesse, W. D., 2017. *Introduction to Mineralogy*. Oxford University Press. 398.
- Philbrick, J. B. S., 2016. *A Geochemical Analysis of the Arkansas Novaculite and Comparison to the Siliceous Deposits of the Boone Formation*. MS Thesis, University of Arkansas, 1-60.

- Pin, C., Gannoun, A., & Dupont, A., 2014. Rapid, simultaneous separation of Sr, Pb, and Nd by extraction chromatography prior to isotope ratios determination by tims and mc-icp-ms. *Journal of Analytical Atomic Spectrometry*, vol. 29, 1858-1870.
- Pittenger, G. C. & Konig, R. H., 1977. "Geochemistry, geothermometry and mineralogy of copper, lead, zinc, and antimony deposits of Sevier County, Arkansas." *Symposium on the Geology of the Ouachita Mountains*, vol. 2, 19-26.
- Platt, J. P., 1986. "Dynamics of Orogenic Wedges and the Uplift of High-Pressure Metamorphic Rocks." *Geological Society of America Bulletin*, vol. 97, no. 9, 1037-1053.
- Pogue, J. E., 1915. *The Turquoise*. National Academy of Sciences, vol. 12, 3<sup>rd</sup> memoir, 9-129.
- Porter Geoconsultancy, 2013. "Morenci, Metcalf, Arizona, USA." Porter Geoconsultancy Pty Ltd., 1-3.
- Potra, A., Garmin, W. T., Samuelsen, J. R., Wulff, A., and Pollock, E. D., 2018. Lead isotope trends and metal sources in the Mississippi Valley-type districts from the mid-continent United States. *Journal of Geochemical Exploration*, vol. 192, 174-186.
- Rains, D., Hanson, D., & Worrell, A., 2015. *Mineral Resources of Arkansas*. Arkansas Geological Survey Poster Series.
- Richards, I. J., Connelly, J. B., Gregory, R. T., & Gray, D. R., 2002. "The Importance of Diffusion, Advection, and Host-Rock Lithology on Vein Formation: A Stable Isotope Study from the Paleozoic Ouachita Orogenic Belt, Arkansas and Oklahoma." *Geological Society of America Bulletin*, vol. 114, no. 11, 1343-1355.
- Stacey, J. S. & Kramers, J. D., 1975. Approximation of terrestrial lead isotope evolution by a two-stage model. *Earth and Planetary Science Letters*, vol. 26, no. 2, 207-221.
- Stroud, R. B., Arndt, R. H., Fulkerson, F. B., Diamond, W. G., 1969. *Mineral resources and industries of Arkansas*. U.S. Bureau of Mines Bulletin 645.
- Targeted News Service, 2020. "Rep. Westerman Hosts DOI Deputy Secretary MacGregor." Targeted News Service, Washington D.C.
- Thibodeau, A. M., Killick, D. J., Hedquist, S. L., Chesley, J. T., & Ruiz, J., 2015. "Isotopic evidence for the provenance of turquoise in the southwestern United States." *GSA Bulletin*, vol. 127, no. 11/12, 1617-1631.
- Thibodeau, A. M., Lopez Lujan, L., Killick, D. J., Berdan F. F., & Ruiz J., 2018. "Was Aztec and Mixtec turquoise mined in the American Southwest?" *Science Advances*, vol. 4, no. 6.
- Tosdal, R. M., Wooden, J. L., & Bouse, R. M., 1999. "Pb isotopes, ore deposits, and metallogenic terranes." *Reviews in Economic Geology*, vol. 12, 1-28.

US Climate Data, 2022. Climate: Mena, Arkansas. US Climate Data, version 3.0. Accessed 4/16/2022. [www.usclimatedata.com/climate/mena/arkansas/united-states/usa0376](http://www.usclimatedata.com/climate/mena/arkansas/united-states/usa0376)

Viele, G. W., 1989. The Ouachita Orogenic Belt. In: Hatcher, R. D., Thomas, W. A., Viele, G. W. (Eds.), *The Appalachian-Ouachita Orogen in the United States*. DNAG, the Geology of North America F-2. Geological Society of America, Boulder, Colorado, 555-561.

Weigand, P. C., & Harbottle, G., 1993. "Role of turquoises in the ancient Mesoamerican trade structure, American Southwest and Mesoamerica." *Systems of Prehistoric Exchange*, New York, Plenum, 159-177.

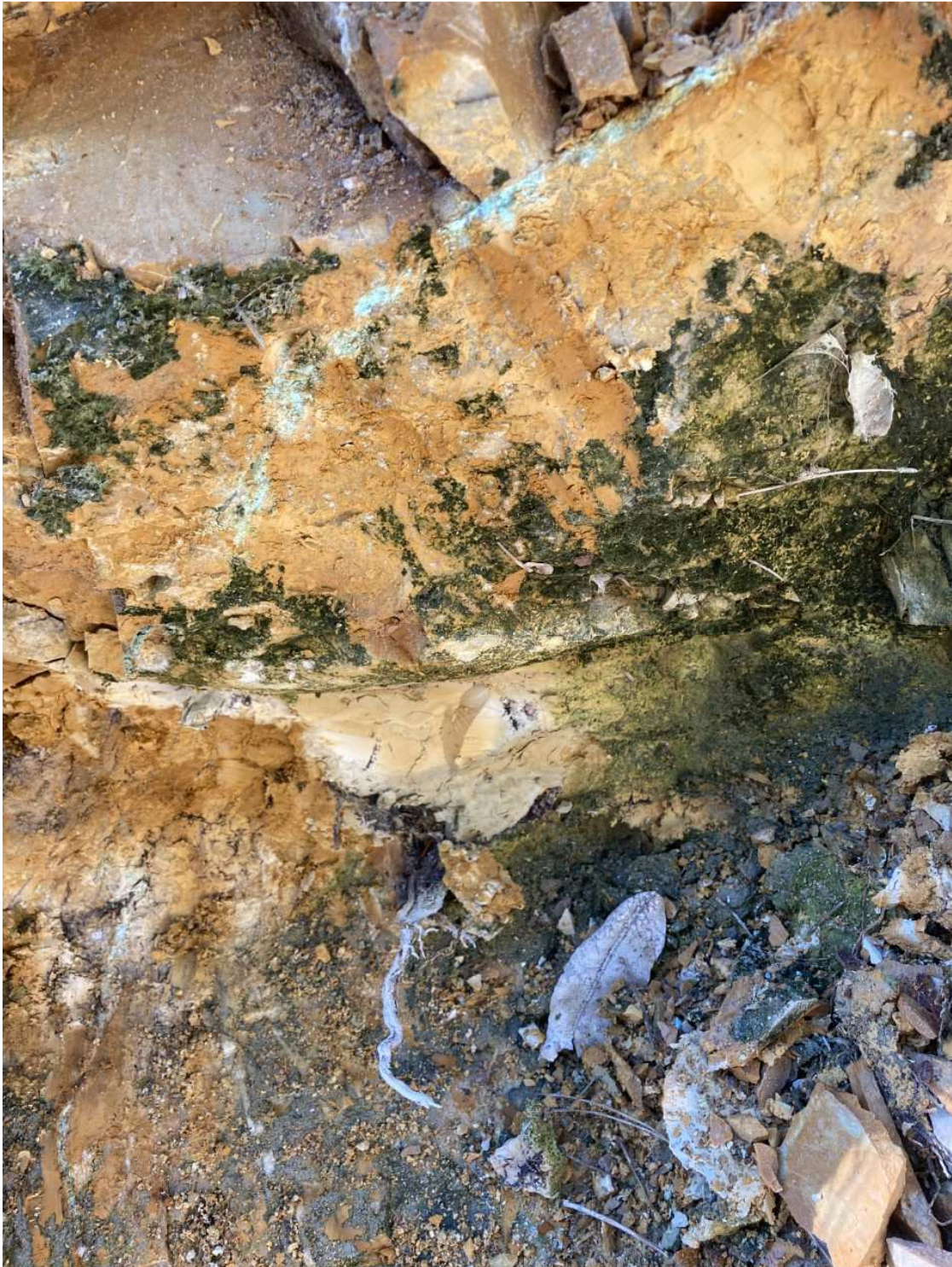
Wigley, J., 2006. "Arkansas Turquoise: How I became a gem miner." *Rock & Gem*, vol. 36, no. 4, 28-30.

Zartman, R. E. & Doe, B. R., 1981. Plumbotectonics—the model. *Tectonophysics*, vol. 75, no. 1, 135-162.

## Chapter 9: Appendices

### *Appendix A: Mona Lisa Mine Photos from 2020-2022 (photos by author and T. Paradise)*

*09/21/2020*

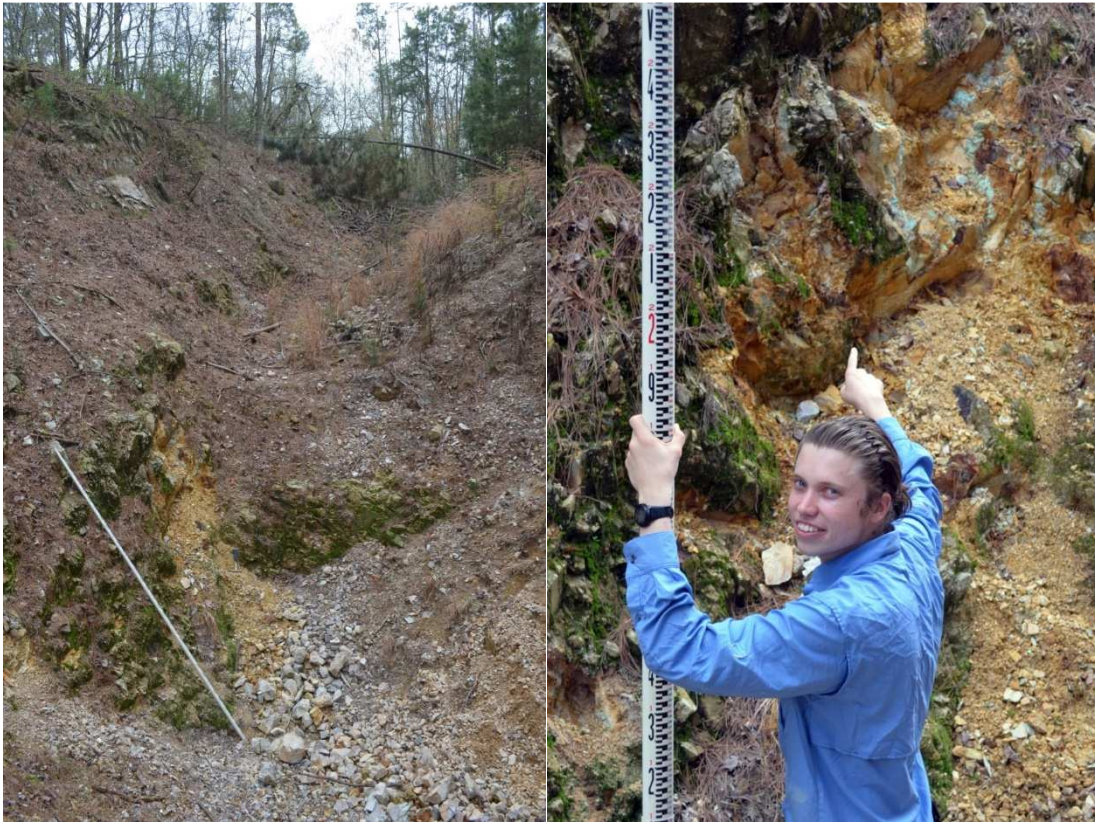








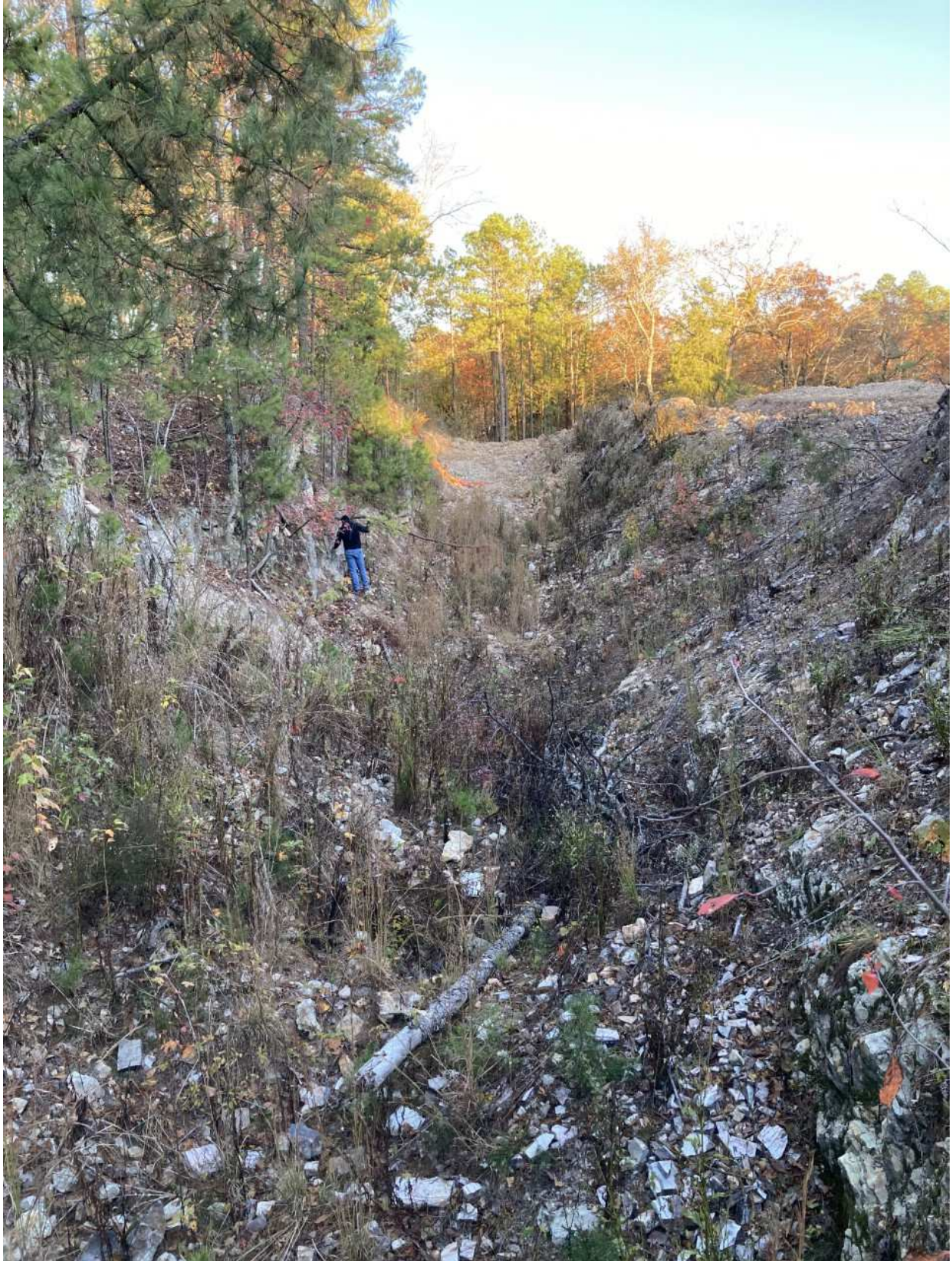
3/27/2021





*11/12/2021 and 11/13/2021*







04/09/2022

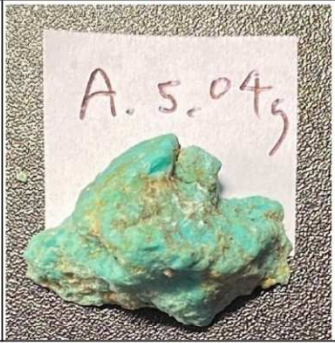





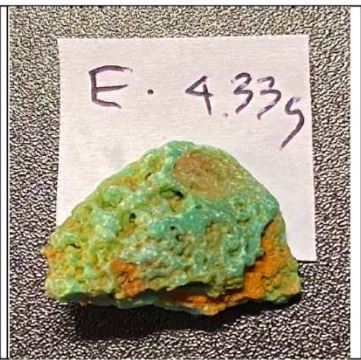




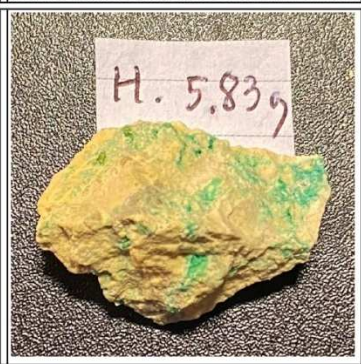






*Appendix B: Sample Images (photos by author and T. Paradise)*

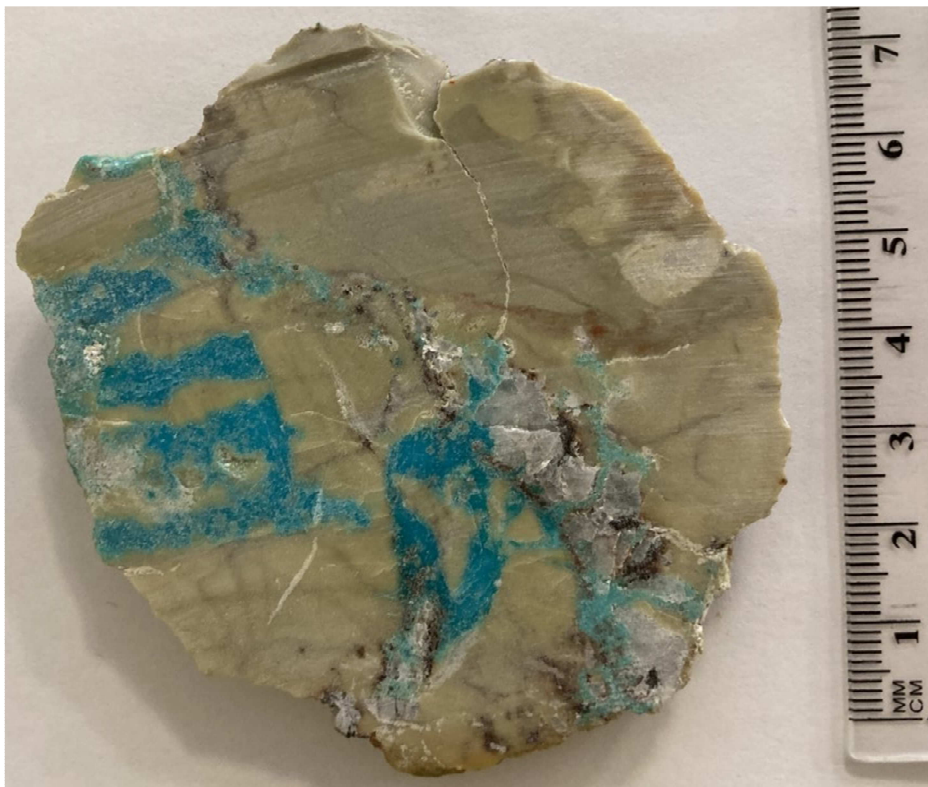
	WEIGHT (g)	L+W+D (mm)	c.MOHS	COMMENTS	XRD Turquoise Samples
<b>A</b>	5.04	26x14x15	6+	fine color (B+), vitreous, silica-like	
<b>B</b>	5.07	24x17x15	6+	good-fine color, vitreous	
<b>C</b>	3.85	19x15x14	6+-4+	white low mohs, blue, vitreous high mohs	
<b>D</b>	3.54	25x18x9	5, 6+	mohs 5 to mohs 6+	

<b>E</b>	4.33	25x19x10	5, 6	
<b>F</b>	2.31	24x13x10	5, 6+	

<b>G</b>	4.33	32x18x9	variscite-like color, parts vitreous, parts friable	
<b>H</b>	5.83	29x20x15	4-6+	

I	8.82	35x20x14	5, 6	beige-yellow mass, dark green seam	
J	5.29	23x20x12	7+	white mass, SILICA-LIKE, vitreous 7+	

*Polished Slab*



*MLI 01*



*MLI 02*



*MLI 03*



*MLI 04*



*MLI 05*



*MLI M*



*Appendix C: Sample Weights for Concentration and Isotope Analysis*

<i>Sample ID</i>	<i>Weight (mg)</i>
TQ-A	254.64
TQ-B	250.98
TQ-C	259.81
TQ-D	356.03
TQ-E	261.66
TQ-F	255.27
TQ-H	250.95
TQ-J	251.66
<b>MLI 01</b>	251.02
<b>MLI 02</b>	250.66
<b>MLI 03</b>	258.6
<b>MLI 04</b>	253.22
<b>MLI 05</b>	254.09
<b>MLI M</b>	251.43



*Appendix D: Elemental Concentrations (ppm) (negative values indicate concentrations outside of calibrated range)*

<i>Sample ID</i>	<i>Li</i>	<i>P</i>	<i>Sc</i>	<i>Ti</i>	<i>V</i>	<i>Cr</i>	<i>Mn</i>	<i>Fe</i>	<i>Co</i>	<i>Ni</i>	<i>Cu</i>	<i>Zn</i>	<i>Ga</i>	<i>Rb</i>	<i>Sr</i>	<i>Y</i>	<i>Zr</i>	<i>Mo</i>	<i>Cd</i>
	<i>ppm</i>	<i>ppm</i>	<i>ppm</i>	<i>ppm</i>	<i>ppm</i>	<i>ppm</i>	<i>ppm</i>	<i>ppm</i>	<i>ppm</i>	<i>ppm</i>	<i>ppm</i>	<i>ppm</i>	<i>ppm</i>	<i>ppm</i>	<i>ppm</i>	<i>ppm</i>	<i>ppm</i>	<i>ppm</i>	<i>ppm</i>
<b>TQ-C Cu/Fe</b>	-13.07	142004.55	3.91	169.73	-725.75	247.33	115.46	21544.15	18.31	22.54	45454.49	5318.78	-1.30	-123.42	602.45	32.59	29.39	15.07	-1.37
<b>TQ-J Cu/Fe</b>	-39.42	148365.41	-24.14	95.57	-535.46	255.56	71.47	14944.40	1.93	5.51	1412.14	1230.11	-1.28	-143.93	11.09	2.80	24.79	16.86	-1.77
<b>MLI 01 Cu/Fe</b>	-41.90	137783.30	6.32	78.28	-739.47	237.62	115.89	89318.06	2.42	-21.49	54316.94	2278.75	-1.28	-144.68	459.78	109.33	27.61	13.70	-1.42
<b>MLI 02 Cu/Fe</b>	-39.00	71348.13	-21.41	85.99	-700.63	260.17	71.68	19067.06	3.70	-13.73	14016.85	2012.09	-1.75	-145.70	15.50	7.82	22.78	10.22	-1.42
<b>MLI 02 Replicate Cu/Fe</b>	-41.96	271523.39	-0.15	85.95	-287.31	248.31	88.26	31104.64	16.34	-9.63	58231.43	1704.02	-0.94	-117.47	40.25	20.97	23.96	14.30	-1.24
<b>MLI 03 Cu/Fe</b>	-41.87	34513.05	-27.57	58.24	-721.36	252.10	62.60	14046.52	-0.64	-21.26	2313.11	1241.60	-1.37	-130.96	3.86	-0.27	20.63	12.73	-1.21
<b>MLI 05 Cu/Fe</b>	-37.82	110352.09	-14.76	344.69	-780.66	239.56	119.79	23179.38	15.51	66.93	31655.90	14887.01	-1.93	-106.07	993.19	117.69	42.69	13.10	-0.53
<b>TQ-A Pb/Sr</b>	0.00	63484.43	3.97	5.60	17.08	3.36	5.60	3164.51	2.26	1.36	13830.95	500.43	0.19	0.05	36.91	14.22	0.36	0.13	0.10
<b>TQ-B Pb/Sr</b>	0.10	56920.97	10.13	8.58	360.14	3.56	4.92	2397.27	8.35	8.20	8573.58	155.81	0.45	0.65	129.74	87.75	0.37	0.14	0.02
<b>TQ-C Pb/Sr</b>	0.03	56295.34	17.67	11.75	28.42	2.99	9.41	2114.45	8.24	3.56	13725.87	641.01	0.18	0.20	220.54	19.53	0.24	0.10	0.04
<b>TQ-D Pb/Sr</b>	0.12	48257.05	11.23	7.80	319.54	5.17	5.26	2920.13	6.23	6.59	7847.23	130.02	0.39	0.75	99.59	37.96	0.95	0.16	0.02
<b>TQ-E Pb/Sr</b>	0.12	71050.44	22.14	16.10	240.36	5.19	7.01	6789.09	4.33	5.71	10539.52	151.59	0.35	1.15	2.96	4.04	1.29	0.47	0.02
<b>TQ-F Pb/Sr</b>	0.25	69221.14	15.31	16.95	557.62	7.08	7.09	3663.89	8.89	10.55	12485.92	241.01	0.59	1.44	62.11	45.15	4.34	0.17	0.03
<b>TQ-H Pb/Sr</b>	0.12	69309.37	23.89	14.67	37.79	3.86	14.84	2988.70	10.76	7.69	19051.14	1001.26	0.21	0.38	266.48	26.12	0.34	0.10	0.06
<b>TQ-J Pb/Sr</b>	0.00	97017.99	2.62	2.12	254.67	1.80	0.84	693.01	0.78	0.46	801.40	60.18	0.23	1.26	0.27	2.18	0.13	0.21	0.01
<b>MLI 01 Pb/Sr</b>	0.04	50171.16	18.84	13.61	39.95	2.97	20.94	25383.07	1.40	0.84	16714.99	383.20	0.24	0.25	192.27	84.48	1.73	0.11	0.05
<b>MLI 02 Pb/Sr</b>	0.03	80096.48	13.24	4.28	207.95	4.43	4.90	5125.45	4.57	2.62	14785.63	132.38	0.40	0.76	11.66	10.48	0.70	0.15	0.02
<b>MLI 03 Pb/Sr</b>	0.00	27678.48	1.33	1.60	104.84	18.23	0.11	105.74	0.10	0.16	1932.12	8.59	1.59	0.16	0.38	0.98	0.02	0.01	0.01
<b>MLI 04 Pb/Sr</b>	0.14	68973.00	15.90	8.26	373.57	4.74	10.25	12365.47	4.54	3.84	16739.13	219.37	0.45	1.24	11.75	4.72	0.48	0.23	0.02
<b>MLI 05 Pb/Sr</b>	0.00	65805.27	12.48	32.78	38.60	4.31	25.92	5797.63	10.16	3.10	16852.39	925.41	0.19	0.42	701.62	89.62	0.11	0.23	0.22
<b>MLI M Pb/Sr</b>	9.89	15179.64	3.03	467.25	188.00	20.28	21.61	2994.80	8.96	381.81	579.36	783.84	1.22	0.93	55.76	27.73	25.21	0.33	0.52

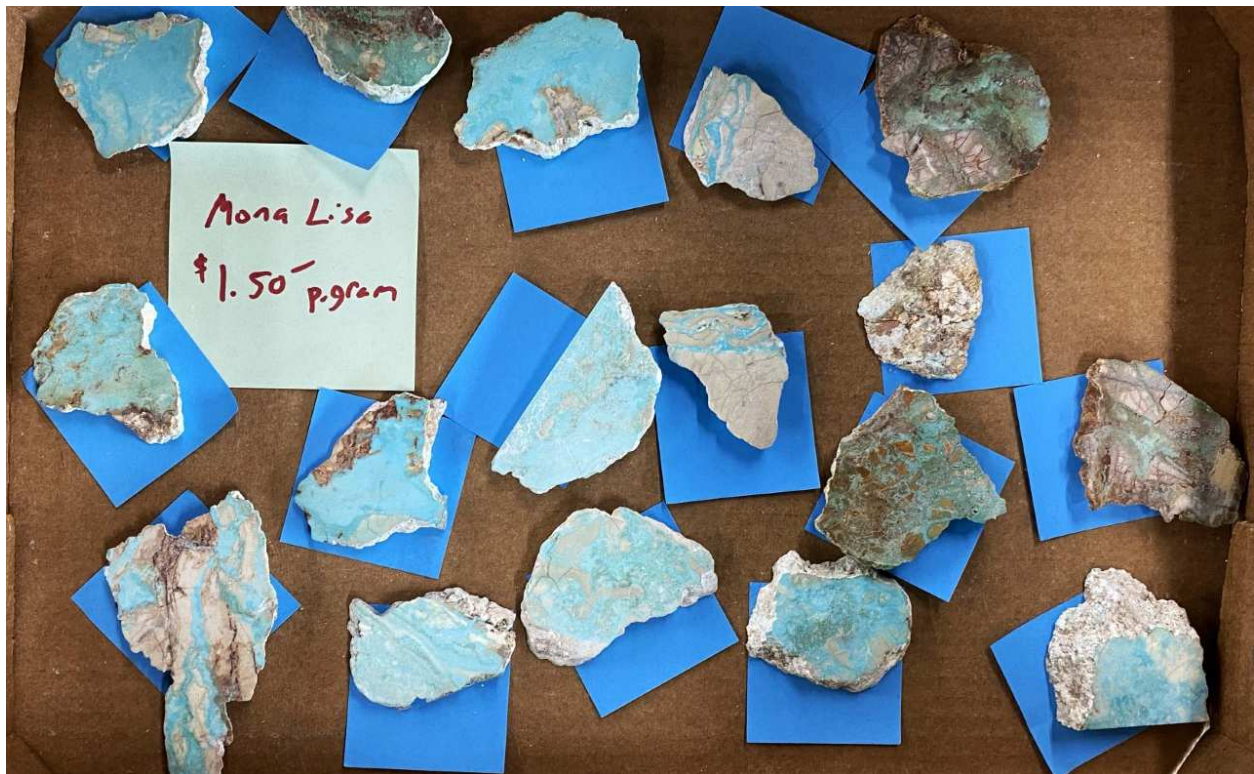
*Appendix D: Elemental Concentrations (ppm) (continued)*

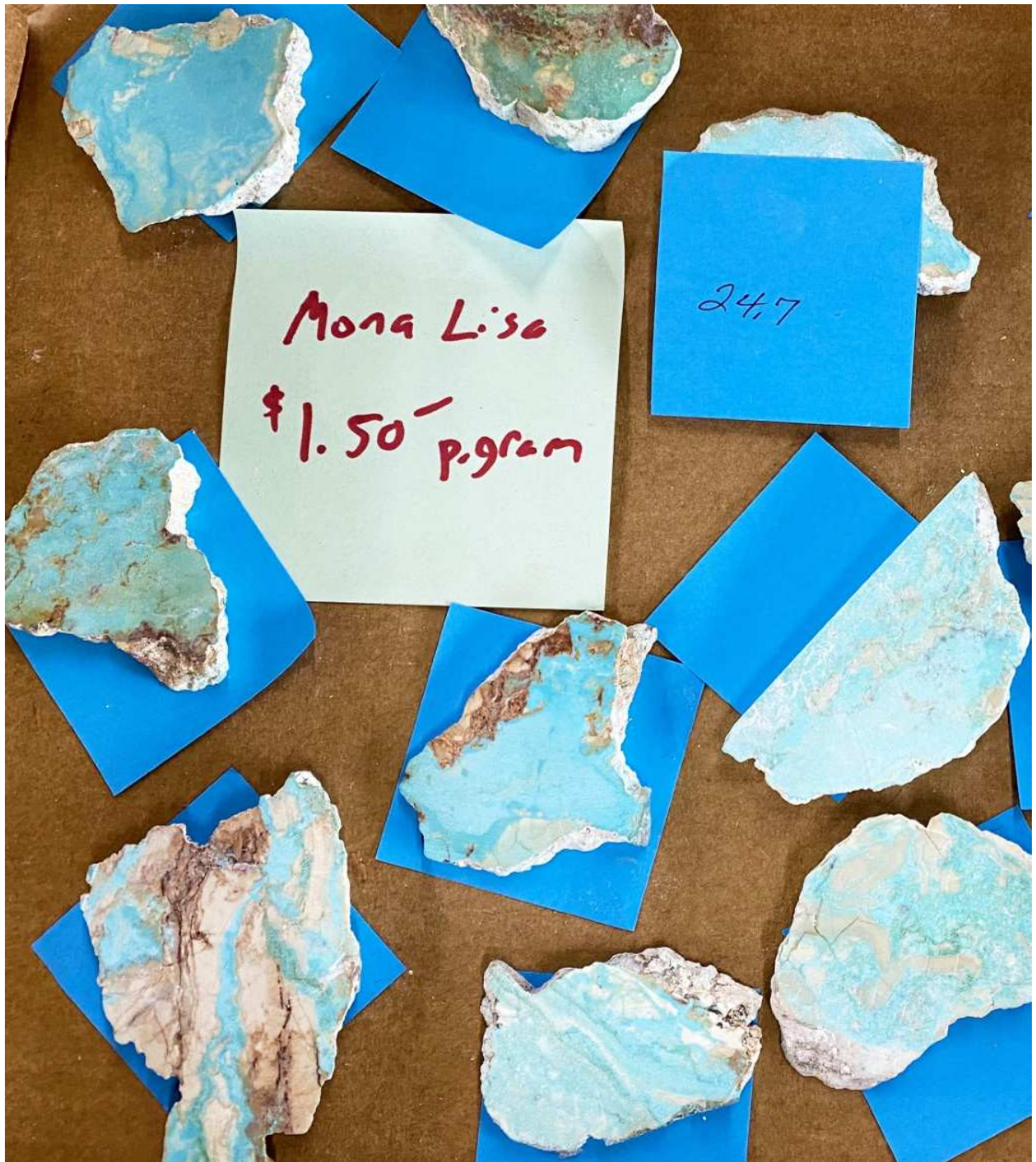
<i>Sample ID</i>	<i>Ba</i>	<i>La</i>	<i>Ce</i>	<i>Pr</i>	<i>Nd</i>	<i>Sm</i>	<i>Eu</i>	<i>Gd</i>	<i>Tb</i>	<i>Dy</i>	<i>Ho</i>	<i>Er</i>	<i>Tm</i>	<i>Yb</i>	<i>Lu</i>	<i>Re</i>	<i>Pb</i>	<i>Th</i>	<i>U</i>
	<i>ppm</i>	<i>ppm</i>	<i>ppm</i>	<i>ppm</i>	<i>ppm</i>	<i>ppm</i>	<i>ppm</i>	<i>ppm</i>	<i>ppm</i>	<i>ppm</i>	<i>ppm</i>	<i>ppm</i>	<i>ppm</i>	<i>ppm</i>	<i>ppm</i>	<i>ppm</i>	<i>ppm</i>	<i>ppm</i>	<i>ppm</i>
<b>TQ-C Cu/Fe</b>	504.15	4.81	9.98	-0.61	11.36	-1.28	-1.44	-0.59	-2.05	-0.75	-1.57	1.85	-1.78	6.83	-1.19	-1.65	9.46	-45.74	2.93
<b>TQ-J Cu/Fe</b>	796.19	1.30	4.46	-1.38	26.00	-2.24	-1.25	-0.88	-2.06	-1.64	-2.19	-1.03	-2.69	-1.22	-2.31	-1.74	2.01	-48.63	3.67
<b>MLI 01 Cu/Fe</b>	321.61	1.60	4.18	-1.16	11.50	-2.24	-1.83	-1.23	-2.17	-0.05	0.44	13.68	0.21	15.74	0.21	-1.70	-1.26	-48.41	2.02
<b>MLI 02 Cu/Fe</b>	656.32	5.68	9.20	-0.25	35.83	-1.84	-1.65	-0.53	-2.14	-0.93	-2.11	-0.55	-2.60	-0.59	-2.24	-1.79	0.32	-49.28	-0.75
<b>MLI 02 Replicate Cu/Fe</b>	1266.01	25.61	33.14	4.39	45.81	1.53	0.21	3.87	-1.45	2.11	-1.34	1.66	-2.20	0.91	-1.94	-1.79	2.02	-48.48	5.90
<b>MLI 03 Cu/Fe</b>	152.17	-0.01	2.62	-1.58	7.11	-2.28	-1.98	-1.54	-2.29	-2.00	-2.21	-1.50	-2.69	-2.01	-2.35	-1.66	-1.01	-48.47	-2.62
<b>MLI 05 Cu/Fe</b>	4625.26	3.36	5.75	-1.32	35.01	-1.71	0.21	-0.78	-2.14	-1.52	-1.31	8.90	0.46	25.80	1.95	-1.60	-0.85	-43.12	8.35
<b>TQ-A Pb/Sr</b>	3.68	0.00	0.02	0.00	0.00	0.00	0.00	0.00	0.00	0.03	0.06	0.55	0.13	1.00	0.15	0.00	0.05	0.00	1.43
<b>TQ-B Pb/Sr</b>	450.97	8.23	8.75	1.71	8.59	2.93	1.40	7.87	1.48	8.02	1.54	4.21	0.62	4.42	0.73	0.01	2.52	0.07	3.11
<b>TQ-C Pb/Sr</b>	71.55	0.25	0.22	0.04	0.18	0.04	0.05	0.08	0.02	0.13	0.08	0.71	0.18	1.46	0.24	0.00	0.05	0.00	0.91
<b>TQ-D Pb/Sr</b>	326.50	5.98	6.72	1.24	6.33	2.01	0.95	4.93	0.87	4.49	0.81	2.03	0.26	1.73	0.26	0.00	3.54	0.05	2.33
<b>TQ-E Pb/Sr</b>	256.42	0.59	0.80	0.14	0.74	0.21	0.19	0.31	0.05	0.30	0.07	0.24	0.04	0.30	0.04	0.00	0.41	0.05	3.82
<b>TQ-F Pb/Sr</b>	502.25	10.43	11.15	2.33	9.99	3.02	1.26	6.08	1.10	6.16	1.17	3.11	0.44	3.19	0.50	0.01	2.59	0.41	7.37
<b>TQ-H Pb/Sr</b>	92.12	0.62	0.57	0.11	0.48	0.10	0.07	0.14	0.02	0.16	0.10	0.98	0.28	2.39	0.41	0.00	0.12	0.02	1.61
<b>TQ-J Pb/Sr</b>	172.44	0.21	0.35	0.09	0.40	0.13	0.11	0.18	0.04	0.30	0.08	0.30	0.05	0.36	0.05	0.00	0.86	0.00	4.08
<b>MLI 01 Pb/Sr</b>	54.39	0.19	0.20	0.04	0.21	0.06	0.05	0.12	0.03	0.52	0.60	3.40	0.61	4.25	0.61	0.01	0.03	0.00	0.91
<b>MLI 02 Pb/Sr</b>	355.09	9.24	11.53	1.80	6.54	1.29	0.51	1.91	0.28	1.34	0.26	0.75	0.11	0.79	0.12	0.00	0.50	0.03	1.94
<b>MLI 03 Pb/Sr</b>	31.33	0.07	0.12	0.02	0.10	0.04	0.02	0.07	0.02	0.14	0.04	0.12	0.02	0.08	0.01	0.00	0.01	0.01	0.52
<b>MLI 04 Pb/Sr</b>	246.50	1.19	1.38	0.21	0.88	0.20	0.17	0.35	0.06	0.34	0.08	0.27	0.05	0.37	0.06	0.00	0.18	0.04	3.02
<b>MLI 05 Pb/Sr</b>	44.86	0.01	0.01	0.00	0.00	0.00	0.02	0.01	0.00	0.13	0.35	3.95	1.11	11.42	1.77	0.02	0.02	0.00	5.65
<b>MLI M Pb/Sr</b>	66.54	3.77	5.58	0.75	2.90	0.53	0.15	0.65	0.11	0.73	0.38	2.97	0.69	5.55	0.97	0.01	1.47	1.24	6.72

*Appendix E: Full Isotope Results and Uncertainties*

<b>Sample</b>	<b><math>^{208}\text{Pb}/^{204}\text{Pb}</math></b>	<b>Error</b>	<b><math>^{207}\text{Pb}/^{204}\text{Pb}</math></b>	<b>Error</b>	<b><math>^{206}\text{Pb}/^{204}\text{Pb}</math></b>	<b>Error</b>	<b><math>^{87}\text{Sr}/^{86}\text{Sr}</math></b>	<b>Error</b>
<b>TQ-A</b>	38.5129	{1.04E-03}	15.7077	{4.75E-04}	20.7344	{7.50E-04}	0.71234	5.61E-06
<b>TQ-B</b>	38.5858	{1.30E-03}	15.7120	{4.54E-04}	19.8953	{5.64E-04}	0.71456	5.64E-06
<b>TQ-C</b>	38.9758	{1.05E-03}	15.8571	{3.66E-04}	23.1794	{8.64E-04}	0.71230	5.98E-06
<b>TQ-D1</b>	38.4916	{7.72E-04}	15.6797	{2.53E-04}	19.3089	{3.48E-04}	0.71496	4.82E-06
<b>TQ-D2</b>	38.4897	{9.60E-04}	15.6803	{3.80E-04}	19.3094	{4.41E-04}	0.71498	6.94E-06
<b>TQ-E</b>	39.0764	{1.33E-03}	15.7962	{5.39E-04}	21.6647	{7.97E-04}	0.71713	8.77E-06
<b>TQ-F</b>	38.9101	{7.09E-04}	15.7949	{2.86E-04}	21.3226	{3.35E-04}	0.71749	5.87E-06
<b>TQ-H</b>	38.8510	{1.50E-03}	15.7733	{5.46E-04}	22.7770	{7.81E-04}	0.71229	5.75E-06
<b>TQ-J</b>	38.9307	{5.79E-04}	15.7896	{2.25E-04}	21.2573	{2.91E-04}	0.71916	8.97E-06
<b>MLI 01</b>	38.7570	{1.89E-03}	15.7895	{7.04E-04}	21.7871	{1.12E-03}	0.71256	5.46E-06
<b>MLI 02</b>	38.9598	{8.88E-04}	15.7877	{3.32E-04}	21.4767	{4.37E-04}	0.71648	6.66E-06
<b>MLI 03</b>	N/A		N/A		N/A		0.71533	7.56E-06
<b>MLI 04</b>	38.9712	{7.47E-04}	15.7633	{3.05E-04}	21.3593	{3.98E-04}	0.71341	5.23E-06
<b>MLI 05</b>	N/A		N/A		N/A		0.71230	5.21E-06
<b>MLI M</b>	39.2655	{9.86E-04}	15.8273	{3.90E-04}	21.9286	{5.33E-04}	0.71280	5.49E-06

*Appendix F: Mona Lisa Turquoise with Prices (photos by author and T. Paradise)*





Mona Lisa  
\$1.50<sup>-</sup> p.gram

24.7

